International Journal of Bifurcation and Chaos

Symmetry and Network Topology in Neuronal Circuits: Complicity of Form and Function

Ian Stewart
Mathematics Institute, University of Warwick
Coventry, CV4 7AL, United Kingdom
i.n.stewart@warwick.ac.uk

Received (to be inserted by publisher)

Symmetries in the external world constrain the evolution of neuronal circuits that allow organisms to sense the environment and act within it. Many small 'modular' circuits can be viewed as approximate discretizations of the relevant symmetries, relating their forms to the functions they perform. The recent development of a formal theory of dynamics and bifurcations of networks of coupled differential equations permits the analysis of some aspects of network behaviour without invoking specific model equations or numerical simulations. We review basic features of this theory, compare it to equivariant dynamics, and examine the subtle effects of symmetry when combined with network structure. We illustrate the relation between form and function through examples drawn from neurobiology, including locomotion, peristalsis, visual perception, balance, hearing, location detection, decision-making, and the connectome of the nematode *Caenorhabditis elegans*.

Keywords: network; neuroscience; symmetry; synchrony; phase relation; balanced coloring; bifurcation; vision; locomotion; peristalsis; vestibular system; binocular rivalry; auditory cortex; grid cell; decision-making; connectome.

1. Introduction

Throughout much of the animal kingdom, sensory and motor activity is initiated and controlled by networks of neurons, either in the brain or elsewhere in the body. A basic question, in both biology and mathematics, is to understand how the architecture of a network of neurons affects its dynamics. In general terms, this amounts to investigating connections between form and function in such networks. This is a huge topic, which has been studied from numerous points of view, and a comprehensive survey is out of the question, so we focus on the role of symmetry and its influence on network dynamics. Here 'symmetry' includes the usual notion of invariance under a group of transformations, but we also allow local 'groupoid' symmetries, which are often more suited to biology.

An important feature of network dynamics is *synchrony*. This, too, such a large topic that we can only scratch the surface. In its strongest form, two nodes of a network are synchronous if the have identical dynamics; that is, if their behavior yields identical time series. A related notion of *phase synchrony* applies to time-periodic states: now the time series are identical except for a phase shift. There are weaker notions of synchrony in which 'identical' is replaced by 'strongly correlated' or more vaguely 'look similar'. We confine the discussion to exact synchrony and phase relations. This is an idealized modeling assumption, but we argue that it can afford useful insights into real networks where symmetry is imperfect or approximate.

The term 'neural network' has been adopted by the Artificial Intelligence and Machine Learning communities, so for clarity we refer to neuronal networks when the neurons are biological or refer to models of biological neurons. A striking feature of many neuronal networks is *symmetry*. Here the network connections are (more or less) invariant under a group of permutations of the neurons. It is well known from equivariant dynamics that symmetry can create synchrony and phase patterns in a robust, systematic manner [Golubitsky *et al.*, 1988; Golubitsky & Stewart, 2002]. More recently it has also become apparent that while symmetry is sufficient to create such patterns, it is not necessary [Boldi & Vigna, 2002; Stewart *et al.*, 2003; Golubitsky *et al.*, 2005; Golubitsky & Stewart, 2006; DeVille & Lerman, 2013, 2015]. Moreover, generic dynamics and bifurcation in a symmetric network can differ from generic dynamics and bifurcation for the same symmetry group in the equivariant setting, because of network constraints.

This paper has three main themes: mathematical, biological, and philosophical.

The mathematical theme is the exploration of these ideas, focusing mainly on the context of neuronal networks, which allows us to relate the theoretical concepts to biological observations. The mathematical framework is more general, dealing with any network of coupled differential equations, so it applies to many areas of science, but we mostly restrict discussion to neuronal networks to be specific. This paper is not a comprehensive survey — just a selection of interesting and typical examples, combined with an introduction to an approach to a formal theory of network dynamics that has been developed over the past two decades [Stewart *et al.*, 2003; Golubitsky *et al.*, 2005; Golubitsky & Stewart, 2023]. A similar framework presented in a more concrete manner has been proposed in [Field, 2004].

The biological theme examines how symmetry transformations in the external world, arising from fundamental symmetries of physical laws, relate to the topology of neuronal networks for perception and movement. For example, the visual system is capable of perceiving the same object in different orientations, at different distances, and in different locations. The corresponding transformations of the object in 3-dimensional space are rotations, translations, and dilations. They generate a group $\mathbb{E}(3) \times \mathbb{R}^+$, the Euclidean group in $\mathbb{R}^3$ extended by the group of dilations $x \mapsto \mu x$ for $0 < \mu \in \mathbb{R}$. A neuronal network that has evolved to recognize and track the motion of objects must deal with these changes in the input image(s) to the eye(s). It is therefore reasonable to expect the network topology to be invariant under a corresponding transformation group. However, $\mathbb{E}(3) \times \mathbb{R}^+$ is continuous and non-compact, whereas the network is discrete and finite, so some type of approximation is mathematically necessary. Moreover, biological systems generally lack the precision expected in physics or engineering. We do not attempt to formalize this kind of approximation; instead, we present numerous examples.

The third, more philosophical, theme is a contribution to the perennial debate about form and function: which is primary? The networks analyzed here suggest that in at least some cases the answer is 'both' — or 'neither'. Instead, we suggest that biological form and function may coevolve, under constraints caused by common symmetry properties. Equivariance properties of symmetric systems, rooted in the underlying physics, are common to real (biological) systems, the underlying network (real neuronal or idealized model), and model differential equations. The biological function emerges from the natural dynamic properties of the network topology, and in the examples discussed, the same symmetries are present in all three. It seems reasonable to suggest that the evolution of these neuronal circuits may have been constrained by these common symmetries. Symmetries and synchronies therefore provided a potential route that links form to function in an evolutionary context, and provide a framework for relating form and function.

1.1. *Example: Locomotion of* Caenorhabditis elegans

A simple example of these principles is the locomotion of the nematode worm *C. elegans*. This organism has been studied intensively; in particular the arrangement of its cells (which is essentially the same for all specimens) is known, as is the connectome (wiring diagram of nerve cells).

Figure 1 shows the neuromuscular connections involved in locomotion. Figure 2 shows a neuromechanical model obtained as a simplified and idealized version of the nerve and muscle groups and connections. An evident common feature is the repetitive linear arrangement of nerves and muscles.

The primary function of locomotor nerves and muscles is to propel the organism forwards or backwards. *C. elegans* has two distinct neuronal circuits for these two directions of movement, but we ignore this level

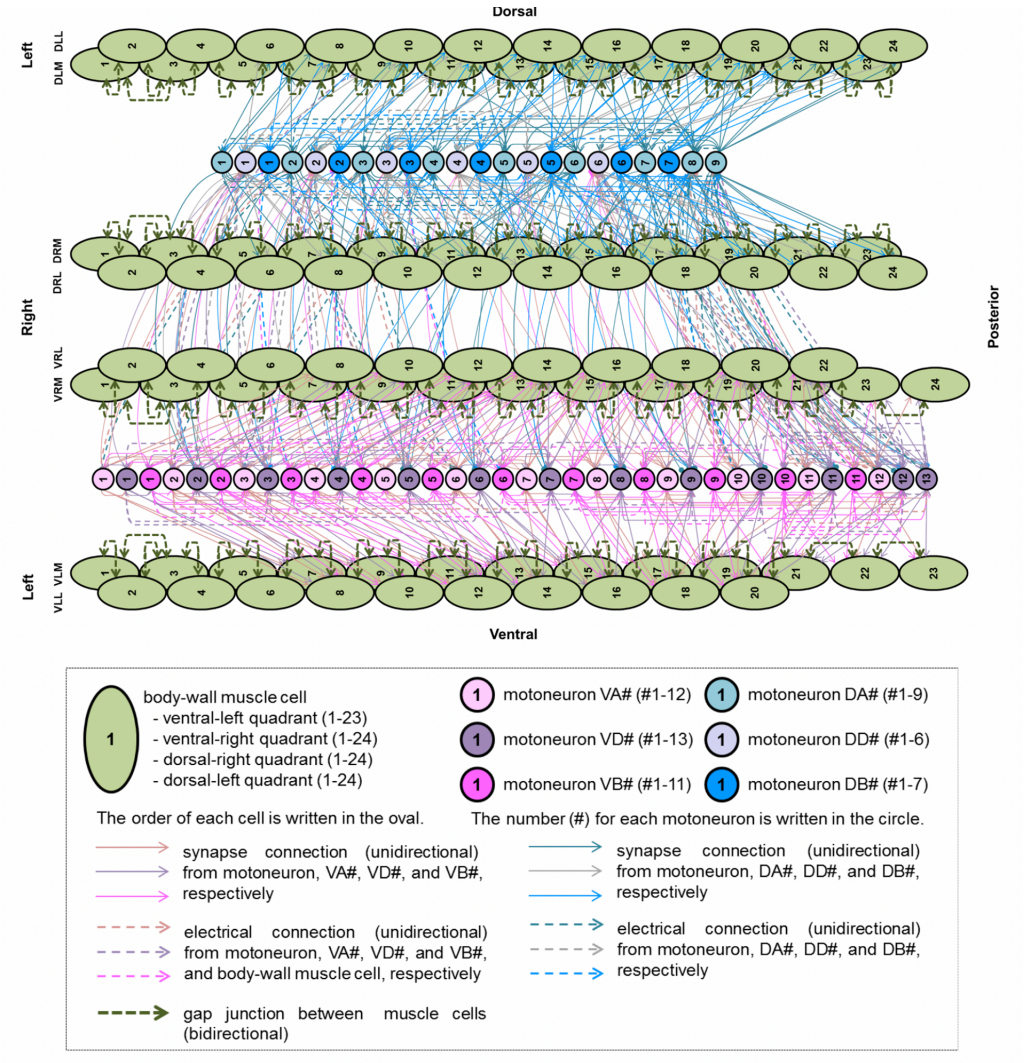

Fig. 1. Neuromuscular connections based on WormAtlas. Synaptic connections and gap junctions of 95 muscle cells and 6 types of motor neuron [Sakamoto *et al.*, 2021, Figure 1].

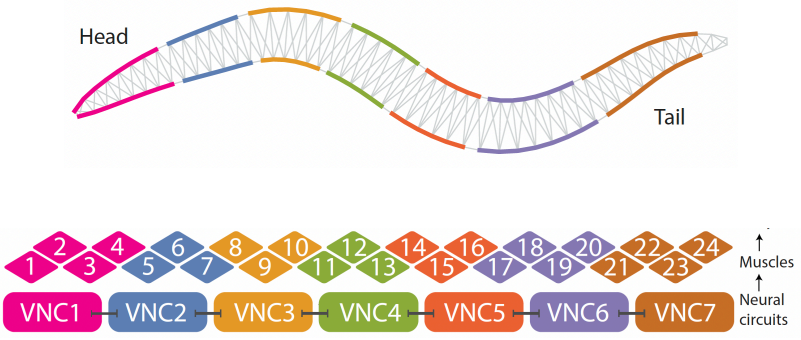

Fig. 2. Neuromechanical model of *C. elegans* locomotion. *Top*: Following [Boyle *et al.*, 2012] the body is modeled in 2D cross-section as a set of interconnected discrete segments. *Bottom*: Following [Izquierdo *et al.*, 2018] muscles are modeled as elements that contract and relax in dorsoventral plane, staggered along ventral and dorsal sides. Five neural units innervate three ventral and three dorsal muscles and two end units innervate four muscles, as shown by colors [Olivares *et al.*, 2021, Figure 1].

of detail and restrict attention to forward locomotion. The transformation group concerned in the physical world is the additive group of translations $\mathbb{R}$ together with time translation (also $\mathbb{R}$). The stationary state is invariant under the subgroup $\mathbf{1} \times \mathbb{R} \subseteq \mathbb{R} \times \mathbb{R}$. When the organism moves, it adopts a sinusoidal shape, corresponding to a periodic traveling wave with spatiotemporal symmetry $\widetilde{\mathbb{R}} = \{(\rho vt, \rho t) : t \in \mathbb{Z}\}$, where ρ is the period. That is, time translation by an integer multiple ρt of the period has the same effect as spatial translation by ρvt, where v represents the speed.

Considering only the spatial part, the physical group $\mathbb{R}$ is replaced in the dynamics by a discrete version $\mathbb{Z}$. The same group $\mathbb{Z}$ is an approximate symmetry of both the set of muscles and of the set of neurons that drive them — approximate in part because the chain is finite, instead of being an idealized bi-infinite chain with exact $\mathbb{Z}$ symmetry. Or, imposing periodic boundary conditions, a finite closed ring. This is true of both the model and (give or take biological imprecision) the actual organism. This underlying transformation group is therefore related to both the form of the network (a linear chain) and the function (linear locomotion). Linearly propagating waves of muscle movements, triggered by linearly propagating waves in chains of neurons, are common to many biological functions requiring linear movement, and even biped and quadruped locomotion can be viewed as traveling waves in short closed rings; see Section 9.

In this example the symmetry structures and their relations are very simple. Later examples suggest that the same principles could apply to other symmetry groups and biological functions.

1.2. *Summary of Paper*

Before embarking on the mathematics, neuroscience-related applications, and examples, Section 2 discusses the relationship between idealized models and messy reality. It provides some justification for the use of idealized models, both practical and theoretical, while pointing out some of the pitfalls. In particular we discuss the relation between exact and approximate symmetries.

Section 3 raises the issue of form *v.* function, in both designed and evolved systems, and suggests that form and function often coevolve, with neither being primary.

Section 4 begins with the importance of synchrony in many aspects of brain behaviour, and explores its relations to symmetry — treating both in an ideal exact form. Two simple networks introduce some of the basic mathematics of these concepts, with an emphasis on how the architecture of a network affects its typical dynamics. Terminology not defined here is explained when needed.

Section 5 is a brief summary of the basics of equivariant dynamics. In particular, we state the Equivariant Branching Lemma, which asserts the generic existence of certain symmetry-breaking equilibria, and the analogous Equivariant Hopf Theorem, which does the same for Hopf bifurcation to a periodic oscillation.

Section 6 summarizes the general theory behind these examples. In particular we show that while symmetry implies certain types of synchrony, synchrony can also arise in the absence of symmetry, through balanced colorings and their associated quotient networks (which clump clusters of synchronous nodes together), and the equivalent formalism of graph fibrations. We also discuss input trees, which determine when it is possible for two nodes to synchronize robustly.

Section 7 delves more deeply into properties of symmetric networks. We discuss symmetry-breaking, and examine the subtle relationsss between equivariant and admissible ODEs for a symmetric network. Among the balanced colorings we distinguish orbit colorings, determined by a subgroup of the symmetry group according to the equivariant theory, and exotic colorings, which are not orbit colorings but are nevertheless balanced. The existence of exotic colorings hints at differences of generic behavior between the network theory and equivariant dynamics.

Section 8 discusses the relevance of balanced colorings to synchrony patterns of individual states, either steady or oscillatory, and to phase patterns of oscillations. Here the key concept is rigidity — the pattern persists after any small admissible perturbation of the ODE. The dynamics leads to strong restrictions on network architecture, modulo some longstanding conjectures that have been proved in important special cases or under slightly stronger hypotheses.

Section 9 begins a series of case studies of symmetry and synchrony in neuronal networks, discussing patterns in legged locomotion ('gaits'), their relation to traveling waves of nerve activity, and how mathematical network models link these two features via spatio-temporal symmetries of symmetric networks.

The related topic of peristaltic waves is also considered. A final subsection shows how a balanced coloring of a suitable asymmetric chain can prove the existence of traveling wave states, and uses simulation to show that a linear chain of FitzHugh–Nagumo neurons subjected to sinusoidal forcing of the initial node can also generate traveling waves.

Section 10 summarizes some models of vision. Topics include the relation between the retino-cortical map and the complex logarithmic function, the symmetry properties of the V1 layer of the cortex and its relevance to edge detection, the application of this structure to hallucination patterns, similar issues of the V2/V3/V4 layers related to the perception of direction, the Klein bottle topology of the orientation field, and Wilson networks as models of visual rivalry and illusions.

Section 11 provides brief discussions of three other types of sensory network: the vestibular system in the inner ear, controlling balance; the auditory cortex in humans and bats; and grid cells, which determine spatial location.

Section 12 discusses models of high-level decision-making in the brain, similar to the original proposal of [Wilson, 2009]. We summarize ideas of [Franci *et al.*, 2022] and place them in the context of this paper. We consider m agents who assign real-number values to each of n options, leading to a model with $\mathbb{S}_m \times \mathbb{S}_n$ symmetry, where $\mathbb{S}_k$ indicates the symmetric group of all permutations of k symbols. An initially indecisive state can undergo symmetry-breaking bifurcations to states in which sets of agents prefer specific sets of options, allowing decisions to be made. There is a natural network model with three distinct types of arrow, and the network topology creates some 'exotic' patterns that cannot be obtained from the symmetry group using equivariant bifurcation theory. The application here is somewhat metaphorical, but it shows that exotic patterns can arise in reasonable models of real-world phenomena.

Section 13 demonstrates that the mathematical methods used to understand the above models is not limited to small networks, by applying them to the connectome of *C. elegans*. Here we summarize one small part of work on symmetry and fibrations in real, large networks [Morone & Makse, 2019; Leifer *et al.*, 2020; Morone *et al.*, 2020; Makse *et al.*, 2021].

Finally, Section 14 provides a summary and conclusions, including a table of relations between form and function, mediated by symmetry, for the examples discussed in the text.

2. Modeling Issues

One possibly contentious issue requires immediate discussion. In the mathematical formalism under consideration, symmetry and synchrony are employed in an idealized manner: they are assumed to be exact. Biology, of course, is not like that. Neurons and the signals they produce may be approximately identical, but never exactly so. We therefore ask whether idealized mathematics can shed useful light on real biological systems. We claim that the answer is affirmative, provided we do not expect too much. Mathematically, an approximately symmetric system can profitably be viewed as a perturbation of an ideal system with exact symmetry. [Morone & Makse, 2019] quantify the notion of an approximate symmetry, which in particular allows statistical estimates of the significance of apparent symmetries. This approach deserves further attention.

A major advantage of assuming exact symmetry is that the mathematics has more structure, and is therefore more tractable, leading to systematic phenomena that can be understood in some detail. Moreover, many of the features thus revealed persist, to some extent, after a symmetry-breaking perturbation. This is a consequence of the mathematical condition of hyperbolicity [Guckenheimer & Holmes, 1983], which by the Kupka-Smale Theorem is valid generically [Kupka, 1963; Smale, 1963; Peixoto, 1966]. It implies that states occurring in the symmetric case persist after such a perturbation, and are 'close' to' the corresponding states of the idealized model. States that are related by symmetry in the idealized model — for instance, periodic oscillations with identical waveforms, or specific phase relations — cease to be related in exactly this way: the waveforms are no longer identical and the phase relations can vary to some extent from the ideal. However, the waveforms and phase relations remain *very similar* when symmetry is slightly broken. In this manner, the idealized model has important implications for a more realistic one, while being more tractable and more comprehensible.

Example 2.1. As an example, consider the *repressilator*, a simple gene regulatory network that creates

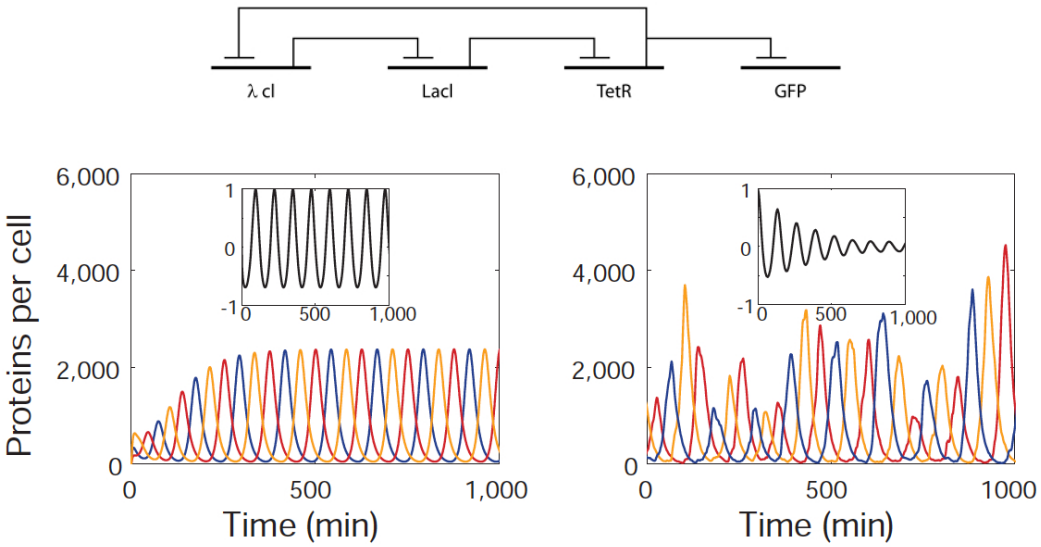

Fig. 3. Repressilator. *Top*: Genetic regulatory network. *Bottom* [Elowitz & Leibler, 2000]: Simulations of oscillations. *Left*: Idealized symmetric model. *Right*: Stochastic version with only approximate $\mathbb{Z}_3$ symmetry.

oscillations. [Elowitz & Leibler, 2000] discuss the exact symmetric model, with three genes and a cyclic symmetry group $\mathbb{Z}_3$. In the network of Figure 3 (top), the repressor protein LacI from *E. coli* inhibits the transcription of the repressor gene *tetR* from the tetracycline-resistance transposon Tn*10*, whose protein product in turn inhibits the expression of a third gene, *cI* from λ phage. Finally, CI inhibits *lacI* expression, completing the cycle.

Elowitz and Leibler initially assume, for simplicity, that all three repressors have the same dynamics, so the equations are $\mathbb{Z}_3$-symmetric. Equivariant bifurcation theory predicts that one generic dynamic state is a discrete rotating wave in which all three nodes oscillate with the same waveform but with successive phase shifts of one third of the period. Numerical simulations of oscillatory motion produces a discrete rotating wave with successive $\frac{1}{3}$-period phase shifts, Figure 3 (bottom left), a typical symmetry-breaking form found in $\mathbb{Z}_3$-symmetric network dynamics [Golubitsky & Stewart, 2002]. Elowitz and Leibler also show that a damped oscillation sustained by stochastic noise produces persistent but aperiodic oscillations of different amplitudes, which have approximately the same $\frac{1}{3}$-period phase shifts, Figure 3 (bottom right). This illustrates how a symmetric model can sometimes be a useful guide to a more realistic one.

Similar remarks apply, *mutatis mutandis*, to synchrony, which we will see is related to, but different from, symmetry. In this paper, we work with exact, idealized, perfectly symmetric or perfectly synchronous models. Provided their limitations are understood and respected, such models can offer useful insights into otherwise intractable systems of real biology.

3. Form and Function

Studies of the brain or subnetworks of the nervous system observe the form of neuronal circuits and aim to infer something about their function and how they perform it. Systematic understanding of the dynamic behavior that is typical for given network topology aids such inferences, and can be seen as a contribution to a wider issue: the relation between form and function. One theme of this paper is that symmetry often helps to elucidate this relationship, because it is often common to both form and function, providing a link between them.

This is not a new idea. In particular, it is known that breaking symmetry by removing a few connections can create highly structured and complex patterns of behavior in densely connected homogeneous networks [Singh, Menon, & Sinha, 2016], which are reasonable models of some regions of the brain with a large number of neurons. [Pillai & and Jirsa, 2017] propose that such processes can be formalized "as a low-dimensional

process emerging from a network's dynamics dependent on the symmetry and invariance properties of the network connectivity". Our aim is to complement such suggestions by embedding them in a rich formal theory of network dynamics and linking this theory to specific examples.

3.1. *Form* v. *Function: Origins in Architecture*

Historically there has been much debate about which of form and function is primary, and not just in neuroscience. The phrase "form follows function" is generally credited to the architect Louis Sullivan in his article "The tall office building artistically considered" [Sullivan, 1896]. The article was in part a reaction against classical design principles, in which the function of a building was of secondary importance to its form. Sullivan argued that the main design principles for a skyscraper, hence its resulting form, were dictated by its function: namely, to contain large numbers of offices. "Following our instincts," he wrote, "we will naturally be led to the canonical skyscraper form." *But* ... "We are doubtless right, in our instinct, but we must seek a fuller justification, a finer sanction, for it." This quest led him to an eloquently stated principle:

> Whether it be the sweeping eagle in his flight, or the open apple-blossom, the toiling work-horse, the blithe swan, the branching oak, the winding stream at its base, the drifting clouds, over all the coursing sun, form ever follows function, and this is the law. Where function does not change, form does not change.

Modernist architects took this principle to heart from the 1930s onwards, using it to dismiss all unnecessary decoration. Eventually, there was a backlash: a reversion to "function follows form", followed by a decoupling of form from function. Numerous buildings were designed primarily to look unusual and interesting; the activities within them were then shoehorned into the resulting structure. Iconic examples include the Guggenheim Museum in Bilbao, Spain; the Atomium in Brussels, Belgium; and the Krzywy Domek (crooked house) in Sopot, Poland.

Sullivan's references to living creatures, from eagles to oaks, contains the seeds of a counter-argument, with wider relevance. Architecture is about *design*, and the form of a designed structure may well be governed by its intended use. But an *evolved* structure, such as an eagle's wing or an oak tree's leaves — or, indeed, a neuronal network — does not arise by specifying a function (fly, collect energy from sunlight, process sensory and motor information) and then constructing an organism or an organ that performs this function. Evolution has no preset goals. Instead, nature creates random variations, and natural selection weeds out those that reduce the organism's chances of survival to breed.

One purpose of this article is to place the form/function debate in a different context. Architects explored three options: form follows function, function follows form, the two are unrelated. They omitted a fourth option: the first two options *both occur*, iteratively and interactively. We now argue that this option is closer to reality.

3.2. *Form and Function in Evolution*

The evolutionary process is widely hailed as 'random', meaning that evolution has no preset goals. Mutations in DNA are unpredictable (though there may be 'hot spots' that mutate at higher than normal rates, and conserved regions where mutations are rare — perhaps because most are fatal), which reinforces the role of randomness. However, variability of viable organisms in evolution is far from random. Mutations at a genetic level are random, though not uniformly so, but mutations are filtered through the processes of developmental biology, which impose constraints. In particular, selection can create a type of dynamic in which phenotypic changes become more predictable.

Classic examples are the evolution of the horse, with a systematic increase in size [Simpson, 1951; MacFadden, 2005], and the arms race between predatory cats and large herbivores [Van Valkenburgh *et al.*, 2016], in which the cats evolve ever longer teeth, and herbivores every thicker hides, both becoming increasingly massive — at which point both die out because they have over-invested in armament and their lifestyles become unsustainable. The entire process was repeated many times over a period of 33 million

years — evidence that it was predictable. A recent example is the effect of weather conditions on Darwin's finches, [Grant & Grant, 2003], who show that phenotypic changes such as beak size would be entirely predictable if the weather could be predicted.

In evolutionary biology, form follows function, but function also follows form, and the process may iterate. Feathers originally seem to have developed for warmth (form following function) [Bock, 2000] and were then co-opted for short hopping flights (function following form). Thus form and function coevolve, with neither necessarily being primary. Coevolution is an example of *complicity* [Cohen & Stewart, 1994]. Here, two different processes combine in a manner that transcends either of them, or even their union. If we envisage each process as an axis in possibility-space — what [Kauffman, 2000, 2008] calls the "space of the adjacent possible" — the combined system ends up exploring regions far from either axis, creating possibilities inherent in neither process.

These remarks can be interpreted in the context of evolving neuronal networks. DNA mutations primarily affect the form of the network. Its natural dynamic then produces its function. But selection for improved (or different) function then favors some mutations over others, and the process repeats. The details of this iterative coevolution are complex and hard to disentangle, but one common thread often runs throughout: the natural physical symmetries of the things being sensed or the motion of the organism are reflected in the similarly symmetric topology of the neuronal network that is responsible for sensory perception and movement, and evolution exploits, conserves, and (if it is advantageous) adapts these symmetries.

The correspondence is not exact: network symmetries are discrete, whereas many physical symmetries are continuous. In such cases, the network tends to 'do the best it can' to emulate continuous symmetries in a discrete setting. Sometimes this tendency can even be formalized as an optimization process. Moreover, for some purposes more extensive breaking of symmetry may have been selected for: a possible example is the still controversial evolutionary history of hexapods, once thought to have evolved from arthropods by fusing segments and losing limbs [Kukalová-Peck, 1987], but now believed to be more closely related to crustaceans [Grimaldi, 2010].

4. Synchrony and Symmetry

Numerous studies have indicated the importance of *synchrony* in the nervous system, and in particular the brain [Singer, 1999; Uhlhaas *et al.*, 2009; Nicosia *et al.*, 2013]. The well-known slogan "neurons that fire together, wire together" underpins Hebbian learning [Hebb, 1949]. Roughly speaking, neurons are synchronous when their periods of activity coincide: they spike or burst at (more or less) the same times. There are many different concepts of synchrony [Golomb *et al.*, 2001; Golomb, 2007]. Here we employ a strong, idealized definition: identical dynamics.

This assumption is not as strong as it might seem. For example, bursting neurons are often modeled as an ODE with two timescales: a fast one for the spiking of the neurons and a slow one that switches activity on and off [Golubitsky *et al.*, 2001; Izhikevich, 2007]. Exact synchrony of the slow oscillations can then create approximate synchrony of the fast ones, with coincident periods of activity but waveforms that differ in fine detail and timing.

Synchrony is often interpreted as evidence for a causal connection, or functional interdependence, between the neurons concerned, hence for their synaptic connections. Thus the dynamics of sets of neurons provides hints about the 'wiring diagrams' of neuronal 'circuits'. An important point here is that synchrony between two neurons need not imply the existence of a *direct* connection between them. This is a key point of [Nicosia *et al.*, 2013], and an example is Figure 16 (left), where there are many synchronous nodes but these are never adjacent.

An equally important extension of this concept is *phase synchrony*. Now the neurons have identical dynamics except for a specific time delay — generally a phase shift in a periodic state. A familiar example is locomotion [McGhee, 1968; Gambaryan, 1974], where the phase shifts are visible in the timing of limb and muscle movements in a gait cycle. In the human walk, there is a half-period phase shift between left and right legs. Quadrupeds use several distinct gait patterns, such as the walk/trot/canter/gallop of the horse; all of these patterns display characteristic phase shifts, as in Figure 4. The same goes for traveling waves of

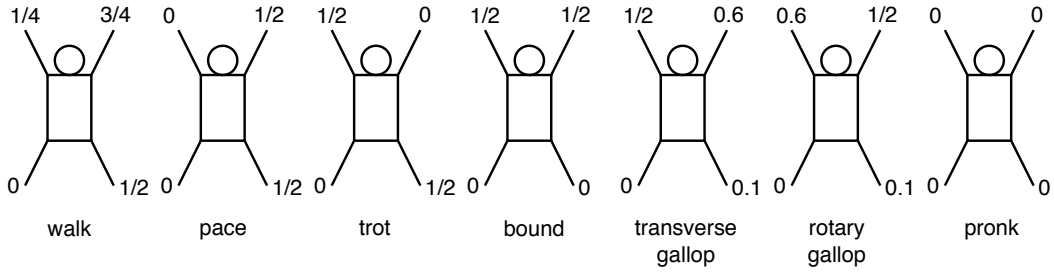

Fig. 4. Phase patterns in common quadruped gaits. Animal viewed from above. Numbers indicate fraction of gait period at which leg hits ground.

leg movements in arthropods, such as centipedes and millipedes, and for peristaltic waves in general, such as the locomotion of *Drosophila* larvae [Gjorgjieva *et al.*, 2013], the curious patterns in the heart chambers of *Hirudo medicinalis* [Calabrese & Peterson, 1983; Olsen & Calabrese, 1996], and, indeed, peristalsis in the intestine [Furness, 2008].

4.1. *Symmetry Induces Synchrony and Phase Patterns*

One consequence of the theory of network dynamics is a rigorous sense in which phase synchrony is indicative of features of the wiring diagram of the neural circuitry that controls the relevant muscle groups. In particular, traveling waves are associated with linear chains of (almost identical) neurons, and cyclically repeated phase shifts are associated with closed rings having cyclic group symmetry $\mathbb{Z}_k$, [Buono & Golubitsky, 2001; Golubitsky & Stewart, 2002]. Many theoretical studies illustrate this connection using numerical solutions of model equations, for example [Kopell & Ermentrout, 1986, 1988, 1990; Kopell, 1988; Kopell & LeMasson, 1994]. A systematic mathematical framework for network dynamics [Stewart *et al.*, 2003; Golubitsky *et al.*, 2005] provides a rigorous foundation for this observed relation between form (circuit diagram) and function (dynamic behaviour). However, it also reveals some subtleties that challenge naive intuition and require a more nuanced view of the links between synchrony and causality.

Fig. 5. *Left*: The metabolator network. *Right*: The Smolen oscillator network. Sharp arrowhead: excitation/activation. Barred arrowhead: inhibition/repression.

A common cause of synchronous dynamics is symmetry. The usual mathematical definition of symmetry is a transformation that preserves structure. A *symmetry* of a network is a permutation of its nodes that preserves the connections between them: see Section 6 for details. A simple example is Figure 5 (left), known as a *metabolator* in gene regulatory networks [Purcell *et al.*, 2010]. Here, swapping nodes 1 and 2 preserves the two types of arrow (directed edge). In biological contexts these two types of arrow are identified with excitation/activation and inhibition/repression. Each node receives one inhibitory/activator arrow from itself (self-regulation) and one excitatory/repressor arrow from the other node. For present purposes the key feature is that the arrows have different types, and each node receives one input of each type.

In the formal theory, every network diagram defines a class of *admissible* differential equations (ODEs) that respects the network architecture. Any more specific model, based on standard functional forms for the equations, is a special case of such ODEs. This remark applies both to models that closely parallel reality, and to standard 'toy' models (such as phase oscillators) that are default choices, chosen for convenience and familiarity.

The metabolator diagram is symmetric under interchange of the two nodes. It leads to admissible ODEs of the form

$$\begin{aligned} \dot{x}_1 &= f(x_1, x_1, x_2) \\ \dot{x}_2 &= f(x_2, x_2, x_1) \end{aligned} \tag{1}$$

where the function f is arbitrary. The same f occurs in both components, and swapping indices 1 and 2 converts the first equation into the second, so the symmetry of the network shows up in the admissible ODEs. So does the connectivity: there is one variable for the node (by convention, the first) and one at the tail of each arrow. Self-loops and multiple arrows are permitted and have their own variables, so the same variable may appear more than once.

Nodes 1 and 2 are (exactly) synchronous if they have the same dynamics; that is, if $x_1(t) = x_2(t)$ for all times t. Setting both equal to $y(t)$ the two equations become

$$\begin{aligned} \dot{y} &= f(y, y, y) \\ \dot{y} &= f(y, y, y) \end{aligned} \tag{2}$$

This repeats the ODE for y twice, which is fortunate, because any difference between these two equations would lead to a contradiction, indicating that no synchronous state exists. Thus any solution of the common equation $\dot{y} = f(y, y, y)$ corresponds to a synchronous solution $(y(t), y(t))$ of (1), and *vice versa*.

Remark 4.1.

(a) It is not quite true that *any* difference between these two equations would lead to a contradiction. Formally different equations might, by accident or design, agree on the solution $y(t)$. See [Stewart & Parker, 2007, Section 7] and Section 8 for an explanation of why in practice this caveat does not allow other kinds of synchrony in any practical manner.

(b) A synchronous solution need not be stable, even when it exists. A *synchrony-breaking* perturbation is one that destroys the synchrony, by making $x_1(t)$ and $x_2(t)$ slightly different. If this perturbation grows, the synchronous state is unstable.

More generally, the same kind of discussion shows that in a symmetric network, nodes can synchronize provided they lie in the same orbit of the symmetry group; that is, some symmetry maps one node to the other. Thus symmetry is *sufficient* for (stable or unstable) synchrony.

4.2. *Symmetry is Not Necessary for Synchrony*

A general question now arises: is symmetry *necessary* for synchrony? It was this question that motivated formulating a general theory of network dynamics, because the answer is 'no'. Consider Figure 5 (right), known as a *Smolen oscillator* in gene regulatory networks [Smolen *et al.*, 1998]. This network is not symmetric: swapping nodes 1 and 2 changes arrows from excitatory to inhibitory, and conversely, which would have a substantial effect on the dynamics.

A modeling issue (to which we return in Example 5.4) must now be decided. Namely: whether nodes 1 and 2 are assumed to have the same node type, or a different node type. From a general network point of view, it is reasonable to assign them the same node type, in which case nodes 1 and 2 are input-isomorphic and admissible ODEs have the form

$$\begin{aligned} \dot{x}_1 &= f(x_1, x_1, x_2) \\ \dot{x}_2 &= f(x_2, x_1, x_2) \end{aligned} \tag{3}$$

Again the same function f occurs in both components, but now, swapping indices 1 and 2 does not convert the first equation into the second. Nodes 1 and 2 are synchronous if $x_1(t) = x_2(t)$ for all times t. Setting both equal to $y(t)$ the two equations once more reduce to (2), and any solution of the common equation $\dot{y} = f(y, y, y)$ corresponds to a synchronous solution $(y(t), y(t))$ of (1), and *vice versa*.

On the other hand, we assign different node types to nodes 1 and 2, then nodes 1 and 2 are not input-isomorphic and admissible ODEs have the form

$$\begin{aligned} \dot{x}_1 &= f(x_1, x_1, x_2) \\ \dot{x}_2 &= g(x_2, x_1, x_2) \end{aligned} \tag{4}$$

Generically, there is no synchronous state, so the dynamics is different.

Remark 4.2. The Smolen oscillator occurs in GRN models, and the above distinction depends on the type of model. In some phenomenological models, all nodes are assumed to have the same internal dynamics,

in which case equation (3) is appropriate. However, this assumption is not always realistic, because in neuronal networks a given node either has only activator output arrows, or only inhibitor output arrows. In vertebrates, the type of neuron is determined by the transmitter that it releases. For excitatory neurons the transmitter is glutamate; for inhibitory neurons its is γ-amino-butyric acid (GABA). However, in insects GABA can be either excitatory or inhibitory [Ffrench-Constant *et al.*, 1993].

This suggests that the internal dynamic of an activator node is different from that of an inhibitor node, so such nodes should not be node-equivalent. Both choices are of mathematical interest.

The existence of synchronous states for equation (3) is governed by a more general notion of symmetry. The terminology in this case differs among different areas of research, where the concept arose independently: it is known as a *fibration symmetry*, a *balanced coloring*, or an *input symmetry*, see Section 6. The crucial property here is that when certain nodes are required to have identical dynamics (synchrony) the entire system of admissible ODEs leads to a *consistent* set of equations for the synchrony classes (also called *clusters* [Belykh & Hasler, 2011; Pecora *et al.*, 2013] or *partial synchrony* [Pogromsky, 2008]).

If the functions f in (1) and (3) are the same, then the ODE (2) for synchronous states is the same for both networks. The difference shows up when synchrony is broken, both in the dynamic behaviour and in the stability of states, including stability of the synchronous state to synchrony-breaking perturbations.

The relation of symmetry to phase patterns is subtler. Networks with trivial symmetry can exhibit nontrivial phase patterns in a structurally stable (technically: 'rigid') manner. Therefore symmetry of the network is not necessary for phase patterns to occur. However, assuming a highly plausible conjecture, and some technical conditions on network topology (such as transitivity), generic phase patterns are determined by a cyclic group of symmetries of the *quotient network* by the relation of synchrony. See Section 8. In this sense, symmetry is necessary and sufficient for phase synchrony.

5. Equivariant Dynamics

The network formalism of [Stewart *et al.*, 2003; Golubitsky *et al.*, 2005; Golubitsky & Stewart, 2023] is modeled on analogies with equivariant dynamics [Vanderbauwhede, 1980; Cigogna, 1981; Dancer, 1980, 1983; Golubitsky *et al.*, 1988; Olver, 1993; Golubitsky & Stewart, 2002]. Equivariant dynamics examines how the symmetries of a differential equation affect the behavior of its solutions, especially their own symmetries, which may differ from those of the equation. We summarize some of the basics. We focus on ODEs, although many ideas carry over to PDEs and to discrete dynamical systems (iterated maps).

For simplicity, assume that the state space of the system is $X = \mathbb{R}^n$ and consider an ODE

$$\dot{x} = f(x) \qquad x \in X \tag{5}$$

where $f : X \to X$ is smooth (infinitely differentiable, C^∞). Symmetries enter the picture when a group of linear transformations Γ acts on X. We require all elements of Γ to map solutions of the ODE to solutions. By [Golubitsky & Stewart, 2002, Section 1.2] this is equivalent to f being Γ-*equivariant*; that is:

$$f(\gamma x) = \gamma f(x) \tag{6}$$

for all $\gamma \in \Gamma, x \in X$. The proof is a simple application of uniqueness of solutions for given initial conditions. We call (5) a Γ-*equivariant ODE*.

The *group orbit* of a point x is $\Gamma x = \{\gamma x : \gamma \in \Gamma\}$. Equivariance implies that whenever $x(t)$ is a solution, so is any $\gamma x(t)$ in the group orbit $\Gamma x(t)$. That is, solutions come in group orbits. This is where the symmetry of the ODE 'goes to' when solutions break symmetry spontaneously: the group orbit remains symmetric but the symmetry is distributed over the entire orbit instead of being concentrated at one solution. Condition 6 captures the structure of ODEs that arise when modeling a symmetric real-world system. It states that the map f inherits the symmetries of the system, in the sense that symmetrically related points in state space have symmetrically related tangent vectors to the flow of the ODE.

5.1. *Isotropy Subgroups and Fixed-Point Subspaces*

We remarked above that the symmetries of a solution may differ from the symmetries of the equation. We now explain how this can happen and formalize the resulting structure.

First, suppose that an equilibrium x_0 is *unique*. Then $\gamma x_0 = x_0$ for all $\gamma \in \Gamma$, so the solution is symmetric under Γ. However, when uniqueness fails — which is common in nonlinear dynamics — equilibria of a Γ-equivariant ODE need not be symmetric under the whole of Γ. This phenomenon, called *(spontaneous) symmetry-breaking*, is a general mechanism for pattern formation, and occurs for more complex dynamics than just an equilibrium.

To formalize 'symmetry of a solution' we introduce a key concept:

Definition 5.1. If $x \in X$, the *isotropy subgroup* of x is

$$\Sigma_x = \{\sigma \in \Gamma : \sigma x = x\}$$

This group consists of all σ that fix x. There is also a dual notion: if $\Sigma \subseteq \Gamma$ is a subgroup of Γ, its *fixed-point subspace* is

$$\mathrm{Fix}(\Sigma) = \{x \in X : \sigma x = x \quad \forall \sigma \in \Sigma\}$$

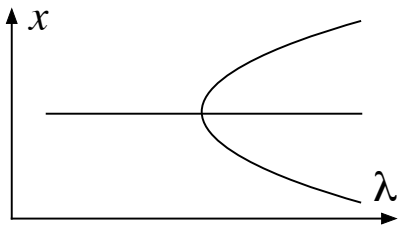

Fig. 6. Pitchfork bifurcation. The diagram shows how equilibrium values of x depend on the parameter λ.

Example 5.1. A simple example is the *pitchfork* bifurcation, Figure 6, given by the equilibria of the family of ('normal form') ODEs

$$\dot{x} = f(x, \lambda) = \lambda x - x^3$$

The function f is equivariant for the group $\Gamma = \mathbb{Z}_2$ acting by $x \mapsto -x$. Equilibria are given by $x = 0$ and $x^2 = \lambda$. The latter give nonzero solutions $x = \pm\sqrt{\lambda}$ only for $\lambda > 0$. The isotropy subgroup of 0 is $\mathbb{Z}_2$, but that of $\sqrt{\lambda}$ and $-\sqrt{\lambda}$ is the trivial subgroup $\mathbf{1}$.

The zero solution is stable for $\lambda < 0$ but unstable for $\lambda > 0$. The solutions $\pm\sqrt{\lambda}$ are stable, but exist only for $\lambda > 0$. In the terminology of bifurcation theory, the trivial branch of equilibria at $x = 0$ *loses stability* as the bifurcation parameter λ passes through 0, and two new branches of stable equilibria appear. Although individual equilibria lose the $\mathbb{Z}_2$ symmetry, the set of *all* equilibria retains $\mathbb{Z}_2$ symmetry.

A simple 'real-world' example of pichfork bifurcation is a vertical rod in the plane, held up by a spring, buckling under a vertical load λ. As λ increases through a critical value, the vertical state ceases to be stable and the rod buckles either to left or right. Another is Euler buckling of a horizontal rod in the plane under a symmetrically placed load, [Zeeman, 1977, Chapter 16] or [Poston & Stewart, 1978, Chapter 13].

Clearly $\mathrm{Fix}(\Sigma)$ comprises all points $x \in X$ whose isotropy subgroup contains Σ. Fixed-point spaces play a central role in equivariant dynamics because they have an important property: they provide a natural class of subspaces that are invariant for any Γ-equivariant map f:

Proposition 1. *Let $f : X \to X$ be a Γ-equivariant map, and let Σ be any subgroup of Γ. Then $\mathrm{Fix}(\Sigma)$ is an invariant subspace for f, and hence for the dynamics of (5).*

The proof is so simple that we give it here:

Proof. If $x \in \mathrm{Fix}(\Sigma)$ and $\sigma \in \Sigma$ then $\sigma f(x) = f(\sigma x) = f(x)$, so $f(x) \in \mathrm{Fix}(\Sigma)$. ■

We can interpret $\mathrm{Fix}(\Sigma)$ as the space of all states that have symmetry (at least) Σ. Then the restriction $f|_{\mathrm{Fix}(\Sigma)}$ determines the dynamics of all such states. In particular, we can find states with a given isotropy subgroup Σ by considering the (usually) lower-dimensional system determined by $f|_{\mathrm{Fix}(\Sigma)}$.

If $x \in X$ and $\gamma \in \Gamma$, the isotropy subgroup of γx is conjugate to that of x:

$$\Sigma_{\gamma x} = \gamma \Sigma_x \gamma^{-1}$$

Therefore isotropy subgroups occur in conjugacy classes, which correspond to group orbits of the solutions. Thus for many purposes we can consider isotropy subgroups only up to conjugacy. The conjugacy classes of isotropy subgroups are ordered by inclusion. The resulting partially ordered set is called the *lattice of isotropy subgroups* or *isotropy lattice* [Golubitsky *et al.*, 1988], although technically it need not satisfy all lattice axioms [Davey & Priestley, 1990]. If we do not pass to conjugacy classes, it is a genuine lattice. It classifies possible sequences of successive symmetry-breaking bifurcations.

5.2. *Symmetry-Breaking Bifurcation*

Consider a 1-parameter family of maps $f : \mathbb{R}^n \times \mathbb{R} \to \mathbb{R}^n$, where λ is a bifurcation parameter, satisfying the equivariance condition

$$f(\gamma x, \lambda) = \gamma f(x, \lambda) \tag{7}$$

for all $x \in \mathbb{R}^n, \lambda \in \mathbb{R}$. (Here Γ acts trivially on λ.) There is a corresponding family of ODEs:

$$\dot{x} = f(x, \lambda) \tag{8}$$

Suppose that $\{(x(\lambda), \lambda)\}$ is a branch of equilibria parametrized by λ. By the Implicit Function Theorem, a necessary condition for the occurrence of local bifurcation from a branch of equilibria at (x_0, λ_0) is that the Jacobian $J = \mathrm{D}f|_{x_0,\lambda_0}$ should have eigenvalues on the imaginary axis (including 0) [Iooss & Joseph, 1990]. A zero eigenvalue usually corresponds to steady-state bifurcation: typically, the number of equilibria changes near (x_0, λ_0), and branches of equilibria may appear, disappear, merge, or split. The possibilities here can be organized, recognized, and classified using singularity theory [Golubitsky & Schaeffer, 1985]. A nonzero imaginary eigenvalue $\mathrm{i}\omega$ (which occurs together with its complex conjugate $-\mathrm{i}\omega$) usually corresponds to Hopf bifurcation [Hassard *et al.*, 1981]. Under suitable genericity conditions this leads to periodic solutions whose amplitude (near the bifurcation point) is small, and whose period tends to $2\pi/\omega$ near the bifurcation point. In either case the corresponding eigenspace is said to be *critical*. Generically, it is an absolutely irreducible representation of Γ, that is, the representation is irreducible and all commuting linear maps are real multiples of the identity [Golubitsky *et al.*, 1988, Chapter XIII Proposition 3.2].

The main existence theorem for steady-state local bifurcation in equivariant dynamics [Vanderbauwhede, 1980; Cigogna, 1981] guarantees the generic existence of branches for *axial* subgroups $\Sigma \subseteq \Gamma$: those with $\dim(E_0 \cap \mathrm{Fix}(\Sigma)) = 1$ where E_0 is the critical eigenspace. It states:

Theorem 1 [Equivariant Branching Lemma]. *Suppose that E_0 is a nontrivial absolutely irreducible representation of Γ acting on $\mathbb{R}^n$ and that $\Sigma \subset \Gamma$ is an axial subgroup of Γ acting on E_0. Then generically there exists a unique branch of equilibria to* (8) *whose symmetries are Σ. Moreover, generically, each branch is either transcritical or pitchfork.*

One technical issue requires mention. Ihrig's Theorem ([Ihrig & Golubitsky, 1984, Theorem 4.2] or [Golubitsky *et al.*, 1988, Theorem XIII.4.4]) states that, subject to mild technical conditions, the existence of a non-zero quadratic equivariant on the critical eigenspace implies that all branches obtained from the Equivariant Branching Lemma are linearly unstable near the bifurcation point. It might seem that this renders such branches useless, but it is common for such branches to regain stability through a further bifurcation. This can be achieved by 'turning round' at a saddle-node point, or though an intersection with a secondary branch. See [Cohen & Stewart, 2000; Stewart *et al.*, 2003] for discussions of this issue in models of sympatric speciation.

5.3. *Equivariant Hopf Theorem*

We now discuss the other generic type of local bifurcation: Hopf bifurcation. This is a fundamental bifurcation process in general dynamical systems [Hassard *et al.*, 1981; Guckenheimer & Holmes, 1983], in which a stable equilibrium loses stability and throws off a limit cycle. The main condition for Hopf bifurcation is that the Jacobian $\mathrm{D}f$ has nonzero imaginary eigenvalues $\pm \mathrm{i}\omega$ at some value $\lambda = \lambda_0$, referred to as *critical eigenvalues*. Some technical conditions are also needed: the critical eigenvalues must be simple, there should be no resonances, and the critical eigenvalues should cross the imaginary axis with nonzero speed.

These conditions are generic in dynamical systems without symmetry. Non-resonance (other than 1:1 resonance which arises for multiple eigenvalues) and the eigenvalue crossing condition are also generic in symmetric systems, but simplicity of the critical eigenvalues is usually not, so the standard Hopf Bifurcation Theorem does not apply. However, there is a version adapted to symmetric systems, involving phase shift symmetries. A phase shift can be viewed as time translation modulo the period T, leading to an action of the *circle group* $\mathbb{S}^1 = \mathbb{R}/\mathbb{Z}$ for which $\theta \in \mathbb{S}^1$ translates time by θT.

At a non-zero imaginary critical eigenvalue, the critical eigenspace E supports an action not just of Γ, but of $\Gamma \times \mathbb{S}^1$. The $\mathbb{S}^1$-action is related to, but different from, the phase shift action; it is determined by the exponential of the Jacobian $J|_E$ on E. Specifically, if the imaginary eigenvalues are $\pm \mathrm{i}\omega$, then $\theta \in \mathbb{S}^1$ acts on E like the matrix $\exp(\frac{2\pi\theta}{\omega} J|_E)$.

The Equivariant Hopf Theorem is analogous to the Equivariant Branching Lemma, but the symmetry group Γ is replaced by $\Gamma \times \mathbb{S}^1$. A subgroup $\Sigma \subset \Gamma \times \mathbb{S}^1$ is $\mathbb{C}$-*axial* if Σ is an isotropy subgroup of the action of $\Gamma \times \mathbb{S}^1$ on E and $\dim_{\mathbb{R}}(E_{\pm \mathrm{i}\omega} \cap \mathrm{Fix}(\Sigma)) = 2$, where $E_{\pm \mathrm{i}\omega}$ is the critical eigenspace.

Theorem 2 [**Equivariant Hopf Theorem**]. *If the Jacobian has non-real purely imaginary eigenvalues, then generically for any* $\mathbb{C}$*-axial subgroup* $\Sigma \subseteq \Gamma \times \mathbb{S}^1$ *acting on* $E_{\pm \mathrm{i}\omega}$*, there exists a branch of periodic solutions with spatiotemporal symmetry group* Σ*. On these solutions,* $\mathbb{S}^1$ *acts by phase shifts.*

Proof. See [Golubitsky & Stewart, 1985, Theorem 5.1], [Golubitsky *et al.*, 1988, Chapter XVI Theorem 4.1], or [Golubitsky & Stewart, 2002, Theorem 4.9]. ■

The proof adapts an idea of [Hale, 1993], which reformulates Hopf bifurcation in terms of *loop space*, the Banach space of all maps $\mathbb{S}^1 \to X$ (with both C^1 and C^0 norms occurring in the proof). The group $\mathbb{S}^1$ acts on loop space by time translation (scaled by the period). Periodic solutions of an ODE correspond to zeros in loop space of an associated nonlinear operator. The technique of Liapunov–Schmidt reduction [Golubitsky *et al.*, 1988] converts this problem into finding the zero-set of a *reduced function* on the critical eigenspace. If the original ODE has symmetry group Γ, the reduced function has symmetry group $\Gamma \times \mathbb{S}^1$.

[Golubitsky & Langford, 1981] use the same technique to reduce the analysis of *degenerate* Hopf bifurcations (not satisfying the eigenvalue crossing condition) to the classification of $\mathbb{Z}_2$-equivariant singularities.

Again, there are representation-theoretic conditions on the critical eigenspace [Golubitsky *et al.*, 1988, Chapter XVI Proposition 1.4]. Generically, it is either non-absolutely irreducible, or a direct sum of two copies of the same absolutely irreducible representation.

5.4. *Examples of Hopf Bifurcation in Networks*

We consider Hopf bifurcation in the two networks of Figure 5, in the case where the steady state is synchronous for all λ, so we can write the equilibrium of (1) and (3) as $(x(\lambda), x(\lambda))$ where $x(\lambda) = x_1(\lambda) = x_2(\lambda)$. Hopf bifurcation can occur only when the state space $\mathbb{R}^k$ of each node is at least 2-dimensional ($k \geq 2$).

Example 5.2. At a synchronous state (x, x, x), the $\mathbb{Z}_2$-symmetric metabolator network of Figure 5 (left) has Jacobian

$$J = \begin{bmatrix} A+B & C \\ C & A+B \end{bmatrix} \quad \text{where} \quad A = \partial_1 f|_{(x,x,x)}\ B = \partial_2 f|_{(x,x,x)}\ C = \partial_3 f|_{(x,x,x)}$$

where ∂_j indicates the partial derivative with respect to the jth variable. (Technically, the relevant point is (x, x, x), because f and g are functions of three variables, albeit with some repeated).

Because of the $\mathbb{Z}_2$ symmetry, J leaves invariant two subspaces

$$U_0 = \left\{ \begin{bmatrix} u \\ u \end{bmatrix} \right\} \qquad U_1 = \left\{ \begin{bmatrix} u \\ -u \end{bmatrix} \right\}$$

where $u \in \mathbb{R}^k$, the state space of a node. The overall state space is $\mathbb{R}^k \oplus \mathbb{R}^k = U_0 \oplus U_1$. Therefore the eigenvectors of J are obtained by setting u to the eigenvectors of $A + B + C$ and $A + B - C$, with corresponding eigenvalues.

There are thus two cases. A *symmetry-preserving* (also *synchrony-preserving*) Hopf bifurcation occurs at a pair of purely imaginary eigenvalues of $A + B + C$. In the resulting oscillatory state, nodes 1 and 2 oscillate in exact synchrony. A *symmetry-breaking* (also *synchrony-breaking*) Hopf bifurcation occurs at a pair of purely imaginary eigenvalues of $A+B-C$. In the resulting oscillatory state, nodes 1 and 2 oscillate half a period out of phase with each other, so there is phase synchrony with phase shift half a period.

Example 5.3.

Recall Remark 4.2, concerning two choices for the node types in the asymmetric Smolen oscillator network of Figure 5 (right). This network closely resembles the metabolator, but its behavior is different — for either choice of node types. In particular, its symmetry group is trivial. Despite this, it has synchronous states satisfying (2), by Section 4.2. Instead of symmetry-breaking bifurcations, we look for synchrony-breaking ones.

First, assume that the two nodes have the same node type, so admissible ODEs have the form (3). There exists a synchronous equilibrium (x, x, x) where $x = x_1(\lambda) = x_2(\lambda)$. At this equilibrium the Jacobian for the Smolen oscillator is very similar to that for the metabolator:

$$J = \begin{bmatrix} A+C & B \\ C & A+B \end{bmatrix} \quad \text{where} \quad A = \partial_1 f|_{(x,x,x)}\ B = \partial_2 f|_{(x,x,x)}\ C = \partial_3 f|_{(x,x,x)}$$

It is still the case that J leaves invariant the subspace U_0, on which it acts like $A+B+C$. The corresponding eigenvectors of J are obtained by setting u to the eigenvectors of $A+B+C$, with corresponding eigenvalues. When eigenvalues are purely imaginary, this case leads to synchrony-preserving Hopf bifurcation, and nodes 1 and 2 oscillate in exact synchrony.

However, J does not leave U_1 invariant. To find the eigenvalues and eigenvectors for the synchrony-breaking case, we must solve the equation

$$\begin{bmatrix} A+C & B \\ C & A+B \end{bmatrix} \begin{bmatrix} u \\ v \end{bmatrix} = \lambda \begin{bmatrix} u \\ v \end{bmatrix}$$

That is, the pair of equations

$$(A+C)u + Bv = \lambda u \qquad Cu + (A+B)v = \lambda v$$

Subtracting, we obtain $A(u-v) = \lambda(u-v)$. So either $u - v = 0$ or λ is an eigenvalue of A with eigenvector $w = u - v$.

If $u = v$ we have the synchrony-preserving case. Otherwise, $u \neq v$ and $v = u - w$, where w is an eigenvector of A with eigenvalue λ. Since $Aw = \lambda w$, the second equation leads to

$$\begin{aligned} Cu + (A+B)(u-w) &= \lambda(u-w) \\ Cu + Au - Aw + Bu - Bw &= \lambda u - \lambda w \\ (A+B+C)u - \lambda u &= Bw \\ u &= (A+B+C-\lambda I)^{-1} Bw \end{aligned}$$

assuming $A + B + C - \lambda I$ is invertible, which it is provided λ is not an eigenvalue of $A + B + C$, a generic condition.

Now there is no fixed phase relation between the two nodes. Indeed, they need not have the same waveform, so they need not be (and generically are not) phase-synchronous. Even when the waveforms are the same, suitable choices of f, hence of A, B, C, presumably give any specific phase shift, though we have not verified this in detail. (It is easy to see that the amplitudes of the two nodes can be different.)

Example 5.4. Again we consider the Smolen oscillator, but now we assume the two nodes have different types, so admissible ODEs are of the form (4). Now the Jacobian has the form

$$J = \begin{bmatrix} A + C & B \\ C' & A' + B' \end{bmatrix}$$

where A, B, C are the three partial derivatives of f and A', B', C' are the three partial derivatives of g, evaluated at an equilibrium. Now there is no invariant synchrony subspace. The Jacobian is an arbitrary 2×2 matrix (subject to signs assigned to excitatory and inhibitory arrows). We still expect both steady-state and Hopf bifurcation to be possible, but the distinction between synchrony-preserving and synchrony-breaking bifurcations is no longer meaningful since there is no synchrony to break or preserve.

The main point here is that in the symmetric case of Example 5.2, symmetry imposes strong constraints, leading to phase synchrony in oscillations with phase shifts either zero or half a period. In the asymmetric case of Example 5.3, synchronous oscillatory states can still occur, for suitable f, but Hopf bifurcation leads either to synchronous oscillations or oscillations in which the two nodes generically have different waveforms, with no universal constraints on phase shifts, if these even make sense.

In contrast, Example 5.4 does not have robust synchronous states, whether steady or oscillatory.

Thus network architecture has a strong influence on dynamics and bifurcations. In order to understand when synchronous states are possible and how they arise, it is necessary to understand this relation to the network architecture.

5.4.1. *Simulations*

We illustrate the above statements in a neurobiology context with simulations of networks of two voltage-coupled FitzHugh–Nagumo neurons [FitzHugh, 1961; Nagumo *et al.*, 1962; Murray, 1989]. For Example 5.2, we use model equations

$$\begin{aligned} \dot{v}_1 &= v_1(a - v_1)(v_1 - 1) - w_1 + cv_1 + dv_2 \\ \dot{w}_1 &= bv_1 - gw_1 \\ \dot{v}_2 &= v_2(a - v_2)(v_2 - 1) - w_2 + cv_2 + dv_1 \\ \dot{w}_2 &= bv_2 - gw_2 \end{aligned}$$

Here v_i is the membrane potential at node i, the variable w_i represents the combined effect of sodium, potassium, and leakage currents at node i, and $a, b, c, d, g \in \mathbb{R}$ are parameters.

Figure 7 shows time series for v_1, v_2, and their superposition for parameter values that lead to synchronous oscillations. Figure 8 shows time series for v_1, v_2, and their superposition for parameter values that lead to oscillations with half-period phase shift. (In the first figure the 'inhibitory' connection has been made excitatory, but with a different strength, in order to create synchrony.)

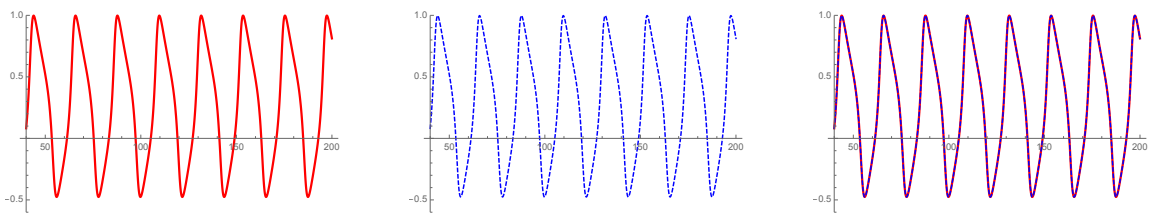

Fig. 7. Synchrony in metabolator network: $a = -.3, b = 0.3, c = -0.1, d = 0.5, g = 0.4$. *Left*: Node 1. *Middle*: Node 2. *Right*: Both nodes superposed.

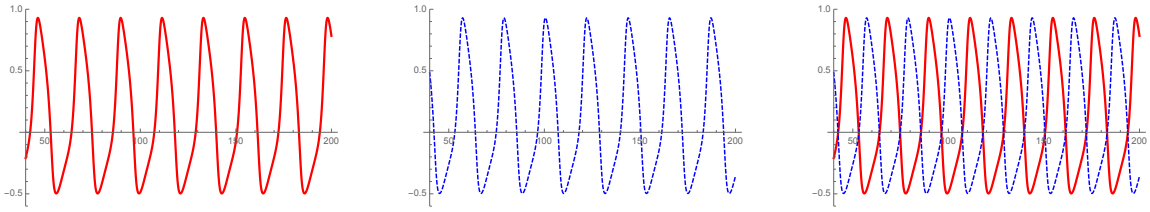

Fig. 8. Half-period phase shift in metabolator network: $a = -.3, b = 0.3, c = 0.2, d = -0.2, g = 0.4$. *Left*: Node 1. *Middle*: Node 2. *Right*: Both nodes superposed.

For Example 5.3, we use model equations with similar variables and parameters:

$$\begin{aligned}
\dot{v}_1 &= v_1(a - v_1)(v_1 - 1) - w_1 + cv_2 + dv_1 \\
\dot{w}_1 &= bv_1 - gw_1 \\
\dot{v}_2 &= v_2(a - v_2)(v_2 - 1) - w_2 + cv_2 + dv_1 \\
\dot{w}_2 &= bv_2 - gw_2
\end{aligned}$$

Figure 9 shows time series for v_1, v_2, and their superposition for parameter values that lead to synchronous oscillations. Figure 10 shows time series for v_1, v_2, and their superposition for parameter values that lead to asynchronous oscillations with different amplitudes (hence different waveforms).

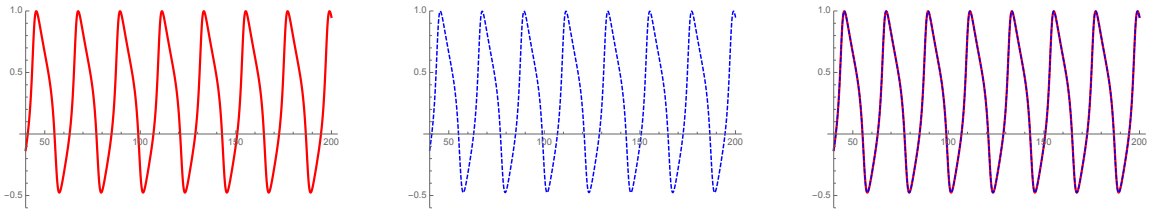

Fig. 9. Synchrony in Smolen oscillator network: $a = -.5, b = 0.3, c = -0.1, d = 0.5, g = 0.4$. *Left*: Node 1. *Middle*: Node 2. *Right*: Both nodes superposed.

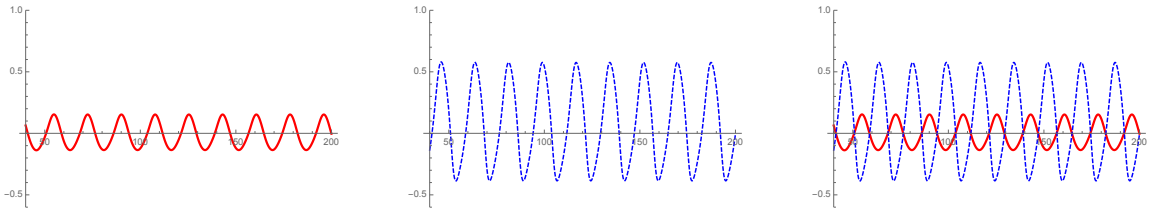

Fig. 10. Distinct waveforms in Smolen oscillator network: $a = -.5, b = 0.3, c = -0.1, d = -0.4, g = 0.4$. *Left*: Node 1. *Middle*: Node 2. *Right*: Both nodes superposed.

6. Networks, Dynamics, Synchrony, and Bifurcations

The formal theory of network dynamics that we describe was introduced in [Stewart *et al.*, 2003], improved in [Golubitsky *et al.*, 2005], and is surveyed in detail in the monograph [Golubitsky & Stewart, 2023]. These sources should be consulted for further information and any terminology not defined here. This formalism represents the network as a labeled directed graph. Nodes (often called 'cells', a term that we avoid because of possible confusion with biological cells) represent individual dynamical systems (ODEs) and arrows (directed edges) represent couplings between them. The output node is at the tail of the arrow and the input node is at the head. Nodes, and arrows, are partitioned into *types*. Nodes of the same type have the same internal dynamic, and arrows of the same type represent the same kind of coupling. Node

types are shown in network diagrams using symbols of distinct shapes (circle, square, triangle ...), and arrow types using distinct arrow symbols (solid/open head, solid/dotted line ...).

Two nodes are *input-isomorphic* if they have the same node type and the same number of arrows of each type as inputs. Associated with each node $c = 1, 2, \ldots, n$ is a *node variable* $x_c \in P_c$, where the *node space* P_c is usually taken to be a real vector space $\mathbb{R}^k$, where k can depend on c. Each diagram determines a class of *admissible ODEs* of the form

$$\begin{aligned} \dot{x}_1 &= f_1(x_1, x_{T(1)}) \\ \dot{x}_2 &= f_2(x_2, x_{T(2)}) \\ &\vdots \\ \dot{x}_n &= f_n(x_n, x_{T(n)}) \end{aligned}$$

where $T(c)$ denotes the tuple of tail node variables:

$$T(c) = (x_{i_1}, \ldots, x_{i_{m(c)}})$$

where $m(c)$ is the number of inputs to node c, and the tail nodes of those inputs are $i_1, \ldots, i_{m(c)}$. Moreover, we require $f_c = f_d$ whenever c and d are input-isomorphic, provided that the variables $x_{T(c)}$ and $x_{T(d)}$ are listed in *standard order*. That is, they are collected in blocks according to arrow-type, and the arrow-types are ordered in the same way for all nodes. (A coordinate-free description can be stated in terms of pullback maps.)

Example 6.1. Consider the 5-node network of Figure 11 (left), illustrating the simplest case where there is one node-type and one arrow-type. All five nodes are input-isomorphic. The admissible maps are those of the form

$$\begin{aligned} \dot{x}_1 &= f(x_1, \overline{x_2, x_5}) \\ \dot{x}_2 &= f(x_2, \overline{x_3, x_5}) \\ \dot{x}_3 &= f(x_3, \overline{x_4, x_5}) \\ \dot{x}_4 &= f(x_4, \overline{x_1, x_5}) \\ \dot{x}_5 &= f(x_5, \overline{x_1, x_2}) \end{aligned} \tag{9}$$

Here the first variable in each component is the node variable, and the second and third variable correspond to the tail nodes of the input arrows. The overline indicates that f is symmetric under interchange of the two variables concerned. (In effect, we assume that a node does not 'know' which nodes its inputs come from, only what these inputs are dynamically.)

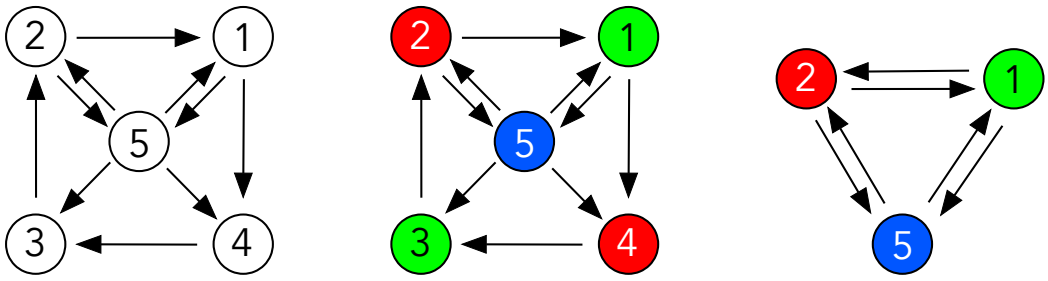

Fig. 11. *Left*: Five-node network. *Middle*: Coloring representing a synchrony pattern. *Right*: Quotient network is a 3-node bidirectional ring.

The same network illustrates several important features of synchrony patterns:

Example 6.2. Assume that the state space for the network of Figure 11 (left) is $P = (\mathbb{R}^k)^5$ for some k. Fully synchronous states have the form

$$x(t) = (u(t), u(t), u(t), u(t), u(t))$$

All five components of (9) reduce to the same form

$$\dot{u} = f(u, u, u, u, u)$$

when we substitute $x_i = u$ for $1 \leq i \leq 5$, so fully synchronous states correspond precisely to solutions of this single ODE. More technically, the diagonal (u, u, u, u, u) is invariant under all admissible maps. Solutions inside this subspace are fully synchronous, with all five nodes behaving identically at all times.

All this may seem a complicated way to state the obvious, but the same reasoning applies to a more interesting synchrony pattern, in which the synchronous clusters are

$$\{1, 3\} \quad \{2, 4\} \quad \{5\}$$

Figure 11 (middle) shows this pattern using the colors green, red, blue. Synchronous nodes are assigned the same color. The corresponding synchrony subspace consists of those points $x \in P$ such that

$$x_1 = x_3 \quad x_2 = x_4$$

That is, the 'polydiagonal' subspace

$$\Delta = \{(x, y, x, y, z)\}$$

We can find solutions with this synchrony pattern using the restriction of (9) to Δ:

$$\begin{aligned} \dot{x} &= f(x, \overline{y, z}) \\ \dot{y} &= f(y, \overline{z, x}) \\ \dot{x} &= f(x, \overline{y, z}) \\ \dot{y} &= f(y, \overline{z, x}) \\ \dot{z} &= f(z, \overline{x, y}) \end{aligned} \tag{10}$$

The third equation is the same as the first, and the second is the same as the fourth. This establishes that Δ is invariant for any admissible map. Eliminating the repeats, we get an ODE in three variables:

$$\begin{aligned} \dot{x} &= f(x, \overline{y, z}) \\ \dot{y} &= f(y, \overline{z, x}) \\ \dot{z} &= f(z, \overline{x, y}) \end{aligned} \tag{11}$$

Solutions of this *restricted ODE* correspond precisely to states with this synchrony pattern.

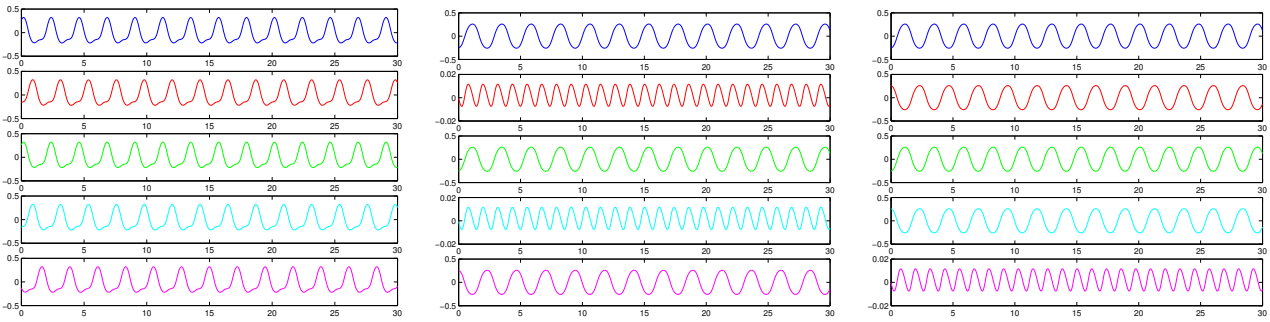

Fig. 12. Simulations of five-node network in Figure 11. Nodes 1–5 in sequence from top to bottom. *Left*: rotating wave. *Middle*: Double frequency in nodes 2 and 4. *Right*: Double frequency in node 5. [Golubitsky & Stewart, 2006].

As confirmation, Figure 12 shows numerical simulations of time-periodic states in this network. These confirm the existence of such patterns. (We do not specify the model equations since the diagrams are purely illustrative.)

These time series exemplify several generic phenomena, made possible by the network structure.

(a) *Left*: A discrete rotating wave with phase shifts $T/3$ from cluster $\{1, 3\}$ to cluster $\{2, 4\}$ and a further phase shift $T/3$ from cluster $\{2, 4\}$ to cluster $\{5\}$, where T is the period.

(b) *Middle*: Clusters $\{1, 3\}$ and $\{5\}$ oscillate with a phase difference of $T/2$. Cluster $\{2, 4\}$ oscillates with twice the frequency of the other clusters.

(c) *Right*: Clusters $\{1,3\}$ and $\{2,4\}$ oscillate with a phase difference of $T/2$. Cluster $\{5\}$ oscillates with twice the frequency of the other clusters.

The simulations show types (a) and (c), with different clusters oscillating with double frequency in (c). Other simulations produce fully synchronous oscillations and patterns of type (b). These simulations are striking, and initially surprising. They would not be surprising if the network were a bidirectional ring with $\mathbb{D}_3$ symmetry — the network of Figure 11 (right). By [Golubitsky & Stewart, 1986] this network typically has four types of periodic state created by Hopf bifurcation: fully synchronous oscillations, and oscillations of the three types (a, b, c) listed above. The explanation is that the equation (11) for the *clusters* happens to be $\mathbb{D}_3$-equivariant.

6.1. *Balanced Colorings*

These results suggest that in some sense a network with $\mathbb{D}_3$ symmetry is 'hidden' somewhere in the 5-node network when the stated synchrony pattern is imposed on the dynamics. To see how, we again look at the restricted ODE (11) on the synchrony subspace Δ.

The above calculation explains the $\mathbb{D}_3$-equivariant behavior, but the explanation rests on two apparent coincidences:

(a) The subspace Δ is invariant for all admissible maps.

(b) The restricted ODEs range precisely over the admissible ODEs for some specific network, whose nodes correspond to the synchronous clusters.

In fact, these features are a consequence of the network architecture and the specified synchrony pattern (coloring). There is a general construction along these lines, leading to the concept of a *quotient network*.

In the network corresponding to the synchronized clusters, each node receives a single input from each of the other two nodes, and these inputs come from arrows of the same type. The same thing happens in the 5-node network if we focus solely on the colors. Each green node receives a single input from a red node and a single input from a blue node, with identical arrow types. The nodes concerned are different for nodes 1 and 3, but they have the correct colors. Similarly each red node receives one input from a blue node and one input from a green node. Finally, the unique blue node receives one input from a red node and one input from a green node.

Since nodes of a given color are synchronized, the signal sent by any red node is identical to that sent by any other red node, and so on. Thus the entire construction works for combinatorial reasons, determined by which colors send signals to which colors. It then becomes possible to identify all nodes of a given color in a consistent, well-defined manner, preserving the ODE.

Such a coloring is said to be *balanced*. Specifically, a coloring of nodes is balanced if nodes of the same color have inputs that are color-isomorphic: there is an input isomorphism preserving the colors of the tail nodes of all input arrows. The key result is that a synchrony pattern determines a flow-invariant subspace if and only if the corresponding coloring is balanced, [Stewart *et al.*, 2003; Golubitsky *et al.*, 2005; Golubitsky & Stewart, 2023]. Such a synchrony pattern is said to be *robust*, because it exists for any admissible ODE.

Algorithms for computing balanced colorings have been developed by [Boldi & Vigna, 2002; Aldis, 2008; Belykh & Hasler, 2011; Kamei & Cock, 2013].

6.2. *Quotient Networks*

The construction of the 3-node network in Figure 11 (right) can be generalized. Given any balanced coloring $\bowtie$ of a network $\mathcal{G}$, the associated *quotient network* $\mathcal{G}_{\bowtie}$ is constructed as follows:

(a) The nodes correspond to the colors.

(b) The input arrows to any node are copied from the input arrows of any node of that color in the original network, preserving arrow-type, with tail nodes given by the color of the corresponding tail node in the original network.

It can then be proved that the admissible ODEs on the quotient network are the same as the restricted ODEs determined by admissible ODEs on the original network [Stewart *et al.*, 2003; Golubitsky *et al.*, 2005]. The quotient network therefore describes the dynamics of the clusters, induced by restriction from the dynamics of the original network.

The original network $\mathcal{G}$ is said to be a *lift* of the quotient network $\mathcal{G}_{\bowtie}$. Any a balanced coloring of $\mathcal{G}_{\bowtie}$ determines a balanced coloring of $\mathcal{G}$ in which nodes of $\mathcal{G}$ have the same color if their images in $\mathcal{G}_{\bowtie}$ have the same color. This coloring of $\mathcal{G}$ is also said to be a lift of the coloring of $\mathcal{G}_{\bowtie}$.

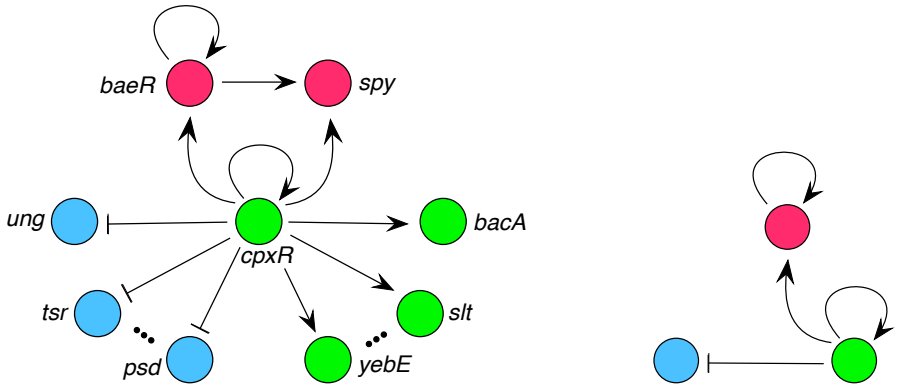

Fig. 13. *Left*: Circuit controlled by *cpxR* gene regulates a series of fibers shown by the colors. Dotted lines: other genes regulated by this circuit, omitted for simplicity. Pointed arrow: activator. Bar: repressor. *Right*: Corresponding quotient network.

Example 6.3. We illustrate the balance condition and the corresponding quotient network in a biological context: a real gene regulatory network. Figure 13 (left) shows a subcircuit of the *E. coli* transcriptional network, regulated by the gene *cpxR*. This circuit has self-regulation loops at *baeR* and *cpxR*. The coloring shown is balanced, thanks to the self-loop at *cpxR*.

Specifically: every red node receives two red inputs and one green input, all activators; every green node receives one green input, also activators; every blue node receives one green input, which is a repressor. Thus nodes of the same color are input-isomorphic by an isomorphism that preserves the types of arrows and the colors of their tail nodes.

The corresponding quotient network, Figure 13 (right), has one node for each color. The input arrows are read off from the original network by copying the input set of any node of the appropriate color, and assigning tail nodes uniquely by their colors.

6.3. *Graph Fibrations*

An alternative description of quotient networks was derived by [Boldi & Vigna, 2002] and [DeVille & Lerman, 2013, 2015] in the context of information processing. Define a *graph fibration* to be a map from a network $\mathcal{G}_1$ to a network $\mathcal{G}_2$ such that:

(a) Nodes map to nodes of the same node-type.
(b) Arrows map to arrows of the same arrow-type.
(c) The input set of any node maps *bijectively* to the input set of its image node.

Example 6.4. In Figure 11, Let $\mathcal{G}_1$ be the left-hand network and $\mathcal{G}_2$ be the right-hand network. Define a map ϕ on nodes by

$$\phi(1) = 1 \quad \phi(2) = 2 \quad \phi(3) = 1 \quad \phi(4) = 2 \quad \phi(5) = 5$$

Denote each arrow e by the pair of head and tail nodes $(\mathcal{H}(e), \mathcal{T}(e))$, which here determine the arrows uniquely because there are no self-loops or multiple arrows. Define the corresponding map on arrows to be induced by the image of the head and tail:

$$\phi(e) = (\phi(\mathcal{H}(e)), \phi(\mathcal{T}(e)))$$

Then it is easy to verify conditions (a,b,c) above, so ϕ is a fibration.

This fibration corresponds to the balanced coloring of Figure 11 (middle): each node maps to its cluster and arrows are mapped to create a color-preserving input isomorphism between $I(c)$ and the image $I(\phi(c)$ for every node c. The balance condition is precisely what is needed to make the map well-defined on arrows.

Indeed, every balanced coloring determines a fibration (even when there are many node- and arrow-types, self-loops, and multiple arrows) in which nodes map to the the corresponding clusters and input arrows are copied to conform to conditions (b) and (c). Conversely, any fibration defines a balanced coloring in which nodes have the same color if and only if they have the same image under the fibration, and the image can be identified with the corresponding quotient network. Thus we have two different but logically equivalent ways to formalize the quotient network construction. Each has advantages in suitable contexts.

As a rough analogy, a quotient group in group theory [Neumann *et al.*, 1994] can either be defined using cosets of a normal subgroup (colors and clusters) or as the image of a homomorphism (fibration).

The mathematical context for balanced colorings, quotient networks, and fibrations replaces the usual symmetry group of network by a different algebraic structure: the set of all isomorphisms between input sets of nodes. This set has a natural structure as a *groupoid* [Higgins, 1971], which is similar to a group, but in which the composition of two elements may not be defined. See [Stewart *et al.*, 2003; Golubitsky *et al.*, 2005; Golubitsky & Stewart, 2006]. Fibration symmetries can be viewed as the groupoid analogue of group symmetries.

6.4. *When Can Two Nodes Synchronize Robustly?*

An important consequence of the above formalism is a necessary and sufficient condition for two nodes to 'be able to synchronize'; that is, for them to have the same color in some balanced coloring. To describe this condition we need the concept of an *input tree*. Given a node c, define $I^1(c)$ to be the network formed by a copy of its input arrows and their tails, with all nodes being considered distinct. Call these tail nodes the *top layer*. Inductively, define $I^{n+1}(c)$ to be the network obtained from $I^n(c)$ by attaching, to all nodes in the top layer, a copy of their input arrows and tail nodes, again with all nodes being considered distinct. Redefine the top layer to be the tail nodes of these new arrows. Finally, let $I^\infty(c)$ be the union of all of the $I^n(c)$, embedded in each other according to the above construction. This construction is essentially the same as the *universal cover* of a directed graph [Leighton, 1982; Neumann, 2011].

We can now state a key result about robust synchrony: two nodes in a network can synchronize robustly if and only if their infinite input trees are isomorphic. The proof is that by [Stewart, 2007] this condition defines the (unique) coarsest balanced coloring (the one with fewest colors) and two nodes can have the same color in *some* balanced coloring if and only if they do so in the coarsest balanced coloring. By [Norris, 1995; Stewart, 2020a], we can replace the infinite input tree in this result by the I^{n-1} tree, where n is the number of nodes, obtaining a finite condition for robust synchrony to be possible. In fact, the following five properties are equivalent:

(a) Nodes c and d can synchronize robustly in some synchrony pattern.
(b) There exists a balanced coloring in which c and d have the same color.
(c) Nodes c and d have the same color in the coarsest balanced coloring.
(d) The input trees $I^\infty(c)$ and $I^\infty(d)$ are isomorphic.
(e) The input trees $I^{n-1}(c)$ and $I^{n-1}(d)$ are isomorphic, where n is the number of nodes.

A useful invariant of the infinite input tree is its *growth rate* or *branching ratio* — the asymptotic ratio of the number of leaves (terminal nodes) in $I^{n+1}(c)$ to the number in $I^n(c)$ [Morone *et al.*, 2020]. For example, Figure 3B (top) of that paper shows a 3-node network for which the numbers of leaves give the Fibonacci sequence, so the growth rate is the golden number $\frac{1}{2}(1+\sqrt{5})$. Nodes that can synchronize robustly have the same branching ratio. However, the converse need not hold.

[Morone & Makse, 2019] apply symmetry group factorization to elucidate the structure-function relation in the neural connectome of *C. elegans*. [Morone *et al.*, 2020; Leifer *et al.*, 2020] suggest that circuits with broken fibration symmetries perform essential logic computations in biological networks, and fibration symmetries also reveal basic building blocks. Similar ideas were proposed in [Nicosia *et al.*, 2013]. [Morone *et al.*, 2020] illustrate their ideas on the genetic transcriptional network of the bacterium *Escherichia coli*. The symmetry viewpoint is used to classify nodes (here genes) according to whether they can, in principle, synchronize their activity. This possibility is interpreted as evidence that the genes concerned can have the same kind of dynamic activity and therefore form one of the building blocks being sought.

Example 6.5.

We return to Figure 13 (left). By Example 6.3 the coloring shown is balanced. Therefore genes of the same color can synchronize robustly. In contrast, genes of different colors cannot synchronize robustly, since they have non-isomorphic input sets. (The *baeR* node has two activator inputs, whereas the *cpxR* node has only one, its self-loop.) This is therefore the coarsest balanced coloring on this network.

As remarked, pairs of nodes that can synchronize robustly must have isomorphic input trees. Figure 14 illustrates this principle for the input trees of three genes: *baeR*, *spy*, and *cpxR*. The first two are isomorphic (to the level shown), the third differs from them both.

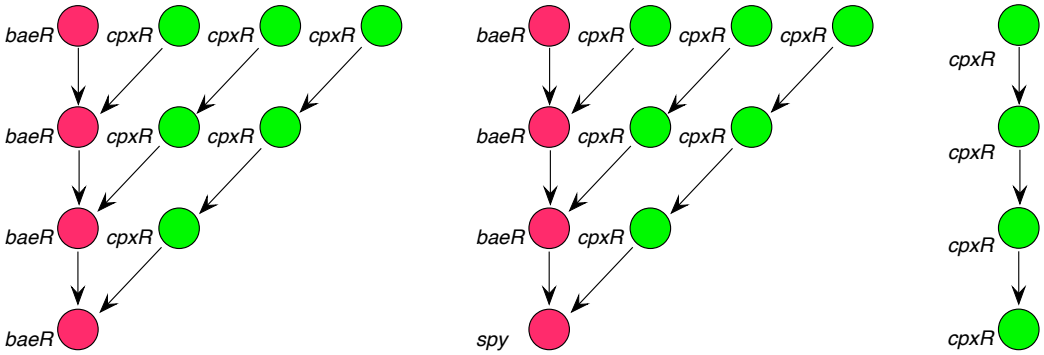

Fig. 14. *Left*: Input tree of *baeR*. *Middle*: Input tree of *spy*. *Right*: Input tree of *cpxR*.

[Morone *et al.*, 2020] discuss several other subcircuits of the *E. coli* transcriptional network from a similar viewpoint. They find that in total this network is organized into 91 fibers. There is a rich variety of input tree topologies, so this approach distinguishes many different types of gene according to possible synchronization.

These methods are not limited to gene regulatory networks. In Section 13 we discuss applications to neuronal networks, classifying neurons in the connectome of *C. elegans* via the symmetries of an important subnetwork. This constitutes a useful step towards further analysis of the dynamics and bifurcations in this network.

7. Symmetry

We have discussed symmetries of a network informally in examples, but it is time to give a formal definition. A *symmetry* of a network is a permutation π of its nodes that induces input isomorphisms between $I(c)$ and $I(\pi(c))$ for all nodes c; that is, π preserves input sets. For example, the network of Figure 11 (right) is symmetric under *all* permutations of its nodes $\{1, 2, 5\}$. The set of all symmetries, in this sense, forms a group under composition of the permutations.

Symmetry has a strong effect on dynamics and bifurcations, permitting the application of general results from equivariant bifurcation theory [Golubitsky *et al.*, 1988]. However, such results must be used with care because network structure can impose extra conditions beyond symmetry. In particular, although admissible maps are equivariant, the converse is generally false [Golubitsky & Stewart, 2023]. So network admissible ODEs can form a proper subset of the equivariant ODEs for the symmetry group.

It is well known that symmetry can lead to synchrony. To be precise, symmetries lead to balanced colorings. If Σ is any group of automorphisms (that is, a subgroup of the automorphism group), then the orbits of Σ determine a balanced coloring, where the colors correspond to the orbits. The associated fibration maps each node to its orbit under Σ, and these orbits constitute the nodes of the corresponding quotient network.

For example in Figure 11 (right), the transposition (12) generates a subgroup of order 2, whose orbits are $\{1, 2\}$ and $\{5\}$. There is a balanced coloring in which nodes 1 and 2 have the same color and the third node 5 has a different color.

What is less well appreciated is that although symmetry is sufficient to create some synchrony patterns,

it need not be necessary. Example 6.1 makes this clear, showing that robust synchrony patterns correspond to balanced colorings. For this reason some authors use the term *fibration symmetry* for a balanced coloring.

7.1. *Symmetry-Breaking*

We distinguish two kinds of symmetry-breaking: spontaneous and forced. *Spontaneous symmetry-breaking* occurs in a parametrized family of ODEs $\dot{x} = f(x, \lambda)$, where f is Γ-equivariant for a group Γ. Suppose that a state $x(t)$ with symmetry group Γ exists for all λ near 0, is stable for $\lambda < 0$, but becomes unstable for $\lambda > 0$. The system typically bifurcates to a stable state whose symmetry group is a proper subgroup of Γ. For instance, in Example 5.1 the ODE has $\mathbb{Z}_2$ symmetry generated by a sign change $x \mapsto -x$. The zero solution also has symmetry $\mathbb{Z}_2$, but each of the branches $\pm\sqrt{\lambda}$ has trivial symmetry $\mathbf{1}$.

In *forced symmetry-breaking*, the Γ-equivariant ODE is modified to $\dot{x} = f(x, \lambda) + g(x, \lambda)$ where g is not Γ-equivariant, so the *equation* has less symmetry. Usually g is small, so the equation is a small perturbation of the original equation by a symmetry-breaking term g. Spontaneous symmetry-breaking is generally better understood than forced symmetry-breaking; the former can be studied rigorously using singularity theory, whereas the latter is often studied using perturbation theory and *ad hoc* choices of g.

7.2. *Equivariance and Admissibility*

It is easy to prove that if a network has symmetry group Γ then every admissible ODE is Γ-equivariant. It is tempting to conclude that the dynamics and bifurcations of such networks are fully prescribed by the Γ-equivariant theory. However, equivariant maps need not be admissible in general, so any results on equivariant ODEs that depend on genericity might not be valid for networks with the appropriate symmetry, and extra care is needed.

This is already the case for very simple networks. The Smolen oscillator of Figure 5 (right) has the trivial symmetry group $\Gamma = \mathbf{1}$ (whether we assume its nodes are identical, or not). Thus the Γ-equivariant systems are arbitrary dynamical systems with no nontrivial symmetry. Generically, such a system has no invariant subspaces. However, the Smolen oscillator with identical nodes has an invariant subspace comprising the synchronous states (x, x). So does *any* network with the same diagram.

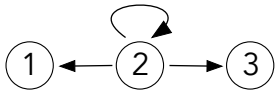

Fig. 15. A 3-node network with symmetry group $\mathbb{Z}_2$ but a generic multiple critical eigenvalue.

Example 7.1. For another simple example: generic steady-state bifurcation in a dynamical system with trivial symmetry arises from a simple critical eigenvalue. The same is true if the symmetry group is $\mathbb{Z}_2$, because both irreducible representations of $\mathbb{Z}_2$ have dimension 1. The network of Figure 15 has $\mathbb{Z}_2$ symmetry. Assume node spaces are 1-dimensional. Its adjacency matrix and admissible systems are:

$$\begin{bmatrix} 0\,1\,0 \\ 0\,1\,0 \\ 0\,1\,0 \end{bmatrix} \qquad \begin{bmatrix} \dot{x}_1 \\ \dot{x}_2 \\ \dot{x}_3 \end{bmatrix} = \begin{bmatrix} f(x_1, x_2) \\ f(x_2, x_2) \\ f(x_3, x_2) \end{bmatrix}$$

with eigenstructure

$$\begin{aligned} \mu_1 &= 1 \ \text{ eigenvector } (1, 1, 1) \\ \mu_2 &= 0 \ \text{ eigenvector } (1, 0, 0) \\ \mu_3 &= 0 \ \text{ eigenvector } (0, 0, 1) \end{aligned}$$

There is a double eigenvalue 0.

Generic symmetry-breaking bifurcation in a $\mathbb{Z}_2$-equivariant dynamical system leads to a pitchfork. The network of Figure 15 is $\mathbb{Z}_2$-symmetric, but its generic bifurcations are different. [Leite & Golubitsky, 2006]

show that generically there are three (orbits of) transcritical branches bifurcating from the trivial solution, only one of which can be stable near bifurcation.

In general, such differences between generic network dynamics and generic equivariant dynamics arise for many reasons, because network structure imposes extra constraints compared to equivariance. These constraints can affect both linear and nonlinear terms, with strong effects on generic bifurcations. The differences are discussed at length in [Golubitsky & Stewart, 2023, Chapter 16].

7.3. *Orbit and Exotic Colorings*

If a network $\mathcal{G}$ has symmetry group Γ, we can use subgroups $\Sigma \subseteq \Gamma$ to construct colorings. Namely, nodes c and σc are assigned the same color, for any $\sigma \in \Sigma$. That is, nodes in the same Σ-orbit are assigned the same color. Accordingly, we call such a coloring an *orbit coloring*. It is easy to prove that any orbit coloring is balanced, because symmetries in Σ map input sets to input sets.

This phenomenon provides a general explanation of similar symmetry-related synchronisation properties, such as the observations of [Nicosia *et al.*, 2013], which are based on an analysis of a Kuramoto model [Kuramoto, 1984]. They observe that if such a system is unable to attain full synchrony, its dynamics organizes into "a regime of remote synchronization where pairs of nodes with the same network symmetry are fully synchronized, despite their distance on the graph". That is, nodes in the same orbit can synchronize robustly, and there is no special reason for nodes in the same orbit to be connected by short chains of arrows.

Balanced colorings provide necessary and sufficient conditions for robust synchrony, including global group-theoretic symmetries but going beyond them. The central point is that a balanced coloring need not be an orbit coloring. Indeed, this is the case for the Smolen oscillator with identical nodes. Its symmetry group is trivial, so the only orbit coloring is the trivial coloring in which nodes 1 and 2 have different colors. Non-orbit balanced colorings are said to be *exotic*.

Example 7.2. The network of Figure 15 has symmetry group $\mathbb{Z}_2$, which swaps nodes 1 and 3 while fixing node 2. There are two subgroups, $\mathbf{1}$ and $\mathbb{Z}_2$, and the corresponding orbit colorings partition the nodes into clusters as $\{\{1\},\{2\},\{3\}\}$ and $\{\{1,3\},\{2\}$ respectively. However, there are three additional balanced colorings: $\{\{1,2,3\}\}$,$\{\{1,2\},\{3\}\}$, and $\{\{1\},\{2,3\}\}$. These are exotic. The corresponding synchrony subspaces explain the unexpected branches in Example 7.1.

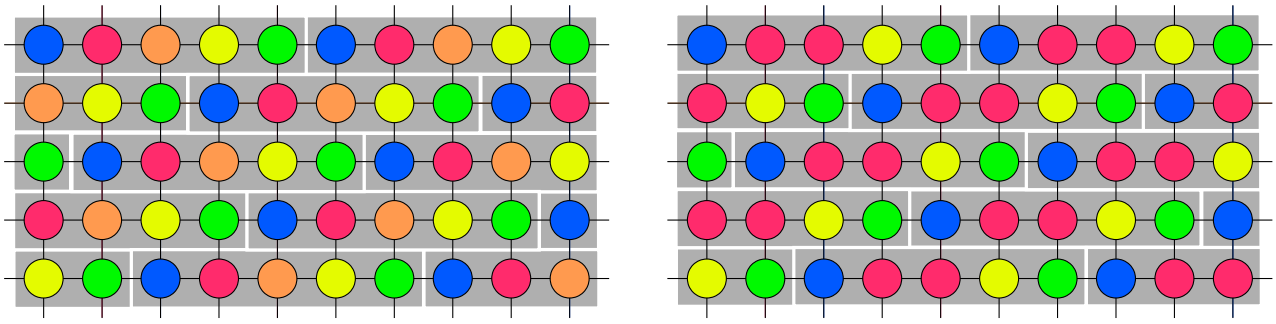

Fig. 16. *Left*: Balanced 5-coloring of $\mathbb{Z}^2$ with NN coupling. *Right*: Balanced 4-coloring of $\mathbb{Z}^2$ with NN coupling obtained by merging red and orange colors. All arrows are bidirectional and of the same type, but arrowheads are omitted for clarity. Gray rectangles are translates of a fundamental domain for the sublattice $\mathcal{K}$ defined by the two spatial periods.

Example 7.3. Exotic colorings can occur even when the network has a rich symmetry group. Figure 16 (left) shows a finite part of a 5-color pattern on a network with the topology of the infinite square lattice $\mathbb{Z}^2$ with nearest-neighbor (NN) connections. For simplicity we omit arrows: all connections are identical and bidirectional. The NN square lattice has an infinite symmetry group, the crystallographic group $\Gamma = \mathbb{Z}^2 \rtimes \mathbb{D}_4$, where $\rtimes$ indicates a semidirect product. This pattern $\bowtie$ is doubly periodic, and it is an orbit coloring for

the sublattice $\mathcal{K}$ generated by the two periods $(5,0)$ and $(2,1)$. As such, it is balanced, for any range of coupling. The gray shading indicates a 1×5 rectangle (the combinatorial version of a fundamental domain) and its translates under $\mathcal{K}$.

For comparison, Figure 16 (right) is a 4-color pattern with the same double periodicity. It is balanced for nearest neighbor (NN) coupling, but it can be proved not to be an orbit coloring. The right-hand coloring is obtained from the left-hand one by merging the colors red and orange. Normally, such a merger can destroy balance, but in this case it does not. The reason can be seen by forming the quotient network of $\mathbb{Z}^2$ by the orbit coloring for $\mathcal{K}$. This turns out to be Figure 17.

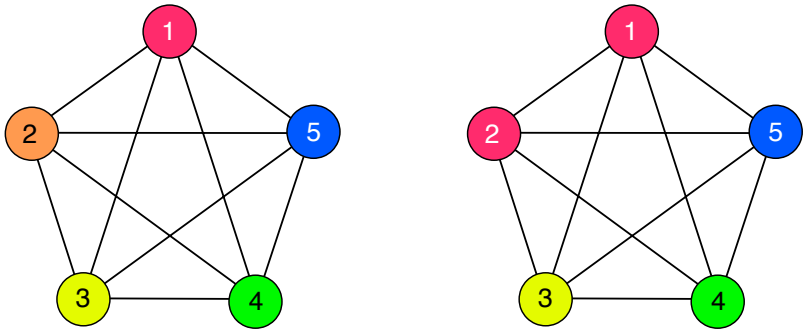

Fig. 17. *Left*: Quotient $\mathbb{Z}^2/\bowtie$ of $\mathbb{Z}^2$ by the 5-coloring has $\mathbb{S}_5$ symmetry and is all-to-all connected. *Right*: Any coloring on $\mathbb{Z}^2/\bowtie$, such as this one, is balanced, so lifts to a balanced coloring of $\mathbb{Z}^2$ with the same lattice periodicity. All arrows are bidirectional and of the same type, but arrowheads are omitted for clarity.

We recognize this quotient $\mathbb{Z}^2/\bowtie$ as the $\mathbb{S}_5$-symmetric all-to-all connected network on five nodes. *Every* coloring of this network is balanced, because all nodes receive the same inputs from other nodes. Each balanced coloring of $\mathbb{Z}^2/\bowtie$ lifts to a balanced coloring of $\mathbb{Z}^2$. If we merge two or more colors of $\bowtie$ *in any manner* on $\mathbb{Z}^2/\bowtie$, we obtain a balanced coloring of $\mathbb{Z}^2$ that is coarser than $\bowtie$. It may or may not be an orbit coloring.

In this example, the symmetry group of $\mathbb{Z}^2/\mathcal{K}$ contains automorphisms that are not induced from automorphisms of $\mathbb{Z}^2$. This type of behavior does not occur for most doubly periodic patterns on $\mathbb{Z}^2$. Indeed, this particular group is the symmetry group of the NN network $\mathbb{Z}^2/\mathcal{K}$ for a sublattice $\mathcal{K}$ *only* when $\mathcal{K}$ is the sublattice above or an image under $\mathbb{D}_4$. Something similar occurs for a few special choices of $\mathcal{K}$; theses sublattices are classified in [Stewart & Gökaydin, 2019] for the square lattice and [Stewart & Gökaydin, 2020] for the hexagonal lattice, in both cases assuming nearest neighbor coupling. A particularly suprising example occurs for the square lattice when $\mathcal{K}=(4\mathbb{Z})^2$: the symmetry group of $\mathbb{Z}^2/\mathcal{K}$ is then the hyperoctahedral group of order 384. The group of symmetries induced from $\mathbb{Z}^2$ has order 128.

Another example of an exotic pattern, which arises in an application to decision-making, occurs in Section 12.

7.3.1. *Implications for Bifurcations to Doubly Periodic Patterns*

The unexpected extra symmetry of $\mathbb{Z}^2/\mathcal{K}$ in Example 7.3 has important implications for the bifurcation analysis of doubly periodic patterns in NN square lattice models [Stewart & Gökaydin, 2019]. The symmetry group of the square lattice is the crystallographic group $\Gamma=\mathbb{Z}^2\rtimes\mathbb{D}_4$, so it is natural to analyze any model with this network structure in the context of Γ-equivariant bifurcations. Here the usual approach is to search systematically for solution branches in fixed-point subspaces of isotropy subgroups Σ.

However, admissibility can introduce additional constraints, not imposed by the global symmetry group of the network. Indeed, in the square lattice with NN coupling, the component for node $(c,d)\in\mathbb{Z}^2$ of an admissible ODE has the form

$$\dot{x}_{(c,d)}=f(x_{(c,d)},\overline{x_{(c+1,d+1)},x_{(c+1,d-1)},x_{(c-1,d+1)},x_{(c-1,d-1)}}) \tag{12}$$

where the overline indicates symmetry under the *vertex group* $\mathbb{S}_4$. In contrast, the Euclidean lattice symmetry group of this component is the subgroup $\mathbb{D}_4$ of $\mathbb{S}_4$. In other words, model equations with lattice structure obey extra constraints, which in principle might change the typical bifurcations. New invariant subspaces can occur, including the synchrony subspaces of exotic colorings. In particular, extra symmetries of the quotient network create orbit colorings of the quotient, which lift to balanced synchrony patterns for the original lattice network — and may be exotic, since the patterns do not arise from symmetries of the lattice.

In this example the quotient network has $\mathbb{S}_5$ symmetry. It can be checked that every $\mathbb{S}_5$-equivariant map can occur as a restricted map by suitable choice of f in (12). The Equivariant Branching Lemma implies that in generic symmetry-breaking bifurcation from the fully synchronous state, there exist steady-state branches whenever $\Sigma \cong \mathbb{S}_m \times \mathbb{S}_{5-m}$, for $m = 1, 2$. These give rise to 2-color synchrony patterns, with m nodes of one color and $5 - m$ nodes of the other color. All such patterns lift to $\mathbb{Z}^2$ with NN coupling, and many of them do not arise from Γ, which induces only $\mathbb{D}_5$ symmetry on the quotient network.

The $\mathbb{S}_5$ symmetry leads to the existence of a quadratic equivariant on the quotient network, so by Ihrig's Theorem all axial branches of an $\mathbb{S}_5$-equivariant ODE are linearly unstable near the bifurcation point. In contrast, this instability property is not what we expect generically for a Γ-equivariant system with the given double periodicity, since this induces a $\mathbb{D}_5$ subgroup of $\mathbb{S}_5$ [Golubitsky *et al.*, 1988, Section 5 Chapter XIII]. Thus exotic symmetries of quotient networks can have a major effect on bifurcations, such as additional branches and changes of stability, which are not predicted by the symmetries of the original lattice model.

Phenomena of this kind are not just theoretical anomalies: they arise in applications. An example of bifurcation to an exotic branch of steady states in an application occurs in a model of decision-making [Franci *et al.*, 2022], see Section 12.6.

8. Rigidity and Balance for Specific States

The notion of a balanced coloring initially arose in connection with 'universal' flow-invariant subspaces: those that are invariant under all suitable maps. In equivariant dynamics 'suitable' means 'equivariant'; in network dynamics it means 'admissible'. The associated synchrony patterns are said to be *robust*.

Robustness is a very strong assumption. However, it turns out that balanced colorings also arise from synchrony and phase patterns of individual states of an admissible ODE, subject only to a natural 'rigidity' condition requiring the pattern to persist after any sufficiently small admissible perturbation. This condition can be viewed as a form of structural stability in the sense of [Smale, 1963]. Rigidity is a reasonable requirement for modeling synchrony and phase patterns in nature, since the predictions ought not to depend in a highly sensitive manner on the precise form of the equations of the model. For example, in the quadruped walk, feet hit the ground in a cyclic order: left rear, left front, right rear, right front. Moreover, these movements are equally spaced in time: phase shifted by one quarter of the period. No exact model is known, but the phase patterns occur in many different animals, so they cannot depend in a sensitive manner on model equations.

We now review the main ideas involved.

In equivariant dynamics, Proposition 1 states that if f is Γ-equivariant and Σ is a subgroup of Γ then $\mathrm{Fix}(\Sigma)$ is flow-invariant. The folk theorem that all flow-invariant subspaces arise in this manner is proved in [Antoneli & Stewart, 2006, Theorem 4.1]. The analogous concepts to Σ and $\mathrm{Fix}(\Sigma)$ in network dynamics are a balanced coloring $\bowtie$ and its synchrony space $\Delta_{\bowtie}$. It is easy to prove that a synchrony subspace $\Delta_{\bowtie}$ is flow-invariant if and only if $\bowtie$ is balanced. Indeed, invariance under all linear admissible vector fields suffices. More generally, a vector subspace is flow-invariant if and only if it is of the form $\Delta_{\bowtie}$ where $\bowtie$ is balanced [Golubitsky & Stewart, 2023, Theorem 10.21]. Here invariance under nonlinear admissible vector fields is necessary.

Flow-invariance is a strong property. Synchrony and phase patterns on individual states are of greater interest. However, it turns out that reasonable (conjecturally generic) conditions on steady and periodic states also imply that the synchrony pattern is balanced, and the phase pattern of a periodic state is determined by a cyclic symmetry group on the quotient by synchrony. This is a strong 'local implies global'

result. In order to avoid 'accidental' counterexamples, two 'structural stability' conditions are imposed. One is hyperbolicity (the state concerned persists after small admissible perturbations) and rigidity (the synchrony or phase pattern also persists). The results in this area are motivated by analogy with equivariant dynamics, where synchrony and phase patterns induced by symmetry can be proved rigid — and hyperbolicity is a generic property.

A network ODE has a hyperbolic equilibrium with a rigid synchrony pattern if and only if that pattern is balanced [Golubitsky *et al.*, 2005; Stewart, 2020b]. Thus a pattern on a single state can force the existence of a flow-invariant subspace. A long-standing conjecture [Golubitsky & Stewart, 2006, Section 10] states the same for a rigid hyperbolic periodic state. This conjecture has been proved for a broad class of networks, including all homogeneous and fully inhomogeneous networks [Golubitsky *et al.*, 2010]. In [Stewart, 2022] it is proved for all networks under a slightly stronger condition than hyperbolicity. There are analogous results for phase patterns [Golubitsky *et al.*, 2012; Stewart, 2022]. Moreover, the original conjectures are valid for networks with at most 3 nodes, and for 1- and 2-colorings [Stewart, 2022].

A striking consequence is that phase patterns are constrained by global group symmetry, rather than fibration symmetry. In a transitive network, rigid phase patterns are always associated with a cyclic group of symmetries of the quotient network formed by identifying synchronous nodes. If this group has order k, the phase shifts are integer multiples of T/k where T is the period [Stewart & Parker, 2008; Golubitsky *et al.*, 2012].

The intuition behind all of these results is that when two nodes are synchronous or phase-related, the same holds for their inputs, if suitably identified. Rigidity is required to avoid contrived counterexamples, and hyperbolicity is assumed to define rigidity.

This completes the theoretical sections of this paper. We now move on to biological examples.

9. Locomotion and Traveling Waves

In Section 1.1 we discussed symmetries of periodic states in connection with the locomotion of *C. elegans*. We now turn to animals with legs, whose patterns of locomotion are called *gaits* [Gambaryan, 1974; Muybridge, 1899], and are classified by the phase shifts associated with the motion of the legs [McGhee, 1968]. Gait patterns in mammals, reptiles, and invertebrates are widely held to be produced by a Central Pattern Generator (CPG), which is a network of neurons in the spinal cord [Grillner & Wallén, 1985; Grillner *et al.*, 1998].

Many gaits, especially the simpler ones, have clear spatiotemporal symmetry: see Figure 4. For example, in the human walk, left and right legs are half a gait period out of phase. In quadrupeds, the walk involves successive $\frac{1}{4}$-period phase shifts as the legs permute in the 4-cycle

$$\rightarrow \text{left rear} \rightarrow \text{left front} \rightarrow \text{right rear} \rightarrow \text{right front} \rightarrow$$

Similarly the bound has left-right synchrony with a half-period rear-front phase shift, the pace has rear-front synchrony with a half period left-right phase shift, and the trot synchronizes diagonal pairs of legs with a half period phase shift between these pairs. These observations suggest that the CPG should be symmetric. As additional evidence, [Wilshin *et al.*, 2017] show experimentally that symmetries of a potential function predict gait transitions in dogs.

In the formal theory, the Rigid Phase Conjecture states that phase shift relations of this kind, if they are preserved by admissible perturbations, imply (subject to some mild technical conditions) that certain quotient networks have cyclic group symmetry. More precisely, the synchrony clusters correspond to a balanced coloring and the quotient network of synchronous clusters must have cyclic group symmetry. The phase shifts relate to this symmetry group according to standard theorems in symmetric dynamics. Thus we can infer that for the quadruped walk, the characteristic quarter-period phase shift implies that the underlying Central Pattern Generator (CPG) network involves a cyclic $\mathbb{Z}_4$ symmetry group; not necessarily acting on the CPG itself, but on its quotient by synchrony.

The Rigid Phase Conjecture has been proved for many networks by [Golubitsky *et al.*, 2010, 2012]. (These papers state the result for any network, but omit a technical condition needed in the proof, which fails for some networks. However, it is valid in many networks, including all homogeneous and fully inhomogeneous ones [Stewart, 2020b].) The highly structured and repeatable phase shifts of primary gaits

add extra motivation for analyzing a symmetric model, whose symmetries must somehow correspond to the observed phase shifts. As just remarked, the nodes of this model could be tightly-bound populations of neurons, but they might correspond to *sets* of neurons synchronized by a balanced coloring, widely distributed along the spinal cord and not communicating directly with each other.

Symmetric models are common in the area. [Kopell, 1988] and [Kopell & Ermentrout, 1986, 1988, 1990] model lamprey and fish CPGs using chains of identical phase oscillators, with either diffusive or synaptic coupling. In their model, synaptic coupling is required to produce locomotion. [Collins & Stewart, 1993a,b; Cohen & Stewart, 1994] suggest modeling gaits as time-periodic states of a symmetric CPG, created by symmetry-breaking Hopf bifurcation from a fully symmetric equilibrium ('stand'). They use equivariant bifurcation theory to classify gait patterns for a variety of hypothetical CPG architectures, both for quadrupeds [Collins & Stewart, 1993b] and for hexapods [Collins & Stewart, 1993a].

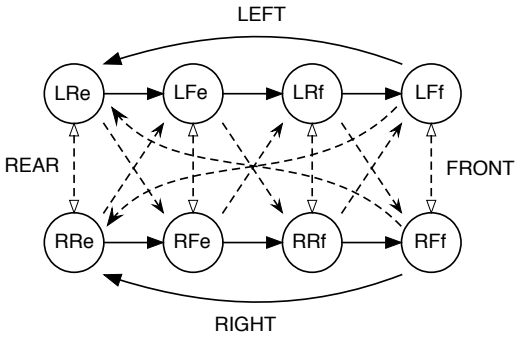

Fig. 18. Model quadruped CPG exhibits the minimal network architecture that naturally supports observed phase patterns while avoiding spurious conjugacies of distinct patterns. Symmetry group is $\mathbb{Z}_4 \times \mathbb{Z}_2$. Three types of short range connections show the symmetry. Longer-range connections (omitted for clarity) could also occur in symmetrically related sets. LR = left rear, LF = left front, RR = right rear, RF = right front, e = extensor, f = flexor.

[Golubitsky & Stewart, 1998; Golubitsky *et al.*, 1999] pointed out that these architectures are unsatisfactory for quadruped gaits, because distinct gaits can be dynamically conjugate and therefore coexist and have the same stabilities for the same parameter values, contrary to observations. They proved that under a specific list of reasonable symmetry hypotheses, the simplest CPG consistent with observations has eight nodes and $\mathbb{Z}_4 \times \mathbb{Z}_2$ symmetry, Figure 18. This network can generate all of the gaits in Figure 4; the pronk, walk, pace, trot, and bound occur as primary Hopf bifurcations and the two gallops occur as secondary 'mixed-mode' bifurcations. A reverse walk is also possible. They suggested that each leg requires two nodes in order to capture the distinction between flexor and extensor muscle groups, so the back-front traveling wave of movement extends to a 4-cycle, and showed that this architecture leads to several predictions that are consistent with observations. Among them is the ability of the same CPG to generate a *jump* or *buck* gait, along with its time-reversal. This gait is not illustrated in Figure 4; it is similar to a bound but with a $\frac{1}{4}$-period phase shift between back and front legs; see [Golubitsky & Stewart, 2002, Figure 3.9] for an example from the Houston Livestock Show and Rodeo. [Buono, 1998, 2001; Buono & Golubitsky, 2001] deduce further predictions, also consistent with observations. They performed numerical simulations with specific equations to show that this network architecture can produce all eight primary gaits with either synaptic or diffusive coupling.

[Pinto & Golubitsky, 2006] consider an analogous 4-node CPG for biped gaits, having $\mathbb{Z}_2 \times \mathbb{Z}_2$ symmetry. They classify all possible spatiotemporal symmetry types of time-periodic state in networks with this architecture using the H/K theorem of [Buono & Golubitsky, 2001]. [Stewart, 2014, 2017] analyzes gait patterns in a rate model for the above biped and quadruped locomotion CPGs.

Similar ideas have been applied to robotics. [Liu *et al.*, 2009] analyze a CPG for a four-legged robot based on a network of van der Pol oscillators, in which the phase shifts for gait patterns are built into the model. Which gait occurs depends on the system parameters. The paper includes simulations for walk, trot, pace, and bound. [Campos *et al.*, 2010] used a similar 6-node CPG to control a hexapod robot, obtaining

the three commonest hexapod (insect) gaits: metachronal, ripple, and tripod. Experiments were performed in simulation using the Webots simulator, an open source physics engine. A model was developed for the Chiara Robot, an open source educational hexapod. [In *et al.*, 2022] present a quadruped robot controlled by a CPG whose design is inspired by [Golubitsky & Stewart, 1998; Golubitsky *et al.*, 1999]. Using hardware simulations of the CPG and video snapshots they show that this electronic CPG and animal robot can exhibit, via symmetry-breaking Hopf bifurcations, all primary gaits predicted by theory, namely forward and backward walk, forward and backward jump, trot, bound, pace, and pronk.

Traveling wave motion much like that for *C. elegans* in Section 1.1 also occurs in vertebrates such as snakes and eels, and in invertebrates such as arthropods, where multiple segments are a discrete version of a continuum. Based on the simplest network that provides a satisfactory GPG for legged locomotion, [Golubitsky *et al.*, 1999] predict that in arthropods such as centipedes and millipedes, the waveform along the animal should contain a half-integer number of waves. This seems to be consistent with observations. Millipede locomotion preserves lateral $\mathbb{Z}_2$ symmetry (mirror-symmetric legs move in synchrony), whereas centipede locomotion breaks lateral $\mathbb{Z}_2$ symmetry (mirror-symmetric legs move a half-period out of phase).

9.1. *Peristalsis*

Many aspects of animal physiology involve the longitudinal propagation of rhythmic patterns, in which chains of neurons oscillate in synchrony or with specific phase relations along the chain. These two types of behavior can be interpreted as standing waves and traveling waves, respectively. An example is the heartbeat of the medicinal leech [Calabrese & Peterson, 1983; Buono & Palacios, 2004] with alternating patterns of standing and traveling waves in two series of heart chambers, one on each side of the animal.

[Furness, 2008] discuss the large-scale neuronal architecture involved in peristalsis, a traveling wave of muscular contractions in the intestine, which is controlled by the enteric nervous system. This system contains millions of neurons, which are mainly bunched into ganglia of two types: myenteric and submucosal. Successive ganglia are connected together and the large scale topology is that of a chain. Mathematical models of enteric neural motor patterns are surveyed in [Chambers *et al.*, 2013]. Specific models are given in [Miftakhov *et al.*, 1999] and [Miftakhov & Wingate, 1993; [Miftakhov & Wingate, 1995]. A common mechanism for such propagating chains involves a CPG, which generates the basic rhythms. This lies at the start of a feedforward network, along which the CPG signals propagate. The next example describes such a model.

Example 9.1. [Gjorgjieva *et al.*, 2013] study neural networks for crawling movement in *Drosophila melanogaster* larvae.

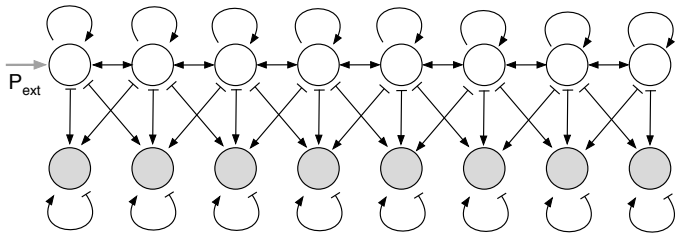

Fig. 19. Model CPG network model of *Drosophila* larva. Network model for peristaltic wave propagation. Each segment consists of an excitatory (white) and an inhibitory (grey) neuronal population. Pointed arrowhead: excitatory. Bar: inhibitory. P_{ext} is an external input acting as a CPG.

Model equations are of Wilson–Cowan type [Wilson & Cowan, 1972], also known as a rate model, see Section 10.6. They take the form

$$\begin{aligned}\tau_E \dot{E}_i &= -E_i + (k_E - E_i)\mathcal{G}_E(bE_{i-1} + aE_i + bE_{i+1} - dI_{i-1} - eI_i - dI_{i+1}\ [+P_{\text{ext}}])\\ \tau_I \dot{I}_i &= -I_i + (k_I - I_i)\mathcal{G}_I(cE_i - fI_i)\end{aligned}$$

where $1 \le i \le 8$. Terms are omitted at the two ends where subscripts outside that range would appear,

and P_{ext} appears only when $i = 8$. Here $\mathcal{G}_E, \mathcal{G}_I$ are sigmoid functions of the general form

$$\mathcal{G}(x) = \frac{1}{1 + \exp(-\lambda(x - \theta))} - \frac{1}{1 + \exp(\lambda\theta)} \tag{13}$$

with parameters λ, θ.

Sample simulations are illustrated in Figure 20. The main point we wish to emphasize is that the network creates traveling waves, which propagate from the rear to the front. When the left and right sides are interchanged, these waves may either be synchronous, or differ by half a period. (In millipede locomotion the two sides are synchronous; in centipedes, antisynchronous.)

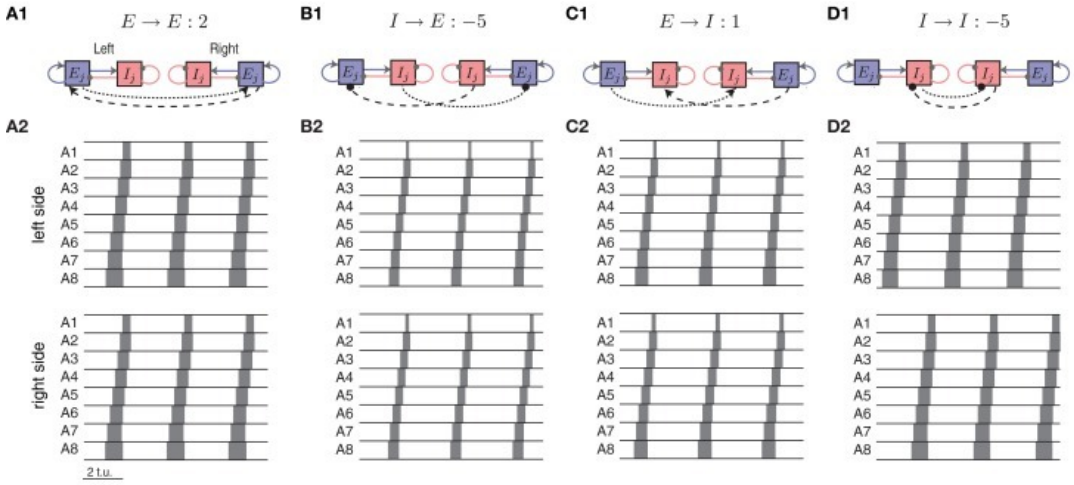

Fig. 20. Two-sided CPG network model in which Figure 19 is replicated for each side of the body. Four types of connections within each segment are illustrated: (A1) excitatory–excitatory, (B1) inhibitory–excitatory, (C1) excitatory–inhibitory, and (D1) inhibitory–inhibitory. (A2, B2, C2, D2) Typical left and right suprathreshold excitatory activity for one example of each of the four types. A2, B2, C2 show left-right synchrony; D2 shows left-right half-period phase shift. [Gjorgjieva *et al.*, 2013].

Gjorgjieva *et al.* conclude that although much is known about the morphology of local and intersegmental interneurons in *Drosophila*, much less is known about the neuronal composition of the crawling CPG. This motivates their use of coupled neuronal populations. The model suggests that strongly connected networks are more likely to generate waves, even when the connection strengths are not precisely tuned (only approximate symmetry). In contrast, weakly connected networks require precise tuning of excitation and inhibition (exact symmetry) to generate propagating waves with suitable timing properties. However, metabolic constraints argue against making connections too strong. They end by emphasizing a key advantage of their approach, which offers "a modeling framework which captures the neuronal dynamics essential for generating propagating peristaltic waves by a simple CPG architecture with a minimal number of parameters".

In this example the most obvious function of the network is to generate neuronal impulses leading to linear motion. The symmetry of a rigid body moving along a line with constant velocity is the subgroup

$$\{(vt, t) : t \in \mathbb{R}\} \subseteq \mathbb{R} \times \mathbb{R}$$

where t is time and v is velocity. If the shape fo the object changes periodically, as it does here, this is replaced by a smaller subgroup

$$\{(\rho vt, \rho t) : t \in \mathbb{Z}\} \subseteq \mathbb{R} \times \mathbb{R}$$

where the period is ρ.

The form of the network is a linear chain, with symmetry the translation group $n \mapsto n + 1, n \in \mathbb{Z}$.

The dynamics is a traveling wave, with symmetry

$$\{(\alpha vt, \alpha t) : t \in \mathbb{Z}\} \subseteq \mathbb{R} \times \mathbb{R}$$

which is the same as that of the moving body.

The symmetry of the network is a discrete approximation to the translation group, and when combined with the dynamic $\mathbb{S}^1$ symmetry of a periodic oscillation, this symmetry group relates the form of the network to its function in the animal.

9.2. *Propagation in Feedforward Chains*

Instead of idealizing the network to an infinite chain or closed ring, we can obtain traveling waves robustly using a finite feedforward chain forced by a CPG. Figure 21 shows an example, closely related to Example 9.1, but simpler.

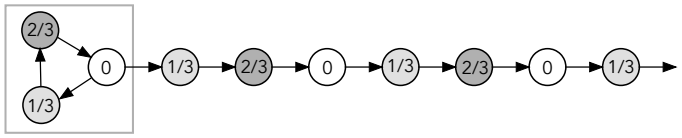

Fig. 21. Feedforward chain of identical nodes with initial CPG (square). In one typical periodic state, all nodes have the same waveform except for phase shifts of $0, 1/3, 2/3$ as indicated.

In this network a ring of 3 nodes (outlined square) forces a linear chain of arbitrary length. We assume all couplings and node dynamics are identical. It can then be proved that the typical time-periodic states include 'traveling waves' in which successive nodes have phases that differ by 1/3 of the period. Varying parameters in model equations can also reverse the direction of travel; that is, swap 1/3 and 2/3. Another possible state exists in which all nodes are synchronous.

The architecture of this network is designed to produce such patterns. The CPG is a unidirectional ring, with symmetry group $\mathbb{Z}_3$ that cycles the three nodes. Equivariant dynamics predicts the existence of a synchronous state and two discrete rotating waves with phase differences 1/3 or 2/3. Network dynamics shows that this state can be 'lifted' from the CPG to the entire network. Specifically, there is a balanced coloring (white, light gray, dark gray) of the nodes. The quotient is the same as the CPG. A rotating wave on the CPG lifts to a traveling wave along the chain.

For reasonable model equations, these traveling waves can be proved to be dynamically stable [Stewart & Wood, 2022; Golubitsky & Stewart, 2023]. In practice they are quite robust, and similar states persist if the nodes and couplings differ — though not by too large an amount. There are many variations with similar properties. The CPG ring can have any number n of nodes, yielding rotating waves where the phase shift from each node to the next is k/n of the period for a fixed but arbitrary integer k. The linear chain can branch like a tree, propagating the traveling wave to many different nodes.

The CPG can be replaced by suitable oscillatory forcing provided the oscillations of nodes in the chain do not depend strongly on the form of the forcing — for example, FitzHugh–Nagumo or other standard model neurons triggered by low-amplitude oscillations that push them above the firing threshold, much as in Example 9.1. For example, Figure 22 shows time series of voltages v_i for a chain of 7 identical identically-coupled Fitzhugh–Nagumo neurons with node 1 subjected to sinusoidal forcing near its natural frequency and node $i-1$ voltage-coupled to node i for $2 \le i \le 7$. The model equations are

$$\begin{aligned}
\dot{v}_1 &= v_1(a - v_1)(v_1 - 1) - w_1 + p \sin qt \\
\dot{w}_1 &= bv_1 - gw_1 \\
\dot{v}_i &= v_i(a - v_i)(v_i - 1) - w_i + cv_{i-1} \quad 2 \le i \le 7 \\
\dot{w}_i &= bv_i - gw_i \quad 2 \le i \le 7
\end{aligned}$$

for parameter values

$$a = -.3 \quad b = 0.3 \quad c = -0.5 \quad g = 0.9 \quad p = .5 \quad q = .25$$

The plot range is $20 \le t \le 120$ to allow transients to die away. Vertical coordinate range is $[-1.2, 1.2]$.

The simulation shows a traveling wave. The waveforms of successive nodes are not identical, but very similar.

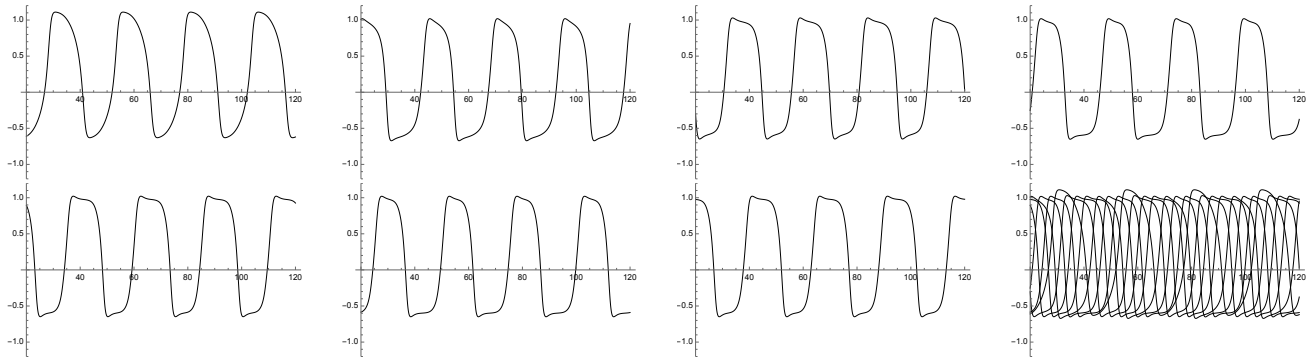

Fig. 22. Time series of voltages v_i for a chain of 7 identical identically-coupled Fitzhugh–Nagumo neurons with sinusoidal forcing. *Top*: neurons 1, 2, 3, 4. *Bottom*: neurons 5, 6, 7, all superposed.

10. Visual Perception

10.1. *Geometry of Retina and Retino-Cortical Map*

The link between form and function is particularly evident in the perceptual systems of animals, which often have strikingly regular physiology. An example is the geometry of the mammalian retina and the associated map to the cortex, Figure 23. The density of cones is highest near the fovea, and becomes rapidly smaller with distance. The density of rods is lowest where that of cones is highest, rises rapidly, and then declines in a roughly linear manner. Rods are widely distributed over the retina while cones are concentrated around the fovea. Peak cone densities in the eye illustrated on the right are 200,482 cones/mm^2 and 15,584 cones/deg^2.

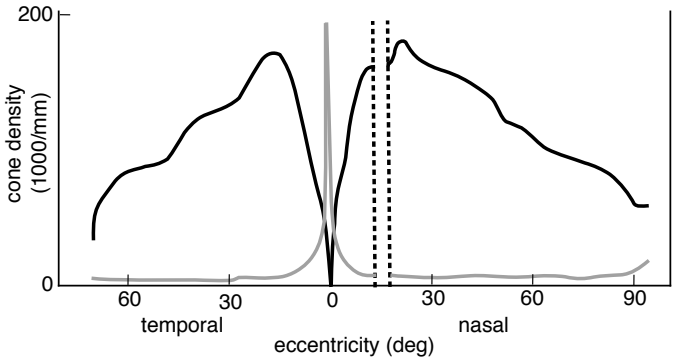

Fig. 23. Density variation of rods and cones in the human retina. Graphs of density against eccentricity (black = rods, grey = cones) redrawn from [Osterberg, 1935].

The density variations make intuitive sense: the greater density of receptors near (but not necessarily at) the center leads to improved visual acuity when observing those parts of the object concerned near the center of the visual field. A more specific observation was made by [Roberts, 1981], discussing a remark by I.J. Good:

> There is a coordinate transformation from a logarithmic polar system (at the retina) to a cartesian system (at the cortex), implemented entirely in the hardwiring of the optic nerve... I rotated the input image and almost fell off my chair. The output is identical, merely translated vertically... I tried scaling the input image, and again the output is identical, merely translated horizontally... This would appear to solve one of the most difficult problems in computer image recognition, replacing it with the much simpler challenge of keeping the object of interest centered in the frame of reference.

We explain these observations in terms of a simple equivariance property of the (idealized model)

retino-cortical map, and relate this map to the effect of transformations of images on the evolution of the visual system. (We ignore here the effects of binocular vision, with one retino-cortical map for each eye.)

The probable source of the observed regularity in the distribution of receptors in the retina is the range of visual stimuli experienced when viewing a (rigid) object. The image of an object depends on how the object moves relative to the observer. In particular, the apparent size of the object depends on distance, so it appears to expand or shrink, known mathematically as dilation. It can also rotate in space. So the same object is observed in many different forms, all transformations of the same underlying shape by dilation and rotations. This phenomenon, known as perceptual constancy, is intimately related to symmetry [Pizlo & Acacio de Barros, 2021]. As Roberts pointed out, translations (which would wreck the entire scheme) are removed by, in effect, centering the object. The resulting changes in optical stimuli can be expected, via natural selection for improved ability to recognize objects, to affect the structure of the visual system, and in particular the spatial distribution of rods and cones.

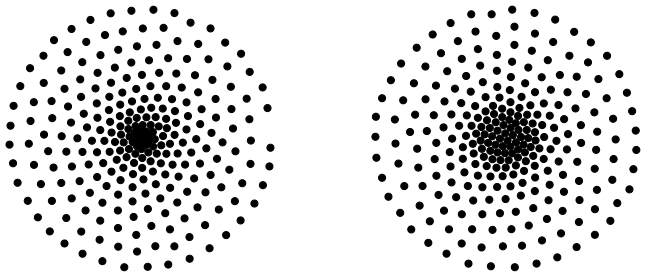

Fig. 24. Kohonen network trained using: *Left*: rotations and dilations, *Right*: rotations, dilations, and small translations. Redrawn from [Clippingdale & Wilson, 1996, Figures 11(d,b)].

[Clippingdale & Wilson, 1993, 1996] model this process using a Kohonen network [Kohonen, 1984], in which the position of nodes (representing rods, say) changes as a consequence of stimuli. An initially random distribution of nodes is subjected to a random rotation and dilation. The distribution is updated by moving each transformed node half way (or more generally, by a fixed proportion) between its original position and the nearest original node. Then the original nodes are removed. This process is iterated until the result converges. The resulting distribution is approximately invariant under all rotations and dilations, so that the density increases approaching the center; see Figure 24.

This suggests a group-theoretic explanation of the density distribution in the retina. Clippingdale and Wilson showed that the natural group Γ of transformations of an object (centered by the eye to remove translational motion) created by dilations and rotations leads, in this manner, to a distribution of nodes that is an optimal discrete approximation to an invariant distribution for Γ. That is, the distribution has rotational symmetry and varies logarithmically with the radius, to the best approximation that is possible for a discrete set. This produces higher densities as the radius decreases. The geometry of the nodes therefore replicates that of rods in the retina to reasonable accuracy, outside the central region where cones dominate. Delta-functions supported at these nodes constitute an effective discrete approximation to group-invariant eigenfunctions, yielding efficient image processing. Clippingdale and Wilson say that "global structure bearing a considerable resemblance to that found in the mammalian visual system can evolve as the result of a simple learning rule in networks driven by transformations similar to those typically encountered in vision."

The density variation of receptors in the retina can be understood in terms of a striking symmetry property of Good's model of the retino-cortical map. In suitable coordinates, this map can be modeled as the complex logarithm

$$f : \mathbb{C} \to \mathbb{C} \quad f(z) = \log z$$

Here we focus on the symmetry properties of log with respect to rotations and dilations of $\mathbb{C}$ fixing the origin. We consider the domain $Z = \mathbb{C}$ to be the retina, with *log-polar* coordinates $z = \mathrm{e}^{\rho+\mathrm{i}\theta} \equiv (r, \theta)$, where the usual radial coordinate is $r = \mathrm{e}^{\rho}$. (The exponential converts multiplication in r to addition in ρ, which

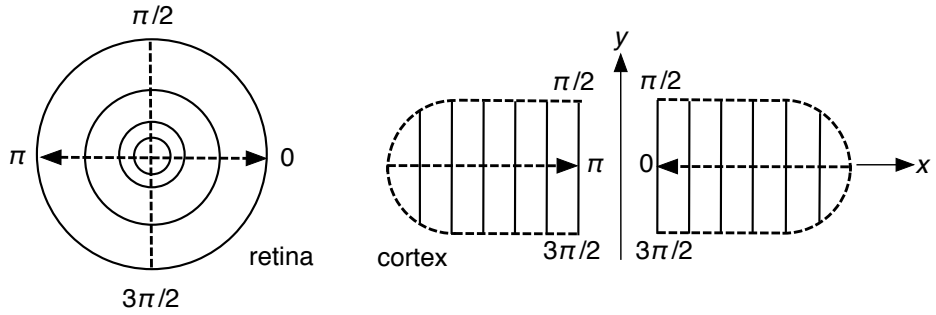

Fig. 25. Retino-cortical map. (In the brain, the two lobes on the right are transposed.)

is convenient for the mathematical discussion that follows.) The logarithm is periodic with period 2πi, so we take the codomain, representing the cortex, to be the cylinder $W = \mathbb{R} \times \mathbb{S}^1$, where $\mathbb{S}^1 = \mathbb{R}/2\pi\mathbb{Z}$ is the circle. 'Unwrapping' $\mathbb{S}^1$ to a period-2π structure on $\mathbb{R}$ and restricting to $[0, 2\pi]$ we effectively get cartesian coordinates (x, y) where $x \in \mathbb{R}, y \in [0, 2\pi]$ and 2π is identified with 0 to give $\mathbb{S}^1$. Now we can interpret the complex logarithm as a map

$$\log : Z \to W : \log(\mathrm{e}^{\rho+\mathrm{i}\theta}) = (\rho, \theta)$$

We show that this map has a natural equivariance property with respect to dilations and rotations.

The group $\Gamma = \mathbb{R}^+ \times \mathbb{S}^1$ acts on both $\mathbb{Z}$ and W, with different actions. Let $\gamma \in \Gamma$, so

$$\gamma = \mathrm{e}^{s+\mathrm{i}\phi} \quad s \in \mathbb{R}^+, \phi \in \mathbb{S}^1$$

On Z we define an action

$$\gamma \bullet z = \gamma z$$

and on W we define an action

$$\gamma * (\rho, \theta) = (\rho + s, \theta + \phi)$$

Now log is equivariant for the two actions $\bullet$ and $*$ of Γ. That is,

$$\log(\gamma \bullet z) = \gamma * \log(z)$$

To see why, compute:

$$\gamma * \log(\mathrm{e}^{\rho+\mathrm{i}\theta}) = \gamma * (\rho, \theta) = (\rho + s, \theta + \phi)$$
$$\log(\gamma \bullet z) = \log(\mathrm{e}^{s+\mathrm{i}\phi}\mathrm{e}^{r+\mathrm{i}\theta}) = (\rho + s, \theta + \phi)$$

Equivariance with respect to these two actions preserves symmetry. The relevant isotropy subgroups are

$$\Sigma_z = \{\sigma \in \Gamma : \sigma \bullet z = z\}$$
$$\mathrm{T}_z = \{\sigma \in \Gamma : \sigma * z = z\}$$

Now

$$\sigma \in \Sigma_z \Leftrightarrow \sigma \bullet z = z \Leftrightarrow \log(\sigma \bullet z) = \log(z) \Leftrightarrow \sigma^* \log(z) - \log z \Leftrightarrow \sigma \in \mathrm{T}_z$$

so $\Sigma_z = \mathrm{T}_z$. The same holds if z is replaced by any subset U of Z. Now U represent an image on the retina, derived from an object in the external world, and $\log(U)$ is the corresponding image on the cortex under the retino-cortical map. Thus U and $\log(U)$ have the same symmetries.

More generally still, if two images U, V on the retina are related by a transformation γ, so that $V = \gamma \bullet U$, then the same holds on the cortex: $\log(V) = \gamma * \log(U)$. This is Roberts's remark, expressed in the language of group actions.

We suggest that this equivariance property, which is well known in various terminology in the literature, determines the relation between form and function in the retina. That is, the wiring of retina to cortex via the optic nerve has evolved so that dilations and rotations are preserved.

10.2. *V1 Layer and Hallucination Patterns*

The link between form and function, unified by common symmetries or discrete approximations to such symmetries, is further illustrated by the structure of the V1 layer of the visual cortex, which detects the orientation of contours in the visual field. Figure 26 shows a portion of V1 from the visual cortex of a macaque monkey. Colors correspond to neurons that detect an edge in that orientation. The colors merge continuously except at isolated points where all colors exist in a pinwheel configuration. These points are singularities of the orientation field.

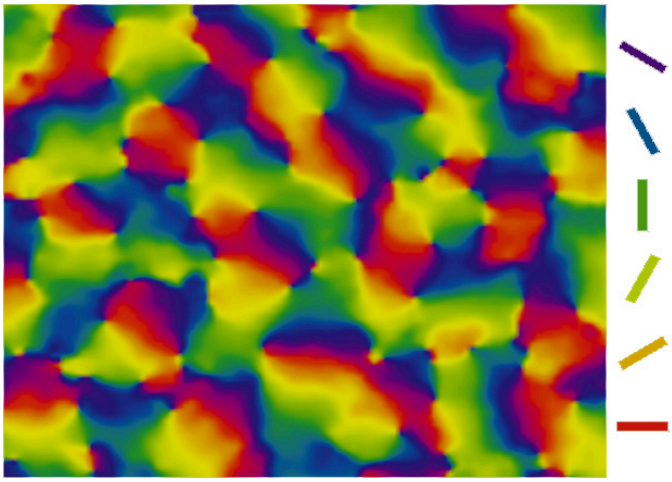

Fig. 26. Pinwheels in macaque cortex V1. colors: orientation that creates the most activity in each region of the cortex. Perceived orientation (shown down right side of image) changes smoothly except at singularities where all colors meet. [Blasdel, 1992] ©1992 Society for Neuroscience.

[Hubel, & Wiesel, 1962] showed that V1 is divided into small regions called *hypercolumns*. Cells in each hypercolumn receive inputs from a small region of the retina. The network structure of a hypercolumn renders it sensitive to a contour in that region, and specific sets of neurons fire corresponding to the orientation of that contour. These direction-sensing neurons are wired together within the hypercolumn by all-to-all inhibitory couplings, creating a *winner-takes-all* dynamic in which the hypercolumn responds most strongly to only one orientation. Figure 27 is a schematic representation of four neighboring hypercolumns.

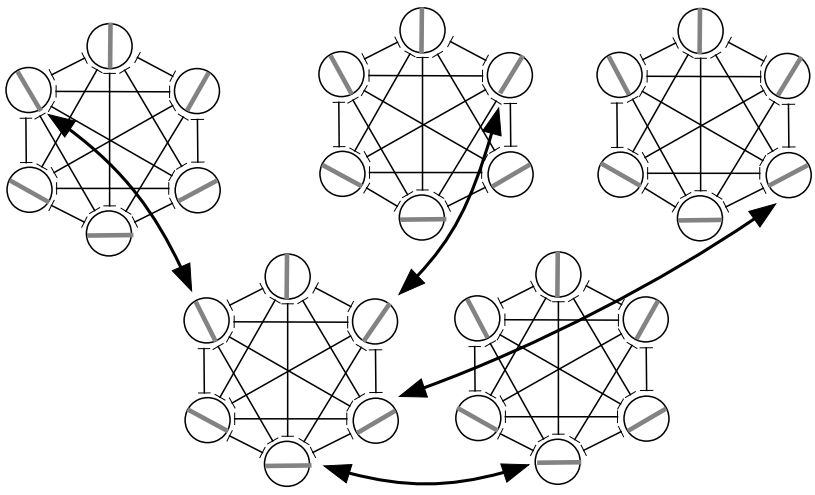

Fig. 27. Four hypercolumns, showing inhibitory all-to-all connections (bars) within a hypercolumn and longer-range excitatory connections (arrows) between a few nearby hypercolumns. (Schematic with 6 orientations and 5 hypercolumns.)

The figure also shows some connections between distinct hypercolumns (arrows). Voltage-sensitive dyes reveal that a cell in a given hypercolumn is linked by excitatory connections to those hypercolumns that lie on (or near) a line in V1 pointing in that direction [Iacaruso *et al.*, 2017]. These connections are of medium range, and it seems likely that the strength of signals decreases with distance. The effect of the overall wiring diagram is to extrapolate any contours that are detected, increasing the sensitivity of V1 to lines that continue in the same orientation. However, these extrapolated contours can be overridden by a sufficiently strong signal indicating a change in direction or the absence of a contour. Thus the form of the wiring diagram reflects the function 'detect contours', which has evolved to do so in an environment subject to random disturbances. Specifically, the objects in the outside world to which the eye responds can appear in many locations and orientations, corresponding to transformation by elements of the symmetry group of the plane; that is, the Euclidean group $\mathbb{E}(2)$. This group is seen in a discretized form as the symmetry group of the array of hypercolumns in V1. A smoothed continuum model is equivariant for a suitable representation of $\mathbb{E}(2)$, see below.

Objects are also subject to dilations created by changes in distance from the eye. These transformations lead to a larger group, which (modulo translations) played a prominent role in Section 10.2 in connection with the geometric distribution of rods and cones in the retina. In this example, the network is a discrete analog of the state space of external stimuli, locations, and so on. The states of the network correspond to stimuli. Physical symmetries act on state space, and correspond to approximate symmetries of the network. The isotropy subgroup of a state determines some of its properties, and is preserved when passing from physical space to the network, up to the same approximation.

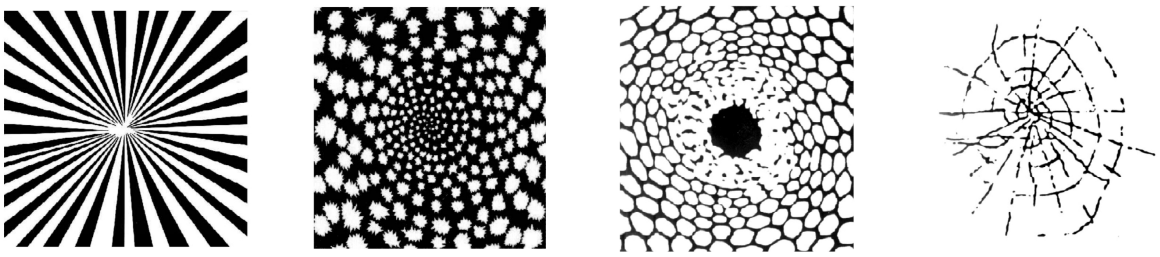

Fig. 28. Typical geometric visual hallucinations. *From left to right*: Funnel and spiral images seen following ingestion of LSD, redrawn from [Siegel & Jarvik, 1975]. Honeycomb generated by marijuana, redrawn from [Siegel & Jarvik, 1975]. Cobweb petroglyph redrawn from [Patterson, 1992]. All figures from [Bressloff *et al.*, 2002].

Geometric visual hallucinations occur after exposure to flickering lights, the administration of anaesthetics, binocular pressure on a subject's eyeballs, and ingesting drugs such as LSD and Marijuana. [Klüver, 1966] organized reported images into four classes: Gratings, lattices, fretworks, filigrees, honeycombs and checkerboards; Cobwebs; Tunnels and funnels, alleys, cones, vessels; Spirals. These patterns can either be stationary or rotate about the center of the visual field.

It is striking that these patterns have a similar density distribution to that of the visual receptors. [Ermentrout & Cowan, 1979] suggested that hallucination patterns might be generated by traveling waves in V1, interpreted via the retino-cortical map. This map, which corresponds roughly to the wiring diagram from retina to cortex, can be expressed in terms of the logarithmic map from the unit disc in the complex plane, representing the retina, to a plane representing V1; see Figure 25. The inverse map, the complex exponential, converts parallel lines in the plane to circles and spirals in the disc. A pattern of parallel waves in V1 is therefore interpreted by the visual system as if it originated in the retina, and its inverse transform in the disc is a pattern of concentric circles or families of spirals. As the waves move across V1, the circles are perceived as expanding and the spirals as rotating.

The original model for this process involved a continuum approximation to the Wilson-Cowan equations, leading to a partial differential equation (PDE) with the symmetry of the plane — that is, the Euclidean group $\mathbb{E}(2)$. It was also assumed that this group occurs in its natural representation by rotations, translations, and reflections of the plane. [Bressloff *et al.*, 2001] observed that the natural continuum

version of an idealized wiring diagram of V1 leads to a different 'shift-twist' action of $\mathbb{E}(2)$. A plane filled with infinitesimal hypercolumns is modelled as a circle bundle over $\mathbb{R}^2$, where a circle at a given point represents all of the orientations sensed by the corresponding hypercolumn. The translations in $\mathbb{E}(2)$ continue to act as geometric translations of the plane. However, rotations are 'twisted' so that as well as rotating the plane itself, they also rotate the circles corresponding to the hypercolumns. This change to the representation affects the irreducible components of the representation, hence the generic bifurcations, hence the predicted range of hallucination patterns. These predictions correspond more closely to observations than those resulting from the natural representation of $\mathbb{E}(2)$.

10.3. *V2/3/4 Layers*

Other layers of the visual cortex also have patterns of connectivity that reflect their functions. In the V2/V3 layers, it has long been thought that the selectivity of a neuron to the orientation and direction of a stimulus arises from the pattern of connections in these layers. Verification has proved elusive, but recently [Rossi *et al.*, 2020] showed that "the excitatory and inhibitory intracortical connections to a layer 2/3 neuron accord with its selectivity by obeying precise spatial patterns." Specifically, they showed that in the mouse cortex, presynaptic excitatory neurons are widely distributed in layers 2/3 and 4, and are distributed coaxial to the preferred orientation of that neuron, with stronger links to the region opposite to its preferred direction. Inhibitory neurons are different: they reside in layer 2/3 and have stronger links to the region near that neuron and ahead of its preferred direction. The asymmetry enhances the ability to detect directions, since reversing a direction does not preserve the connections. Similar asymmetry occurs in the retina, also related to direction sensing. So again we see that the form of the neuronal network has been tailored to the function that it performs, and it seems plausible that both form and function coevolved under natural selection.

10.4. *The Klein Bottle in Our Heads*

The arrangement in Figure 26 is constrained by topological properties of the orientation field. There are only two ways to arrange the series of colors round a singularity so that they change continuously: either the colors follow the sequence in a clockwise direction, or in an anticlockwise one. The picture shows examples of both. The presence of singularities is unavoidable because the cortex has to use many pinwheels to detect a complete line.

Now we ask how the brain combines this orientation information with information on how an edge is moving. Directions have an arrow — north is opposite to south, although both lie on the same straight line — and after a rotation of π radians the arrow reverses. A full 2π is needed to get a direction back to where it started. In contrast, edges do not have an arrow, so return to the same position after only π. Somehow the cortex has to make both of these things work at the same time.

Along a loop round a singularity, the orientations vary continuously, but the direction field flips from a given direction to the opposite one. These statements led [Tanaka, 1995] to conclude that the receptive fields connect to each other with the topology of a Klein bottle, Figure 29 (far right). This prediction has now been verified experimentally in various animals, including owl monkeys, cats, and ferrets, and presumably humans as well. If so, we have Klein bottles in our heads, which help us perceive moving objects.

The reason why Klein bottle topology is appropriate can be explained group-theoretically. Begin with the cylinder $C = \mathbb{R} \times \mathbb{S}^1$ with coordinates (x, θ). If we identify $[r, \theta]$ with $(r + 2, \theta)$ this becomes the torus $[0, 2] \times \mathbb{S}^1$ with the ends $\{0\} \times \mathbb{S}^1$ and $\{2\} \times \mathbb{S}^1$ identified; that is, $\mathbb{T}^2 = \mathbb{R}/2\mathbb{Z} \times \mathbb{S}^1$. This space has a commutative group structure in which

$$(u, \theta) + (v, \phi) = (u + v, \theta + \phi)$$

The Klein bottle differs from the torus in that the ends of a cylinder must be identified with *opposite* orientations. (In vision, this corresponds to the a feature of the direction field: a direction reverses after rotation through π.) To obtain this identification we consider the map $\alpha : \mathbb{T}^2 \to \mathbb{T}^2$ defined by

$$\alpha(u, \theta) = (u + 1, -\theta)$$

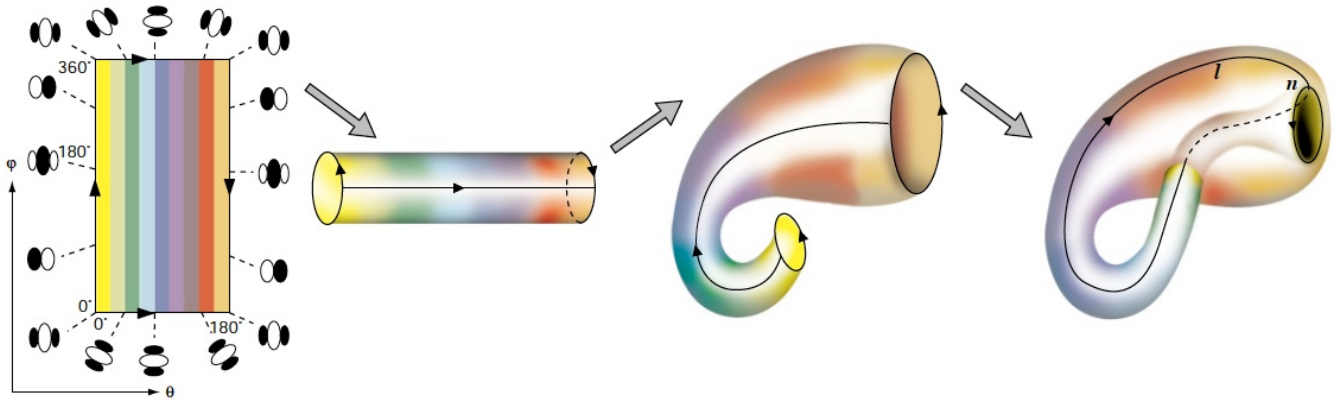

Fig. 29. Symmetry properties of simple cell receptive fields lead to Klein bottle topology. Plot of receptive-field phase against receptive-field orientation (far left). A continuous surface across which these parameters vary smoothly can (only) be constructed by joining together opposite edges of the rectangle to form a Klein bottle (far right). [Swindale, 1996] modified from [Tanaka, 1995].

This map is an involution: it satisfies $\alpha^2 = \mathrm{id}$. Identifying every point (u, θ) with its image $\alpha(u, \theta)$ yields a quotient space topologically equivalent to the Klein bottle. This is the usual representation of a Klein bottle as a rectangle with opposite edges identified: preserving the orientation of one pair and reversing the orientation of the other pair, Figure 29 (left).

10.5. *Models with Spherical Symmetry*

Related models of V1 combining orientation information with the spatial frequency of grids have been proposed. As we have seen, the orientation detected by a hypercolumn can be represented by a single angular coordinate with the topology of a circular ring, the circle $\mathbb{S}^1$. This in particular leads to an orientation tuning curve resulting from breaking the corresponding $\mathbb{O}(2)$ symmetry. Hypercolumns also detect the spatial frequency of grids of parallel lines, and [Bressloff & Cowan, 2002, 2003] extend the ring model to represent spatial frequency as well as orientation. These two variables, for any specific hypercolumn, are represented as distinct angular coordinates (longitude and latitude) on a sphere, with the poles corresponding to high-frequency perception (fine grids) and low-frequency perception (coarse grids). The transformation groups concerned are $\mathbb{O}(3)$, the orthogonal group in three dimensions, and its subgroup $\mathbb{SO}(3)$ of rotations. These groups act on the network topology of the hypercolumn and do not correspond directly to spatial organization in the cortex. The authors consider pattern formation by symmetry-breaking corresponding to low-order spherical harmonics, which determine irreducible representations, and show that this process provides a mechanism for the existence of localized orientation and spatial frequency preferences and tuning, similar to ideas of [De Valois & De Valois, 1988]. The spherical topology and its association with orientation preference pinwheels imply that tuning curves for orientation and spatial frequency are not separable. The authors remark that "representing the topology of a hypercolumn as a sphere is a natural way to accommodate the orientation pinwheels while providing a recurrent mechanism for generating two-dimensional spatial frequency tuning."

10.6. *Rivalry and Visual Illusions*

Yet another example of the form/function connection and its relation to common symmetries is apparent in models of two perceptual phenomena: binocular rivalry and visual illusions. The network structure has not yet been related to real brains, but the results indicate that simple circuits of the same general type are capable of producing the observed phenomena. So it would not be surprising if the brain used something similar — though probably in a more complex and more distributed form.

Two intriguing phenomena involving visual perception, which shed some light on how the visual system works by showing how it can 'go wrong', are:

(Binocular) rivalry: Two different images, presented one to each eye, lead to alternating percepts, possibly of neither image separately [Wilson, 2003, 2007; Breese, 2009].

Illusions: A single image can be perceived in several ways [Leopold & Logothetis, 1999; Eagleman, 2001].

Figure 30 shows two famous illusions: the Necker cube [Necker, 1832], which alternates between two apparent orientations, and the rabbit/duck illusion of [Jastrow, 1899].

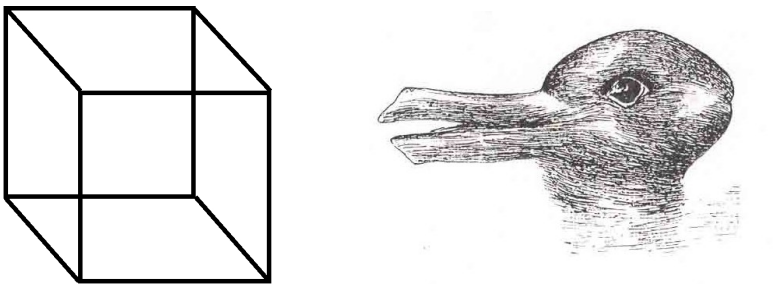

Fig. 30. Two classic multistable illusions. *Left*: Necker cube. *Right*: Rabbit/duck.

[Wilson, 2009] suggested that high-level decision-making in the brain, of which rivalry is an example, can be thought of as competition between patterns, described by a collection of *attributes*. He proposed that patterns are stored in an array whose columns represent attributes and whose rows represent *levels* of those attributes. A *pattern* is then a choice of one level for each attribute. We call such an array a *Wilson network*.

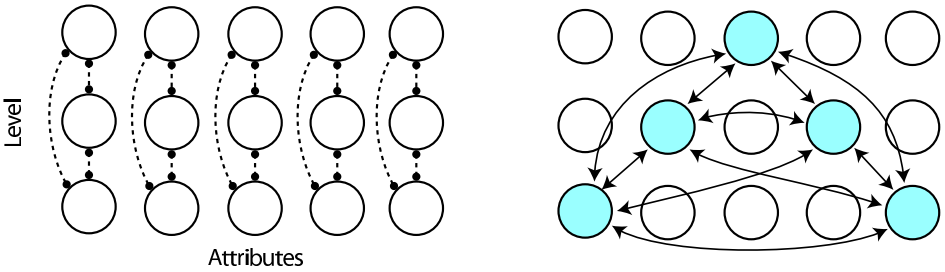

Fig. 31. Architecture for a Wilson network. *Left*: Inhibitory connections between nodes in an attribute column. *Right*: Excitatory connections in the cyan learned pattern.

For example, the Wilson network in Figure 31 has five attribute columns and each attribute has three levels. A 'rate model' ODE associates two variables with each node, an activity variable and a fatigue variable. Rate (or Wilson-Cowan) models use a specific parametrized family of ODEs based on neurophysiology [Wilson & Cowan, 1972; Ermentrout & Terman, 2010; Diekman *et al.*, 2012, 2013]. Such models are standard in this area. The nodes are numbered $i = 1, 2, \ldots, n$. The state of node i is described by a vector $x_i = (x_i^E, x_i^H) \in \mathbb{R}^2$, where $x_i^E \in \mathbb{R}$ is the *activity variable* and $x_i^H \in \mathbb{R}$ is the *fatigue variable*. A key ingredient is the *connection matrix*

$$A = (\alpha_{ij}) \quad 1 \le i, j \le n$$

where α_{ij} is the strength of the connection from node j to node i (positive for excitation, negative for inhibition). This matrix encodes the network structure and the type of connection. The rate equations then have the form:

$$\begin{aligned} \varepsilon \dot{x}_i^E &= -x_i^E + \mathcal{G}\left(-g x_i^H + \textstyle\sum_j \alpha_{ij} x_j^E + I_i\right) \\ \dot{x}_i^H &= x_i^E - x_i^H \end{aligned} \tag{14}$$

for $1 \leq i \leq n$. Here $g > 0$ is the strength of reduction of the activity variable by the fatigue variable, $\varepsilon \ll 1$ is the timescale on which the variables x_{ij}^E, x_{ij}^H evolve, and I_i is an external signal strength to node i. For simplicity we usually let $I_i = I$ for all i. Sometimes (in some rivalry models, for instance) some nodes have $I_i = 0$ instead (nodes not in any learned pattern).

In (14) the nodes are coupled through a *gain function* $\mathcal{G}$, which nominally satisfies

$$\mathcal{G}(z) = 0 \text{ for all } z \leq 0 \tag{15}$$

A common choice of gain function is

$$\mathcal{G}(x) = \frac{0.8}{1 + e^{-7.2(x-0.9)}} \tag{16}$$

Here $\mathcal{G}(x)$ is very small for negative x, but is not identically zero. Thus the state of a 'passive' node is very close to zero, but not exactly zero. This assumption is convenient for simulations and is standard in the literature.

Patterns are encoded by choosing, in each column, the level at which the activity variable is maximal for that column. There are two types of coupling. First, there is all-to-all inhibitory coupling within each column, indicated by the dashed arrows in Figure 31 (left). This assumption promotes winner-take-all dynamics in each column. Second, *learned patterns* are encoded by excitatory connections between levels associated with the pattern, Figure 31 (right). This model mimics Hebbian learning [Hebb, 1949]. Initially all attributes and levels are treated equally. The all-to-all inhibitory connections in columns lead to the wreath product symmetry group $\mathbb{S}_m \wr \mathbb{S}_n$. The topology (form) of the network then evolves/learns to associate combinations of nodes with patterns (function). This association is achieved by forced symmetry-breaking, Section 7.1.

[Diekman *et al.*, 2012] observed that the dynamics associated with Wilson network can lead to patterns that are not learned, which they call *derived patterns*. Thus it might be possible to predict unexpected percepts in binocular rivalry. [Kovács *et al.*, 1996] reported a series of psychophysics experiments, one of which presented a picture of a monkey to one eye of the subject and a jungle scene (with text) to the other eye, Figure 32 (left). (The 'monkey' appears to be a juvenile orangutan, which is an ape, but 'monkey' is the traditional description.) The results were as expected: subjects reported alternation between the monkey and text pictures.

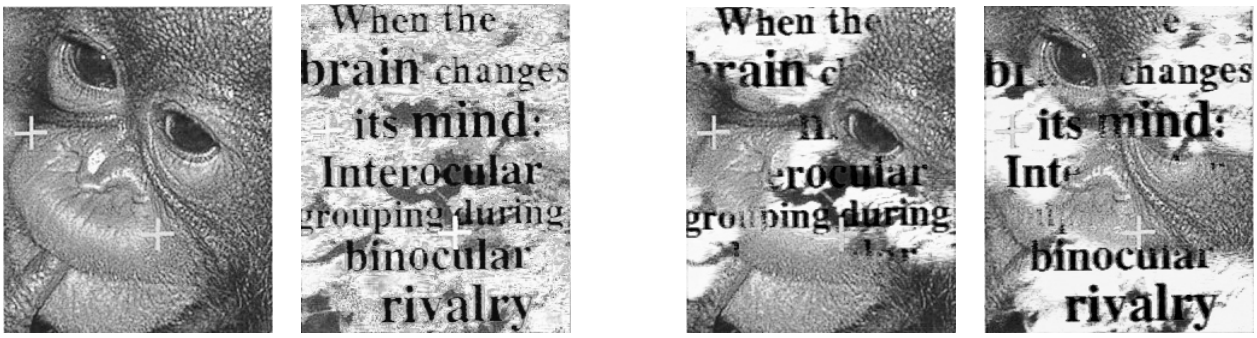

Fig. 32. *Left*: Pictures shown to subjects in the conventional monkey-text experiment of [Kovács *et al.*, 1996]. (Originals in color.) *Right*: Pictures shown to subjects in the scrambled monkey-text experiment.

The two images were then subdivided by three lines into six pieces each, and scrambled by interchanging three pairs of pieces. The two scrambled images, Figure 32 (right), were again presented one to each eye. For approximately half the time, subjects reported seeing just the two scrambled images. However, for the remaining time, subjects reported the reassembled whole images of Figure 32 (left). The subjects had not been presented with the original whole images, yet they reported four percepts: two learned and two not learned.

[Diekman *et al.*, 2012] proposed using Wilson networks to explain these additional percepts. The scrambled monkey-text experiment can be modeled by a two-level, two-attribute Wilson network with two

learned patterns. The images in Figure 32 are conceptualized as rectangles divided into two (disconnected) regions, one white and the other gray; see Figure 33 (left). The first attribute in the network corresponds to the portion of a rectangular image in the white region, and the second attribute corresponds to the portion of that rectangular image in the gray region. In the Kovács experiment the possible levels of each attribute are the portion of the monkey image in the associated region and the portion of the text image in that region.

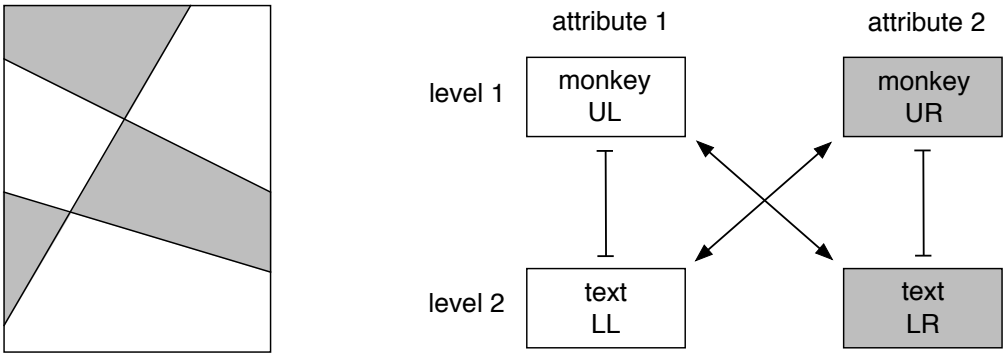

Fig. 33. *Left*: Distinct regions (white, gray) in scrambled monkey-text experiment. *Right*: Two-attribute two learned pattern Wilson network for scrambled monkey-text experiment with reciprocal inhibition in attribute columns and reciprocal excitation in learned patterns. Here UL, LL, UR, LR are the activity variables in the appropriate nodes.

There are four percepts associated with this Wilson network. Denote the activity variables in the nodes by UL (upper left), UR (upper right), LL (lower left), and LR (lower right). Then the theory of symmetric Hopf bifurcation [Golubitsky *et al.*, 1988] yields four patterns:

UL>LL and UR<LR: mixed image
UL<LL and UR>LR: mixed image
UL>LL and UR>LR: monkey
UL<LR and UR<LR: text

The first two are the original images presented to the eyes and the third and fourth are the 'derived' images reported by some subjects.

Recent developments introduce changes in the symmetry of the network modelling geometric constraints. An example is a rivalry experiment proposed by [Tong *et al.*, 2006], abstracted from the multi-location rivalry experiments in [Kovács *et al.*, 1996]. A generalized rivalry network model of [Diekman *et al.*, 2013; Diekman & Golubitsky, 2014] leads to predictions for this experiment. Recently, [Golubitsky *et al.*, 2019] performed Tong's experiment and found results that are consistent with the predicted Wilson model results.

Similar models of visual illusions have also been studied. [Curtu, 2010] and many others consider a 2-node rate model. [Stewart & Golubitsky, 2020] analyze a 16-node model that is a more refined representation of the geometry of the Necker cube, embedding geometric constraints from the real world into the network topology.

We return to Wilson's original motivation in Section 12, where we discuss an application to decision theory [Franci *et al.*, 2022]. The networks concerned are also $m \times n$ arrays, but the connections differ, leading to the symmetry group $\mathbb{S}_m \times \mathbb{S}_n$, which is a subgroup of $\mathbb{S}_m \wr \mathbb{S}_n$.

11. Other Sensory Networks

There are many other examples of the role of symmetries in the form and function of neuronal circuits. In this section we discuss three of them: the vestibular system, the auditory cortex, and grid cells.

11.1. *Vestibular System*

The vestibular system in almost all vertebrates controls balance via six semicircular canals, three in each inner ear, which detect angular accelerations of the head in three mutually orthogonal coordinate planes. Signals from the canals are transmitted to eight (groups of) neck motoneurons, which activate eight corresponding muscle groups. These signals may be either excitatory or inhibitory, depending on the direction of acceleration. [McCollum & Boyle, 2004] analyzed experimental observations to deduce the innervation patterns from canals to muscles, and to classify connections as excitatory or inhibitory. They observed that in the cat, the network of neurons concerned possesses the symmetry of a cube (equivalently, of its dual, the octahedron): the *octahedral group*, which comprises 48 transformations.

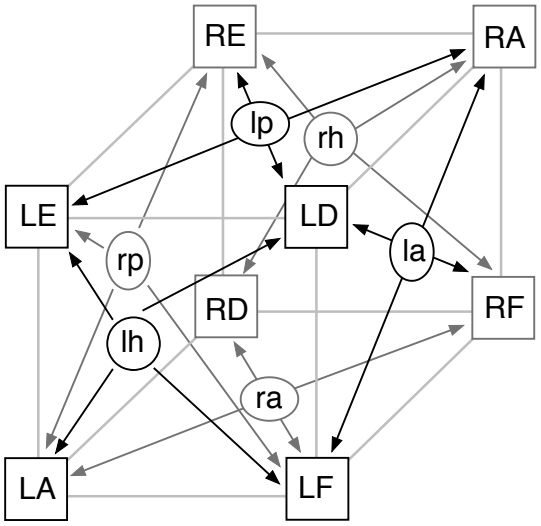

Fig. 34. Schematic of inhibitory connections from canals to muscles drawn on a cube. Canals are at (for clarity, near) centers of faces, muscles at vertices. Connections run to each vertex from the three adjacent faces. Black arrows: connections on visible faces. Dark grey arrows: connections on hidden faces. Light grey lines: not connections, but the edges of the cube, to emphasize the geometry.

Using their results, [Golubitsky *et al.*, 2007] constructed an explicit schematic wiring diagram. The octahedral symmetry is made visible by placing the muscle group nodes at the eight vertices of a cube and the canal nodes at the centers of its six faces. Figure 34 shows the inhibitory connections; excitatory connections, omitted for clarity, run from each canal to the complementary set of muscles. Here the three canals located in each ear are horizontal h, anterior a, and posterior p, and are denoted by lh, la, lp, rh, ra, rp, where l = left and r = right. The eight neck muscles consist of two flexors at the front (LF, RF), two extensors at the back (LE, RE), and four side (shoulder) muscles: alternating (LA, RA) and directed (LD, RD). There are six possible spatiotemporal patterns of time-periodic states that can bifurcate from an equilibrium representing an immobile head. In a simple caricature of the physical actions of the muscle groups, all six patterns correspond to natural head motions.

The octahedral symmetry reflects the geometry of the semicircular canals and their three orthogonal directions in physical space. There is a series of maps: from physical space to the network of canals, from those to the network of muscle groups, and thence to the position and motion of the head. All of these maps are equivariant for the octahedral group. Moreover, the motion of the head feeds back to the brain via the vestibular system, completing a feedback loop. Equivariance ensures that signals from the brain to the muscles, controlling head position, are consistent with those from the inner ear to the brain, detecting its position — clearly a desirable feature. The same principle affects how form and function are related at each stage.

11.2. *Auditory Cortex*

A famous early contribution to the mathematical study of human perception was made by [Fechner, 1860], who coined the term 'psychophysics'. The Weber-Fechner law states that the relationship between stimulus and perception is logarithmic. This is reasonably true for perception of loudness, embodied in the decibel scale of measurement. The equivariance property of the logarithm implies that equal ratios of loudness are perceived as equal intervals. (Of course the 'law' is at best approximate and not universal.)

The structure of the auditory cortex determines the perception of sound. Current information on 'wiring diagrams' is perhaps less specific than for the visual cortex, but there are clear indications of mathematical structure. The main governing feature is frequency; in particular the frequency response of neurons increases from one end of the cortex to the other. The auditory cortex is composed of distinct fields whose structure and function differ. Rodents have two fields, whereas the rhesus monkey has 15. It is not known how many fields there are in the human auditory cortex, or where they are located. As for vision, the auditory cortex identifies specific features of sounds and their spatial locations. For example, layer A1 encodes complex aspects of auditory stimuli without explicit representation of simpler features such as frequency [Chechik & Nelken, 2012].

The structure of the auditory cortex of echolocating animals (bats) has been widely studied, in part because these animals substitute echolocation for vision. [Dear *et al.*, 1993] report structural similarities between bat auditory cortex and mammalian visual cortex. The cover of that issue of *Nature* made the point more pithily: "How bats' ears see" [Greiter & Firzlaff, 2017] investigate the representation of three-dimensional space in the auditory cortex of the bat *Phyllostomus discolor*. Their observations demonstrate that neurons in the cortex respond to specific positions in space, so they can encode three-dimensional spatial information. [Calford *et al.*, 1985] find that significant parts of the body-surface map in the cortex of the fruit-bat *Pteropus poliocephalus* are reversed in comparison with that in other mammals. Given the upside-down posture adopted by the bat at rest, this suggests that the cortex analyzes spatial information in terms of the habitual orientation of an animal's body. This is also a simple example of equivariance under a spatial transformation — but here it is equivariance between networks in different species.

11.3. *Grid Cells*

[Hafting *et al.*, 2005] discovered that rat brains have special neurons, known as *grid cells*, that detect spatial location; see also [Moser *et al.*, 2014]. These neurons are situated in the medial entorhinal cortex, a central processing unit for location and memory. Like the visual cortex, this has a layered structure, and the pattern of firing is specific to each layer. In experiments, electrodes are placed in the brains of rats, which move freely in an open space. Grid cells fire whenever the rat is in one of a number of tiny patches of the space, and these patches form a hexagonal grid. Grid cells create a cognitive map that provides a coordinate system, telling the rat's brain the animal's location. Their activity is updated continually as the animal moves. Some cells fire fire independently of the direction in which the rat is heading; others depend on that direction.

The layers of grid cells are thought to compute the rat's location by integrating tiny movements. Mathematically, this process can be realized using vector calculations, in which position of a moving object is determined by adding together lots of small changes, each with its own magnitude and direction — like navigation by 'dead reckoning'. The computation can also be reset by selecting a new initial location. Feedback from the environment can also cause resetting, but is not required for the the grid neuron system to function.

[Wei *et al.*, 2015] deduce the organization of grid cells from an optimization principle: that the brain should encode spatial location at whatever resolution is required using as few neurons as possible — which is what happens for the retina model of Section 10. Their model implies that grid cells are located on hexagonal lattices, whose sizes form a geometric progression with common ratio $\sqrt{\mathrm{e}} \approx 1.65$ in the ideal model, and in the range $1.4 - 1.7$ in practice. Both features of the model agree with observations. [Hafting *et al.*, 2005] observe a hexagonal lattice structure. The grid size is largest at the ventral end of the cortex and smallest at the dorsal end. [Giocomo *et al.*, 2011] observe a ratio of 1.63 ± 0.035 in wild-type mice. These results indicate that the geometry of grid cells is a good discrete approximation to a distribution

that is symmetric under translations and dilations of the plane. Translation invariance leads to the lattice structure, which is hexagonal because this gives the closest pack in the plane. Dilation invariance leads to the geometric progression of scales — another example of the equivariance properties of the logarithm.

We can also speculate about the intriguing results of [Gardner *et al.*, 2022], who relate grid cell topology to the concept of a continuous attractor network (CAN). Such networks have a large number of neurons, hence a large-dimensional state space, but the natural dynamics is confined to a low-dimensional subset (attractor) of state space, which is insensitive to external inputs. This happens because the network connections constrain the dynamics of large populations of neurons. They discuss two examples: head direction cells, which represent the animal's orientation in the plane, and grid cells, which represent its position. The corresponding CAN models preserve the corresponding symmetry groups: rotation for head cells, two independent translations for grid cells. The attractor for the former is a circle; for the latter (imposing double periodicity) it is a torus.

The authors use high-site-count Neuropixels silicon probes to record hundreds of grid cells in a rat simultaneously. They deduce the topology of the attractor using a nonlinear dimensionality reduction procedure. First, to make the results robust to noise, they use principal component analysis (PCA) [Hotelling, 1933; Stewart, 1993; Pearson, 1901; Jolliffe, 2002] and retain the first six principal components. These are then analyzed using uniform manifold approximation and projection (UMAP) to reduced the dynamics from 6 dimensions to 3. The results confirm the occurrence of a torus. Its presence can be seen visually, and can be quantified using persistent cohomology, a recent mathematical technique that computes topological invariants of data point clouds at different levels of resolution, thereby revealing the topological form on different scales. Applications are widespread; for its use in neuroscience see [Rybakken *et al.*, 2019]. As the rat moves in space, the active zone of grid cells moves across the torus. The dynamics on the torus and the geometry of the rat's location also correspond is other ways.

These results fit into the spirit of this paper, but in a different manner. The network architecture is constrained so that its *dynamics* has the same symmetry properties as the external geometry. These symmetries are presumably encoded in some discrete manner in the network architecture, possibly induced from symmetries of something akin to a quotient network.

12. Decision-Making

Wilson networks were originally proposed in [Wilson, 2009] to model high-level decision-making in the brain, and this idea was followed up mathematically in [Franci *et al.*, 2022] using network dynamics to classify equilibrium patterns of decision-making by groups of humans, animals, and robots. Numerous references to the decision-making literature can be found in that paper. An early mathematical model of opinion formation through social influence in groups dates back is the linear averaging model of [DeGroot, 1974], leading to many different models of opinion formation [Friedkin *et al.*, 1999; Deffuant *et al.*, 2000; Hegselmann & Krause, 2002; Bizyaeva *et al.*, 2022].

Wilson's proposal is best considered as a metaphor rather than a literal description of any real neuronal network. Inasmuch as its nodes may correspond to reality, they would represent populations of neurons, not individuals. We discuss the idea here because it exemplifies several key features of network dynamics in a context related to the brain.

12.1. *Influence Networks*

Consider a number m of *agents* choosing among n *options*. This set-up might represent a swarm of bees selecting a new home, a flock of birds making navigational decisions when migrating, or humans considering policies to mitigate climate change. In these systems the aim is to attain *consensus*, group agreement. Other examples are bacterial communities differentiating into multiple cell types through molecular quorum sensing, and task allocation in a robot swarm. Here the aim is *dissensus*, group disagreement, because the optimal response requires diversity of choices. The emergence of dissensus from consensus can be viewed as a synchrony-breaking bifurcation in a dynamical system. Consensus corresponds to synchronous states (all agents behave identically) and dissensus to asynchronous states.

To implement this approach we represent the state of a model system as an $m \times n$ matrix z, whose entries z_{ij} are real numbers that quantify the value that agent i places on option j. The model assumes that initially all z_{ij} are equal, without loss of generality to 0 (consensus) and then evolve dynamically to an equilibrium state that may break this uniform synchrony pattern (dissensus). In the models discussed here, this evolution is determined by an admissible ODE for an *influence network* whose nodes are the agent/option pairs (i, j) with node variables z_{ij}, and whose arrows represent how each agent's preferences are influenced by those of other agents, and by their own preferences for other options. The initial aim is to classify model-independent behaviors; these can then be sought in more specific models. Here we focus on synchrony patterns arising through synchrony-breaking bifurcation.

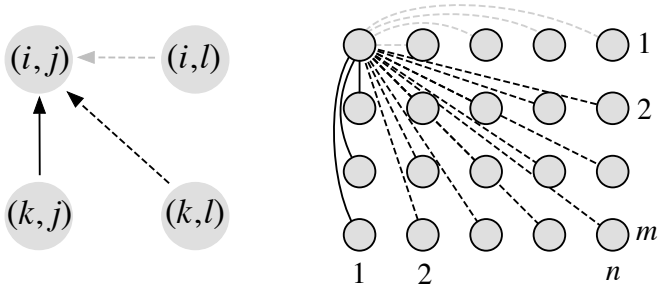

Fig. 35. An $m \times n$ influence network $\mathcal{N}_{mn}$ has three distinct arrow-types: gray dashed *row* arrows, solid black *column* arrows, and black dashed *diagonal* arrows. *Left*: Inputs to node (i, j). *Right*: Arrows inputting to node $(1, 1)$ (arrowheads omitted). There is a similar set of arrows inputting to any other node.

Each variable z_{ij} is associated to a node (i, j) in an *influence network* $\mathcal{N}_{mn}$. This is an $m \times n$ array of identical nodes with three types of arrow, illustrated in Figure 35 with arrowheads omitted for clarity. An arrow from node (k, l) to node (i, j) means that the value assigned by agent i to option j is influenced by the value assigned by agent k to option l. The arrow-type distinguishes different types of influence.

12.2. *Symmetry Group*

The influence network $\mathcal{N}_{mn}$ has symmetry group $\Gamma = \mathbb{S}_m \times \mathbb{S}_n$, where $\mathbb{S}_m$ swaps rows (agents) and $\mathbb{S}_n$ swaps columns (options). These symmetries reflect the assumption that agents and options are *a priori* indistinguishable in the decision-making process. The different arrow-types correspond to the orbits of $\mathbb{S}_m \times \mathbb{S}_n$ acting on pairs of nodes, with a fourth orbit corresponding to the 'internal arrows' of the nodes:

Row arrow: nodes (i, j) and (i, k) in the same row, $k \neq j$.
Column arrow: nodes (i, j) and (k, j) in the same column, $k \neq j$.
Diagonal arrow: nodes (i, j) and (kl) not n the same row or column, $i \neq j$ and $k \neq l$.
Internal node arrow: nodes (i, j) and (i, j).

Admissible systems of ODEs are Γ-equivariant. The converse fails for most m, n, but the linear admissible ODEs are the same as the equivariant ones [Stewart, 2021]. With these arrow-types, $\mathcal{N}_{mn}$ is the 'group network' corresponding to $\mathbb{S}_m \times \mathbb{S}_n$ acting on the set of pairs (i, j) [Antoneli & Stewart, 2007]. As such, it has two universal properties [Golubitsky & Stewart, 2023, Theorem 26.17]:

Let $\mathcal{G}$ be any network with symmetry group $\mathbb{S}_m \times \mathbb{S}_n$. Then:
(a) Every $\mathcal{G}$-admissible map is $\mathcal{N}_{mn}$-admissible.
(b) Every balanced coloring of $\mathcal{N}_{mn}$ is also balanced for $\mathcal{G}$.

12.3. *Irreducible Representations of* Γ

In equivariant bifurcation theory, a key role is played by the irreducible representations of the symmetry group Γ acting on the state space $\mathbb{R}^{mn} = \{z_{ij} : 1 \leq i \leq m, 1 \leq j \leq n\}$. Such a representation is *absolutely irreducible* if all commuting linear maps are scalar multiples of the identity [Golubitsky *et al.*, 1988, Chapter XII Sections 2–3]. In the equivariant case, generically, the kernel of the Jacobian (critical eigenspace for

steady-state bifurcation) is an absolutely irreducible representation. Because the linear admissible ODEs for $\mathcal{N}_{mn}$ are the same as the Γ-equivariant ones, this statement remains valid for the network case and admissible ODEs.

The state space $\mathbb{R}^{mn}$ decomposes into four Γ-invariant subspaces:

$$\mathbb{R}^{mn} = V_{\mathrm{s}} \oplus V_{\mathrm{c}} \oplus V_{\mathrm{dl}} \oplus V_{\mathrm{d}} \tag{17}$$

where

$$\begin{aligned} V_{\mathrm{s}} &= \text{all entries of } z \text{ equal} \\ V_{\mathrm{c}} &= \text{all rows of } z \text{ identical, with sum 0} \\ V_{\mathrm{dl}} &= \text{all columns of } z \text{ identical, with sum 0} \\ V_{\mathrm{d}} &= \text{all rows and all columns of } z \text{ have sum 0} \end{aligned} \tag{18}$$

whose dimensions are respectively $1, n-1, m-1, (n-1)(m-1)$. Each of these subspaces is an absolutely irreducible representation of Γ. They can be interpreted in decision-theoretic terms:

V_{s}: *fully synchronous* subspace — all agents assign the same value to every option.

V_{c}: *consensus* subspace — all agents express the same preferences about the options.

V_{dl}: *deadlock* subspace — each agent is deadlocked and agents are divided about the option values.

V_{d}: *dissensus* subspace — agents express different preferences about the options.

Bifurcations whose critical eigenspace is V_{s} are synchrony-preserving. Those with critical eigenspace V_{c} or V_{dl} are essentially $\mathbb{S}_n$- or $\mathbb{S}_m$-equivariant systems, which have been studied in the context of evolutionary models [Cohen & Stewart, 2000; Stewart *et al.*, 2003]. We focus on the most interesting case, the dissensus subspace V_{d}.

To prove existence of certain synchrony patterns we apply a network analog of the Equivariant Branching Lemma, which includes some exotic patterns as well as axial orbit colorings. For simplicity, assume that each node space of $\mathcal{G}$ is 1-dimensional and that $\dot{x} = f(x, \lambda)$ is a 1-parameter family of admissible ODEs. Let Δ be the diagonal space of fully synchronous states. By admissibility, $f : \Delta \times \mathbb{R} \to \Delta$. Suppose that f has a steady-state bifurcation point $x_0 \in \Delta$ for some λ_0. Given a coloring $\bowtie$, let its synchrony subspace be $\Delta_{\bowtie}$.

Instead of an axial isotropy subgroup, we require:

Definition 12.1. Let K be the kernel (critical eigenspace for steady-state bifurcation) of the Jacobian $J = \mathrm{D}f|_{x_0,\lambda_0}$. Then a balanced coloring $\bowtie$ with synchrony subspace $\Delta_{\bowtie}$ is *axial relative to* K if

$$K \cap \Delta = \{0\} \qquad \dim(K \cap \Delta_{\bowtie}) = 1 \tag{19}$$

There is then a natural analog of the Equivariant Branching Lemma:

Theorem 3 [Synchrony-Breaking Branching Lemma]. *With the above assumptions and notation, let $\bowtie$ be an axial balanced coloring. Then generically a unique branch of equilibria with synchrony pattern $\bowtie$ bifurcates from x_0 at λ_0.*

Proof. See [Franci *et al.*, 2022, Theorem 8.2]. ■

Setting $K = V_{\mathrm{d}}$, this result implies the generic existence of bifurcating branches for all axial balanced colorings relative to V_{d}.

12.4. *Latin Rectangles*

It remains to classify the axial balanced colorings relative to V_{d}. This leads naturally to a combinatorial structure that generalizes the concept of a Latin square:

Definition 12.2. A *Latin rectangle* is an $a \times b$ array of colored nodes, such that:

(a) Each color appears the same number of times in every row.

(b) Each color appears the same number of times in every column.

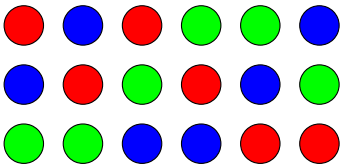

Fig. 36. 3×6 Latin rectangle with 3 colors.

An example with three colors is shown in Figure 36. Definition 12.2 is not the usual definition of 'Latin rectangle', which does not permit multiple entries in a row or column and imposes other conditions [Wikipedia, 2023].

There are number-theoretic conditions on a and b, restricting the possible sizes of Latin rectangles. Specifically, the proportion of nodes with a given color in each column is the same as the proportion in each row (and in the whole array). If that proportion is the fraction p/q in lowest terms, then q must divide both a and b. So, for instance, there is no 3×5 Latin rectangle with more than one color, because q must equal 1. In a 4×6 Latin rectangle with two colors, they must occur three times in each row and twice in each column, because the proportions $1/4, 3/4$ are ruled out since 4 does not divide 6.

12.5. *Classification of Balanced Colorings of Influence Networks*

Using network methods it is straightforward to classify all possible balanced colorings of influence networks $\mathcal{N}_{mn}$:

Theorem 4. *A coloring of $\mathcal{N}_{mn}$ is balanced if and only if it is conjugate under $\mathbb{S}_m \times \mathbb{S}_n$ to a tiling by rectangles, meeting along edges, such that:*

(a) *Each rectangle is a Latin rectangle.*

(b) *Distinct rectangles have disjoint sets of colors.*

Proof. See [Franci *et al.*, 2022, Theorem 9.4]. ■

By 'meeting along edges' we mean that the sets $\{1, \dots m\}$ of row indices and the sets $\{1, \dots m\}$ of column indices split into a sequence of disjoint intervals, in order from left to right (respectively top to bottom)

$$\{1, \dots m\} = I_1 \cup \cdots \cup I_s$$
$$\{1, \dots n\} = J_1 \cup \cdots \cup J_t$$

and the rectangles are the sub-arrays $B_{ij} = I_i \times J_j$. Figure 37 is an example.

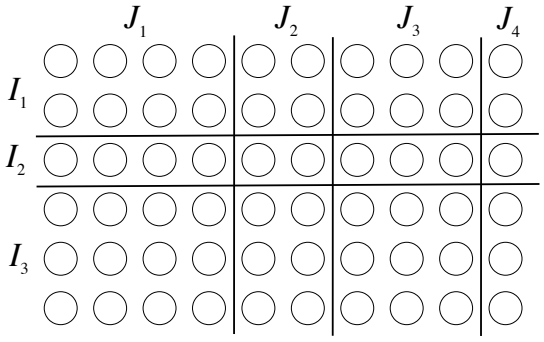

Fig. 37. Rectangular decomposition. Each sub-array must be a Latin rectangle, and distinct sub-arrays have disjoint color-sets.

Henceforth we abbreviate colors by R (red), B (blue), G (green), Y (yellow), and P (purple). Theorem 4 leads to a complete classification of axial colorings on influence networks:

Theorem 5. *The axial colorings on the dissensus space V_{d}, up to reordering rows and columns, are:*

(a) $\begin{bmatrix} B_0 & B_1 \end{bmatrix}$ *where $B_0 = 0$ is a rectangle with one color (Y) and B_1 is a Latin rectangle with two colors (R, B). The fraction $0 < \rho < 1$ of red nodes in every row of B_1 is the same as the fraction of red nodes in every column of B_1. Similarly for blue nodes. If z_R is the value of red nodes and z_B the value of blue nodes, then $z_B = -\frac{\rho}{1-\rho} z_R$. Possibly B_0 is empty.*

(b) $\begin{bmatrix} B_0 \\ B_1 \end{bmatrix}$ *where $B_0 = 0$ is a rectangle with one color (Y) and B_1 is a Latin rectangle with two colors (R, B). The fraction $0 < \rho < 1$ of red nodes in every row of B_1 is the same as the fraction of red nodes in every column of B_1. Similarly for blue nodes. If z_R is the value of red nodes and z_B the value of blue nodes, then $z_B = -\frac{\rho}{1-\rho} z_R$. Possibly B_0 is empty; if so, this pattern is the same as (a) with empty B_0.*

(c) $\begin{bmatrix} B_{11} & B_{12} \\ B_{21} & B_{22} \end{bmatrix}$ *where the B_{ij} are non-empty rectangles with only one color. The four colors (R, B, G, P) are distinct. Let z_{ij} be the value associated to the color of B_{ij} and let B_{11} be $r \times s$, B_{12} be $r \times (n-s)$, B_{21} be $(m-r) \times s$ and B_{22} be $(m-r) \times (n-s)$. Then*

$$z_{12} = -\frac{s}{n-s} z_{11} \qquad z_{21} = -\frac{r}{m-r} z_{11} \qquad z_{22} = \frac{s}{n-s}\frac{r}{m-r} z_{11}$$

Proof. See [Franci *et al.*, 2022, Theorem 9.2]. ■

Remark 12.1. In cases (a) and (b) the theorem implies that axial patterns either have two colors, one corresponding to a negative value of z_{ij} and the other to a positive value; or, when the block B_0 occurs, there can also be a third value that is zero to leading order in λ. Since row-and column-sums are zero to leading order on V_{d}, color Y indicates a neutral opinion while R, B correspond to values with opposite signs.

In case (c) there are four colors. This case represents *polarized* opinion. The agents split into two subsets. Agents in the same subset agree on all option values. Agents in different subsets disagree on all option values, assigning opposite signs to them. This again follows from the zero row- and column-sums in V_{d}, to leading order. If $z_{11} > 0$ then $z_{22} > 0$, while $z_{12} < 0$ and $z_{21} < 0$.

A complete classification can be obtained for $m \times n$ arrays when either $m \leq 4$ or $n \leq 4$. Larger values of m, n lead to a combinatorial explosion of possible Latin rectangles, but some general structure can be found [Golubitsky & Stewart, 2023, Section 24.17].

Example 12.1. Applying Theorem 5 for $m = 4, n = 6$ and eliminating patterns that lie in the same Γ-orbit, we find 16 representatives of the orbits of axial colorings of $\mathcal{N}_{46}$; see Figure 38. There are 3 patterns with 2 colors, 7 with 3 colors, and 6 with 4 colors. (Here we consider two patterns to be the same if they are in the same Γ-orbit, up to a bijective change of colors.

12.6. *Exotic Axial Patterns*

The 3- and 4-color patterns in Figure 38 are orbital. Among the 2-color patterns, the first pattern in row 1 is clearly orbital. The second pattern is exotic by [Franci *et al.*, 2022, Theorem 9.7], and is in the same orbit as the exotic pattern in Figure 13 (left) of that paper. The third lies in a different orbit from the other two because all six column colorings are different, a property that is preserved by Γ but fails for the other 2-color patterns. Perhaps surprisingly, it is orbital. This can be checked by a routine calculation, in which rows and columns are systematically swapped. First, bring any given red node to position $(1, 1)$. Then bring the other red node in column 1 to position $(2, 1)$. Now permute columns so that successive columns $2, 3, \ldots 6$ have the same pattern as the original. This process succeeds in finding an automorphism of the pattern that maps any red node to $(1, 1)$. The group generated by these automorphisms is therefore transitive on the red nodes, so its orbits are the set of red nodes and its complement, the set of blue nodes. Thus this pattern is an orbit coloring.

Remark 12.2. The essential point here is that the 6 columns of this pattern are precisely the 6 possible arrangements of 2 red and 2 blue nodes in a column of size 4. Permuting rows does not change that

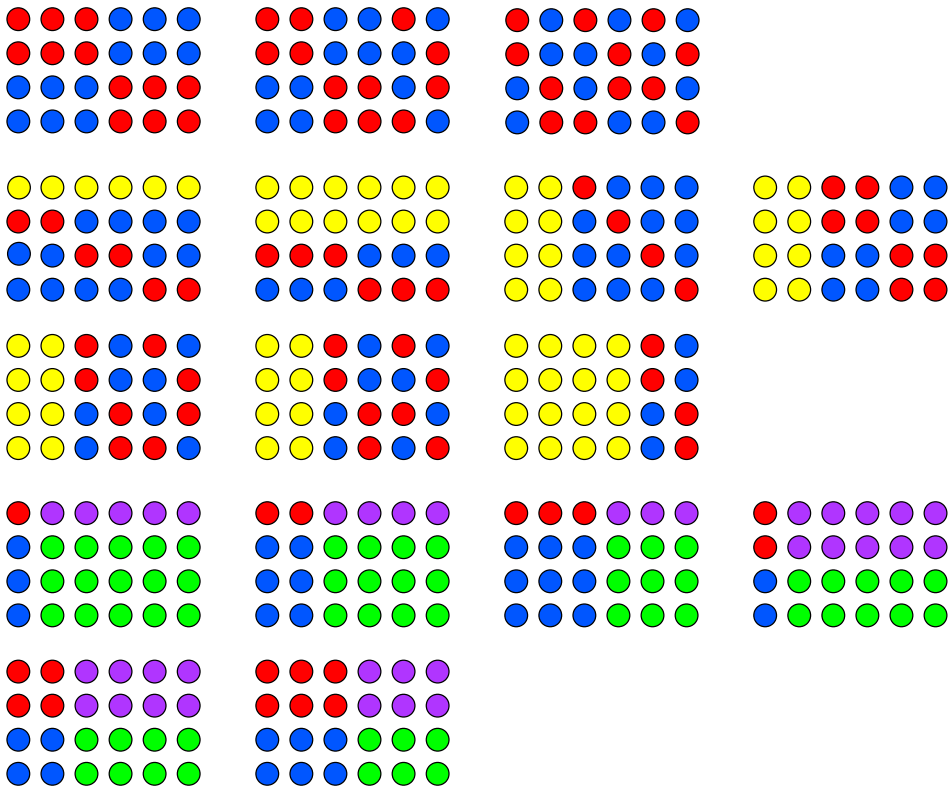

Fig. 38. The 16 Γ-orbits of axial colorings of $\mathcal{N}_{46}$. The second pattern in row 1 is exotic. All others are orbital.

statement. Therefore, once a given red node has been moved to position $(1,1)$ and the other red node in that column has been moved to $(2,1)$, finding an automorphism reduces to permuting the remaining five columns in a unique manner.

This procedure leads to explicit generators for the isotropy group Σ, but as stated it leads to a complicated list with no obvious structure. Presumably there is a more elegant description.

There are many exotic $m \times n$ patterns for larger m, n. Distinguishing them from orbital patterns is a nontrivial task. The main general result, [Franci *et al.*, 2022, Theorem 9.7], provides a sufficient condition for a pattern to be exotic, but it applies only to $4 \times n$ patterns.

12.7. *Stability of Dissensus Bifurcation Branches*

Recall Ihrig's Theorem from Section 5.2: subject to mild technical conditions, the existence of a non-zero quadratic equivariant on the critical eigenspace implies that all branches obtained from the Equivariant Branching Lemma are linearly unstable near the bifurcation point. Since there is a non-zero quadratic equivariant on V_{d}, Ihrig's Theorem applies to orbital dissensus bifurcation branches. This appears to cast doubt on the utility of the Equivariant Branching Lemma in these models, but the resolution is straightforward: globally, those branches can regain stability through saddle-node or secondary bifurcations as in [Cohen & Stewart, 2000; Stewart *et al.*, 2003]. Each of these processes can create jump bifurcations, an important prediction.

We do not know whether a similar result applies to exotic dissensus bifurcation branches, but the usual proof of Ihrig's Theorem does not extend to admissible maps.

Simulations of a specific model ODE leading to various axial patterns, including (a conjugate of) one the exotic pattern of Figure 38, are described in [Franci *et al.*, 2022, Section 10]. The model ODE employed is inspired by [Bizyaeva *et al.*, 2022]. These simulations show that both types of pattern can be stable for values of the bifurcation parameter close to the bifurcation point. (The z_{ij} are not close to zero, so this does not contradict Ihrig's Theorem.)

13. *C. elegans* Connectome

Our final example provides an accessible intermediary between the small networks that are commonly used to illustrate the general theory of network dynamics, as described in previous sections, and the large biological networks of 'big data', notably the human brain/connectome, which are the subject of intense research. The general theory is valid for networks of any size, but this does not guarantee that key concepts such as balanced colorings and symmetries occur in these larger networks, or shed any light on their activity even if they do. We end this paper with an example suggesting that these concepts can also be useful for large realistic networks of significance for neuroscience.

The complete neuronal network, or *connectome*, of the nematode *C. elegans* contains 302 neurons; the wiring diagram has 890 gap junctions and 6393 synapses [Varshney*et al.*, 2011]. [Morone & Makse, 2019] observe that despite these comprehensive data, "the design principles that explain how the connectome structure determines its function remain unknown". They explore the role of symmetries (global and fibration), showing that the balanced colorings determined by the symmetry group predict possible synchronization. These colorings also partition the neurons in a manner that corresponds to broad functional categories that are consistent with those in the WormAtlas [Altun *et al.*, 2002].

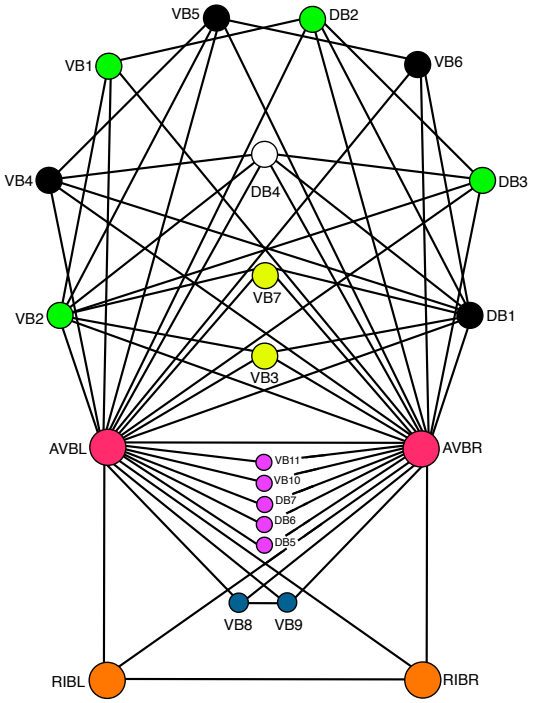

Fig. 39. Slightly idealized forward gap-junction circuit of *C. elegans*. Symmetries act on distinct sets of neurons indicated by different colors that lead to direct product factorization of the symmetry group. The corresponding orbits of neurons match the broad classification of command interneurons and motor neurons from the WormAtlas.

We discuss one example. Figure 39 shows a subnetwork of the *C. elegans* connectome known as the forward gap-junction circuit. This controls forward locomotion in the nematode. The figure is an idealized version with a few extra connections that create perfect symmetry [Morone & Makse, 2019]; this paper also presents the original data for comparison and analyzes 'approximate symmetries'. The symmetry group of this network has order 3840, and is isomorphic to $\mathbb{S}_5 \times \mathbb{Z}_2^5$. Of these symmetries, 120 permute the five motor neurons (DB5, DB6, DB7, VB10, VB11) in all possible ways. Among them are permutations that cycle the five nodes. One possible state for such a symmetry is a traveling wave in which successive nodes have the same waveform but differ in phase by one fifth of the period. We saw in Section 9 that traveling waves form the basis of many locomotion patterns, and the forward motion of *C. elegans* may exploit this possibility.

[Stephens *et al.*, 2008] use PCA to show that the 95% of the variability in the shapes adopted by *C.*

elegans as it moves can be accounted for by just four basic shapes, the first four principal components, which they call *eigenworms*. These four components afford a quantitative description of the worm's locomotion, which leads to model 'equations of motion' for the dynamics. Symmetries might be used to relate the muscle dynamics driving locomotion to the network structures of the forward and backward gap-junction circuits.

The symmetries in this example are global group symmetries. More general fibration symmetries (balanced colorings), which are more local within the network, also occur in 'big data' biological networks, including connectomes and gene regulatory networks, and in particular can be used to classify nodes into functional types and to determine which nodes are able to synchronize robustly.

14. Summary and Conclusions

This paper has four closely related objectives:

(a) To describe the basic concepts of a general theory of dynamics on networks, in principle applicable to a wide range of scientific areas, which has been developed over the past two decades.

(a) To give brief summaries of some of the applications of that theory to networks of interest in neuroscience.

(c) To use those examples to argue that the forms and functions of neural networks in organisms have coevolved, with symmetry as a common feature constraining this coevolution.

Here 'symmetry' comprises both the traditional group-theoretic symmetries widely used in physics and mathematics, and the more general groupoid or fibration symmetries that appear to be more suited to biological networks. Most examples discussed here are group symmetries, but fibration symmetries also occur. In real networks, such symmetries may be only approximate.

(d) To suggest that — at least in many different examples — both form and function have a common feature, the action of symmetry transformations. Equivariance conditions imply that this feature can yield systematic insights into the relations between them.

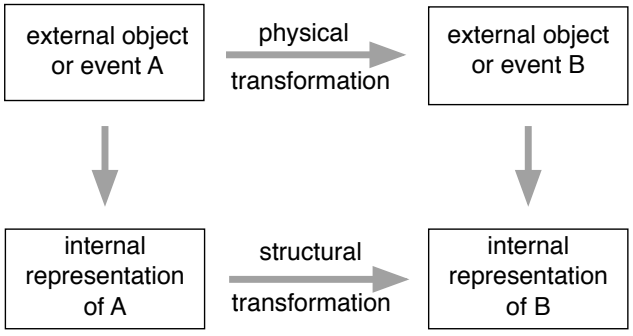

Fig. 40. Equivariance property of representation in the brain of external objects or events. When a physical transformation such as dilation or rotation maps A to B, the structure of the neuronal network concerned should map the representation of A to (something closely approximating) that of B.

Figure 40 is a schematic illustration of (c). Suppose that an object or event A in the external world is represented internally by a state $s(\mathrm{A})$ of a neuronal network, and a transformation ϕ (such as a rigid motion) transforms A to $\mathrm{B} = \phi(\mathrm{A})$. Then the structure of the neuronal network (and other elements of an organism) that generates the internal representation $s(\mathrm{A})$ should also incorporate a map ψ that implements an analogous transformation to $\psi(s(\mathrm{A}))$. In order to provide consistent representations, the equivariance condition

$$\psi(s(\mathrm{A})) = s(\phi(\mathrm{A}))$$

should hold. Moreover, composing ϕs should correspond to composing ψs. This condition implies that the architecture of that network should have the (approximate) symmetries involved in the external transformations. Mathematically, this implies that the network has the same symmetry group, or, when the

structure being preserved is synchrony, a corresponding fibration (equivalently, balanced coloring). This in turn implies that synchronous nodes should have isomorphic input trees, hence the same input tree invariants such as the branching ratio.

These principles are apparent in a variety of neuronal networks, both in reality and in models. The complex logarithm models the retino-cortical map quite well, and is equivariant for rotations and dilations, which occur naturally in images of the same real object. The Kohonen network shows how such a structure evolves naturally by updating images subjected to random transformations of these two kinds.

The structure of the V1 layer of the cortex is also equivariant under these transformations, and when longer-range connections are included, the wiring diagram is ideal for extrapolating line segments detected by hypercolumns. Indeed, the internal structure of each hypercolumn, with all-to-all inhibitory connections, makes it possible for the hypercolumn to select a single direction. Traveling waves in the cortex, which are natural symmetry-breaking patterns for its Euclidean group symmetry, are then perceived as target patterns, spirals, and other typical hallucination patterns, often rotating as the wave moves. These forms are a simple consequence of the equivariance properties of the complex logarithm. Similar remarks apply to the V2, V3, and V4 layers, in connection with direction detection. The Klein bottle structure, initially hypothesized on topological grounds, has been found experimentally; it too is closely related to the group of rotations when the reversal of direction under 180° rotation is taken into account.

Rivalry and visual illusions can be well modelled by Wilson networks, which more generally are models of more general high-level decision-making in the brain. Here the equivariance property is reflected in the organization of the model network, with permutation symmetries on rows and columns, corresponding to an initial assumption that all options are equal, and winner-takes all connections within columns to make it more likely that a definite decision is made. Experiments confirm that subsequent symmetry-breaking trains the network to detect particular patterns, which may include derived patterns: not part of the training set. The possible states of the network depend strongly on which symmetries are represented in its structure, and this in turn is related to real-world geometry.

Locomotion in many different animals is based on generating patterns of traveling waves. The symmetry constraints are that each pair of legs should behave much like each other pair (differences in physiology notwithstanding), and traveling waves require cyclic group symmetries. Left-right bilateral symmetry is an especially strong constraint, leading to lateral synchrony (millipedes) or antisynchrony (centipedes) as remarked in Section 9. The phase patterns of legged locomotion emerge naturally from cyclic symmetries, and this is supported by mathematical theorems. More general traveling waves such as peristalsis conform to the same general structure.

Symmetries also affect the form and function of several other neuronal networks. For the vestibular system, the symmetry group is the octahedral group, related to the three mutually orthogonal semicircular canals. There is indirect evidence that symmetry properties affect the structure of parts of the auditory cortex. Grid cells, used for location, appear to be structured according to a discrete analog of the group of translations and dilations, leading to an efficient representation of the animal's position in space, relative to some resettable initial point. In the model of decision-making, the network is hypothetical, but based on a natural model of identical agents evaluating initially identical options, and the symmetry group arises from these assumptions. Table 14 summarizes the relations between function, form, and symmetry for the examples in this paper.

Finally, we emphasize that the synchrony patterns and symmetries found in the *C. elegans* connectome show that, modulo the imprecision of biological systems, the mathematical structure discussed in this paper can be observed not only in small (possibly artificial) networks, but in large realistic biological networks, especially neuronal ones. Thus the mathematical theory, usually illustrated on small idealized networks for clarity and simplicity, can be applied to real 'big data' networks of significant current research interest. We expect many more applications of this kind to occur, because the underlying principles that form and function coevolve complicitly, and that the structural constraint of symmetry (group or fibration), which is common to both form and function and should affect them both in a consistent manner, is very general.

Table 1: Function, form, and common symmetries (possibly approximate).

CONTEXT	FUNCTION	FORM	SYMMETRY
C. elegans	locomotion	chain	$\mathbb{R}$
repressilator	phase pattern	ring	$\mathbb{Z}_3$
E. coli GRN	gene transcription	central node + links	3-color fibration
quadruped gait	limb phase pattern	bilateral pair of rings	$\mathbb{Z}_4 \times \mathbb{Z}_2$
centipede gait	limb phase pattern	bilateral pair of rings	$\mathbb{Z}_{2n} \times \mathbb{Z}_2$
millipede gait	limb phase pattern	bilateral pair of rings	$\mathbb{Z}_{2n} \times \mathbb{Z}_2$
peristalsis	traveling wave of motion	CPG+chain	fibration
D. melanogaster	peristalsis	CPG+chain	fibration
metabolator	metabolism + genes	2-node symmetric	1-color fibration
Smolen oscillator	oscillation	2-node asymmetric	1-color fibration
retino-cortical map	image recognition	density varies radially	$\mathbb{O}(2) \times \mathbb{R}^*$
visual cortex V1	edge detection	circle bundle over lattice	$\mathbb{E}(2)$ shift-twist
visual cortex V1	edge direction + motion	Klein bottle	$(\mathbb{R}/2\mathbb{Z} \times \mathbb{S}^1)/\alpha$
visual cortex V1	orientation + grid	sphere	$\mathbb{O}(3)$, $\mathbb{SO}(3)$
visual perception	rivalry	4-node monkey-text	$\mathbb{Z}_2 \times \mathbb{Z}_2$
visual perception	rivalry	trained Wilson network	$\subseteq \mathbb{S}_m \wr \mathbb{S}_n$
visual perception	illusions	Necker cube model	$\mathbb{Z}_2 \times \mathbb{Z}_2 \times \mathbb{Z}_2$
vestibular system	balance	cube	octahedral group $\mathbb{O}$
sound perception	loudness	unknown	scaling $\mathbb{R}^*$
auditory cortex	echolocation	lattice	$\mathbb{E}(2)$
decision-making	comparing values	rectangular array	$\mathbb{S}_m \times \mathbb{S}_n$
head direction cells	orientation of head	unknown	$\mathbb{S}^1$
grid cells	location perception	scaled hexagonal lattices	$(\mathbb{D}_6 \ltimes \mathbb{Z}^2) \times \mathbb{R}^*$
C.elegans connectome	forward locomotion	22 nodes	$\mathbb{S}_5 \times \mathbb{Z}_2^5$

References

Aldis, J.W. [2008] "A polynomial-time algorithm to determine maximal balanced equivalence relations," *Internat. J. Bif. Chaos* **18** 407–427.

Altun, Z.F., Herndon, L.A., Wolkow, C.A., Crocker, C., Lints, R., & Hall D.H. [2002] (eds.). *WormAtlas* 2002–2019 ; http://www.wormatlas.org.

Angluin, D. [1980] "Local and global properties in networks of processors," *Proceedings of the Twelfth Annual ACM Symposium on Theory of Computing*, ACM, Los Angeles, 82–93.

Antoneli, F. & Stewart, I. [2006] "Symmetry and synchrony in coupled cell networks 1: fixed-point spaces," *Internat. J. Bif. Chaos* **16** 559–577.

Antoneli, F. & Stewart, I. [2007] "Symmetry and synchrony in coupled cell networks 2: group networks," *Internat. J. Bif. Chaos* **17** 935–951.

Belykh, I. & Hasler, M. [2011] "Mesoscale and clusters of synchrony in networks of bursting neurons," *Chaos* **21** 016106.

Bizyaeva, A., Franci, A., & Leonard, N.E. [2022] "Nonlinear opinion dynamics with tunable sensitivity," *IEEE Trans. Automatic Control*; doi: 10.1109/TAC.2022.3159527.

Blasdel, G.G. [1992] "Orientation selectivity, preference, and continuity in monkey striate cortex," *J. Neurosci.* **12** 3139–3161.

Bock, W.J. [2000] "Explanatory history of the origin of feathers," *Am. Zool.* **40** 478–485.

Boldi, P. & Vigna, S. [2002] "Fibrations of graphs," *Discrete Math.* **243** 21–66.

Boyle, J. H., Berri, S., & Cohen, N. [2012] "Gait modulation in *C. elegans*: an integrated neuromechanical model," *Front. Comput. Neurosci.* **6**; doi: 10.3389/fncom.2012.00010.

Breese, B.B. [2009] "Binocular rivalry," *Psychological Review* **16** (1909) 410–415.

Bressloff, P.C. & Cowan, J.D. [2002] "SO(3) symmetry breaking mechanism for orientation and spatial frequency tuning in the visual cortex," *Phys. Rev. Lett.* **88** 078102.

Bressloff, P.C. & Cowan, J.D. [2003] "A spherical model for orientation and spatial-frequency tuning in a cortical hypercolumn," *Phil. Trans. R. Soc. Lond. B* **358** 1643–1667; doi: 10.1098/rstb.2002.1109.

Bressloff, P.C., Cowan, J.D., Golubitsky, M., Thomas, P.J., & Wiener, M.C. [2001] "Geometric visual hallucinations, Euclidean symmetry, and the functional architecture of striate cortex," *Phil. Trans. R. Soc. Lond. B* **356** 1–32.

Bressloff, P.C., Cowan, J.D., Golubitsky, M., Thomas, P.J., & Wiener, M.C. [2002] "What geometric visual hallucinations tell us about the visual cortex," *Neural Computation* **14** 473–491.

Buono, P.-L. [1998] *A model of Central Pattern Generators for Quadruped Locomotion*, PhD thesis, University of Houston TX.

Buono, P.-L. [2001] "Models of central pattern generators for quadruped locomotion II: secondary gaits," *J. Math. Biol.* **42** 327–346.

Buono, P.-L. & Golubitsky, M. [2001] "Models of central pattern generators for quadruped locomotion: I. primary gaits," *J. Math. Biol.* **42** 291–326.

Buono, P.-L & Palacios, A. [2004] "A mathematical model of motorneuron dynamics in the heartbeat of the leech," *Physica D* **188** 292–313.

Calabrese, R. & Peterson, E. [1983] "Neural control of heartbeat in the leech *Hirudo medicinalis*," *Neural Origin of Rhythmic Movements*, eds. A. Roberts & B. Roberts, *Symp. Soc. Exp. Biol.* **37** 195–221.

Calford, M.B., Graydon, M.L., Huerta, M.F., Kaas, J., & Pettigrew, J.D. *et al.*. [1985] "A variant of the mammalian somatotopic map in a bat," *Nature* 313, 477–479; doi:10.1038/313477a0.

Campos, R., Matos, V., & Santos, C. [2010] "Hexapod locomotion: a nonlinear dynamical systems approach," *IECON 2010 – 36th Annual Conference on IEEE Industrial Electronics Society*, 1546–1551; doi 10.1109/IECON.2010.5675454.

Chambers, J.D., Thomas, E.A., & Bornstein, C. [2013] "Mathematical modelling of enteric neural motor patterns," *Proc. Austral. Physiol. Soc.* **44** 75–84.

Chechik, G. & Nelken, I. [2012] "Auditory abstraction from spectro-temporal features to coding auditory entities," *Proc. Nat. Acad. Sci. USA* 109, 18968–18973. doi:10.1073/pnas.1111242109.

Cicogna, G. [1981] "Symmetry breakdown from bifurcation," *Lett. Nuovo Cimento* **31** 600–602.

Clippingdale, S. & Wilson, R. [1993] "Self-organization in neural networks subject to random transformations," *Proceedings of 1993 International Conference on Neural Networks (IJCNN-93-Nagoya, Japan)* vol. 3, Nagoya, Japan 1993, 2504–2507; doi: 10.1109/IJCNN.1993.714233.

Clippingdale, S. & Wilson, R. [1996] "Self-similar neural networks based on a Kohonen learning rule," *Neural Networks* **9** 747–763.

Cohen A.H., Ermentrout, G.B., Kiemel, T., Kopell, N. Sigvardt, K.A., & Williams, T.L. [1992] "Modelling of intersegmental coordination in the lamprey central pattern generator for locomotion," *Trends Neurosci.* **15** 434–438.

Cohen, J. & Stewart, I. [1994] *The Collapse of Chaos* (Viking, New York).

Cohen,J. & Stewart, I. [2000] "Polymorphism viewed as phenotypic symmetry-breaking," *Nonlinear Phenomena in Biological and Physical Sciences*, eds. Malik, S.K., Chandrasekharan, M.K., & Pradhan,N., (Indian National Science Academy, New Delhi) 1–63.

Collins, J.J. & Stewart, I. [1993a] "Hexapodal gaits and coupled nonlinear oscillator models," *Biol. Cybern.* **68** 287–298.

Collins, J.J. & Stewart, I. [1993b] "Coupled nonlinear oscillators and the symmetries of animal gaits," *J. Nonlin. Sci.* **3** 349–392.

Curtu, R. [2010] "Singular Hopf bifurcations and mixed-mode oscillations in a two-cell inhibitory neural network," *Physica D* **239** 504–514.

Dancer, E.N. [1980] "On the existence of bifurcating solutions in the presence of symmetries," *Proc. Roy. Soc,. Edinburgh* **85A** 321–336.

Dancer, E.N. [1983] "Bifurcation under continuous groups of symmetry," *Systems of Nonlinear Partial Differential Equations*, ed. Ball, J.M., (Reidel, Netherlands).

Davey, B.A., & Priestley, H.A. [1990] *Introduction to Lattices and Order*, (Cambridge University Press,

Cambridge).
Dear, S.P., Simmons, J.A., & Fritz, J. [1993] "A possible neuronal basis for representation of acoustic scenes in the auditory cortex of the brown bat," *Nature* **364** 620–623.
Deffuant, G., Neau, D., Amblard, F., & Weisbuch, G. [2000] "Mixing beliefs among interacting agents," *Advances in Complex Systems* **3** 87–98.
DeGroot, M.H. [1974] "Reaching a consensus," *J. Amer. Statist. Assoc.* **69** 121–132.
De Valois, R.L. & De Valois, K.K. [1988] *Spatial Vision* (Oxford University Press, Oxford).
DeVille, L. & Lerman, E. [2013] "Modular dynamical systems on networks," *J. Eur. Math. Soc.* **17**; doi: 10.4171/JEMS/577.
DeVille, L. & Lerman, E. [2015] "Dynamics on networks of manifolds," *SIGMA* **11**; arXiv:1208.1513v4 [math.DS] 2015.
Diekman, C. & Golubitsky, M. [2014] "Network symmetry and binocular rivalry experiments," *J. Math. Neuro.* **4**; doi 10.1186/2190-8567-4-12.
Diekman, C., Golubitsky, M., McMillen, T., & Wang, Y. [2012] "Reduction and dynamics of a generalized rivalry network with two learned patterns," *SIAM J. Appl. Dynam. Sys.* **11** 1270–1309.
Diekman, C., Golubitsky, M., & Wang, Y. [2013] "Derived patterns in binocular rivalry networks," *J. Math. Neuro.* **3** 6; doi:10.1186/2190-8567-3-6.
Durbin, R.M. [1987] *Studies on the Development and Organisation of the Nervous System of* Caenorhabditis elegans, PhD thesis, University of Cambridge.
Eagleman, D.M. [2001] "Visual illusions and neurobiology," *Nature Reviews: Neuroscience* **2** 920–926.
Elowitz, M.B. & Leibler, S. [2000] "A synthetic oscillatory network of transcriptional regulators," *Nature* **403** 335–338.
Ermentrout, G.B. & Cowan, J.D. [1979] "A mathematical theory of visual hallucination patterns," *Biol. Cybernetics* **34** 137–150.
Ermentrout, G.B. & Terman, D.H. [2010] *Mathematical Foundations of Neuroscience*, (Springer, New York).
Fechner, G.T. [1860] *Elemente der Psychophysik*. Transl. *Elements of Psychophysics*. eds. D.H. Howes & E.G. Boring, (Holt, Rinehart and Winston, New York).
Ffrench-Constant, R.H., Rocheleau, T.A., Steichen, J.C., & Chalmers, A.E. [1993] "A point mutation in a *Drosophila* GABA receptor confers insecticide resistance," *Nature* **363** 449–51.
Field, M. [2004] "Combinatorial dynamics," *Dynamical Systems* **19** 217–243.
FitzHugh, R. [1961] "Impulses and physiological states in theoretical models of nerve membrane," *Biophys. J.* **1** 445–466.
Franci, A., Golubitsky, M., Stewart, I., Bizyaeva, A., & Leonard, N.E. [2022] "Breaking indecision in multi-agent multi-option value dynamics," submitted to *SIADS*.
Friedkin, N.E. & Johnsen, E.C. [1999] "Social influence networks and opinion change," *Advances in Group Processes* **16**, eds. Thye, S.R., Lawler, E.J, Macy, M.W., & Walker, H.A., (Emerald Group, Bingley) 1–29.
Furness, J.B. [2008] *The Enteric Nervous System*, Blackwell, Oxford.
Gambaryan, P. [1974] *How Mammals Run: Anatomical Adaptations*, Wiley, New York 1974.
Gardner, R.J., Hermansen, E., Pichitariu, M., Burka, Y. Baas, N.A., Dunn, B.A., Moser, M.B., & Moser, E.I. [2022] "Toroidal topology of population activity in grid cells," *Nature* **602** 123–128.
Giocomo, L.M., Hussaini, S.A., Zheng, F., Kandel, E.R., Moser, M.B., & Moser, E.I. [2011] "Grid cells use hcn1 channels for spatial scaling," *Cell* **147** 1159–1170.
Gjorgjieva, J., Berni, J., Evers, J.F., & Egle, S.J.[2013] "Neural circuits for peristaltic wave propagation in crawling *Drosophila* larvae: analysis and modeling," *Front. Comput. Neurosci.* **7**; doi: 10.3389/fncom.2013.00024.
Golomb, D. [2007] "Neuronal synchrony measures," *Scholarpedia* **2** 1347.
Golomb, D., Hansel, D., & Mato, G. [2001] "Mechanisms of synchrony of neural activity in large networks," *Handbook of Biological Physics* **4**: *Neuro-Informatics and Neural Modelling*, eds. F. Moss & S. Gielen, (Elsevier Science, Amsterdam), 887–968.
Golubitsky M., Josić K., & Kaper T.J. [2001] "An unfolding theory approach to bursting in fast-slow

systems," *Global Analysis of Dynamical Systems: Festschrift dedicated to Floris Takens on the occasion of his 60th birthday*, eds. Broer, H.W., Krauskopf, B., & Vegter, G., 277–308.

Golubitsky, M. & Langford, W.F. [1981] "Classification and unfoldings of degenerate Hopf bifurcation," *J. Diff. Eqns.* **41** 375–415.

Golubitsky, M., Romano, D., & Wang, Y. [2010] "Network periodic solutions: full oscillation and rigid synchrony," *Nonlinearity* **23** 3227–3243.

Golubitsky, M., Romano, D., & Wang, Y. [2012] "Network periodic solutions: patterns of phase-shift synchrony," *Nonlinearity* **25** 1045–1074.

Golubitsky, M. & Schaeffer, D.G. [1985] *Singularities and Groups in Bifurcation Theory I*, Applied Mathematics Series **51**, (Springer, New York).

Golubitsky, M. & Stewart, I. [1985] "Hopf bifurcation in the presence of symmetry," *Arch. Rational Mech. Anal.* **87** 107–165.

Golubitsky, M. & Stewart, I. [1986] "Hopf bifurcation with dihedral group symmetry: coupled nonlinear oscillators," *Multiparameter Bifurcation Theory*, eds. M. Golubitsky & J. Guckenheimer, Proceedings of the AMS-IMS-SIAM Joint Summer Research Conference, July 1985, Arcata, Contemporary Math. **56**, (Amer. Math. Soc., Providence RI) 131–173.

Golubitsky, M. & Stewart, I. [2002] *The Symmetry Perspective: from equilibria to chaos in phase space and physical space*, Progress in Mathematics **200**, (Birkhäuser, Basel).

Golubitsky, M. & Stewart, I. [2006] "Nonlinear dynamics of networks: the groupoid formalism," *Bull. Amer. Math. Soc.* **43** 305–364.

Golubitsky, M., Stewart, I., Buono, P.-L., & Collins, J.J. [1998] "A modular network for legged locomotion," *Physica* D **115** 56–72.

Golubitsky, M. & Stewart, I. [2023] *Dynamics and Bifurcation in Networks*, (SIAM, Philadelphia), to appear.

Golubitsky, M., Stewart, I., Collins, J.J., & Buono, P.-L. [1999] "Symmetry in locomotor central pattern generators and animal gaits," *Nature* **401** 693–695.

Golubitsky, M., Stewart, I., & Schaeffer, D.G. [1998] *Singularities and Groups in Bifurcation Theory II*, Applied Mathematics Series **69**, (Springer, New York).

Golubitsky, M., L.J. Shiau, L.-J., & Stewart, I. [2007] "Spatio-temporal symmetries in the disynaptic canal-neck projection," *SIAM J. Appl. Math.* **67**; doi: 10.1137/060667773.

Golubitsky, M., Stewart, I., & Török, A. [2005] "Patterns of synchrony in coupled cell networks with multiple arrows," *SIAM J. Appl. Dynam. Sys.* **4** 78–100.

Golubitsky, M., Zhao, Y., Wang, Y., & Lu, Z. [2019] "Symmetry of generalized rivalry network models determines patterns of interocular grouping in four-location binocular rivalry," *J. Neurophysiol.* **122** 1989–1999.

Grant, R.B. & Grant, P.R. [2003] "What Darwin's finches can teach us about the evolutionary origin and regulation of biodiversity," *BioScience* **53** 965–975.

Greiter, W. & Firzlaff, U. [2017] "Representation of three-dimensional space in the auditory cortex of the echolocating bat *P. discolor*," *PLoSONE* **12** e0182461; doi:10.1371/journal.pone.0182461v.

Grillner, S., Parker, D., & El Manira, A.J. [1998] "Vertebrate locomotion—a lamprey perspective," *Ann. New York Acad. Sci.* **860** 1–18.

Grillner, S. & Wallén, P. [1985] "Central pattern generators for locomotion, with special reference to vertebrates," *Ann. Rev. Neurosci.* **8** 233–261.

Grimaldi, D.A. [2010] "400 million years on six legs: On the origin and early evolution of Hexapoda," *Arthropod Structure & Development* **39** 191–203.

Guckenheimer, J. & Holmes, P. [1983] *Nonlinear Oscillations, Dynamical Systems, and Bifurcations of Vector Fields*, (Springer, New York).

Hafting, T., Fyhn, M., Molden, S., Moser, M. B., & Moser, E. I. [2005] "Microstructure of a spatial map in the entorhinal cortex," *Nature* **436** 801–806. doi:10.1038/nature03721

Hale, J.K. [1993] *Infinite-Dimensional Dynamical Systems*, (Springer, New York).

Hall, D.H. & Russell, R.L. [1991] "The posterior nervous system of the nematode *Caenorhabditis elegans*: serial reconstruction of identified neurons and complete pattern of synaptic interactions," *J. Neurosci.*

11 1–22.

Hassard, B.D., Kazarinoff, N.D., & Wan, Y.-H. [1981] *Theory and Applications of Hopf Bifurcation*, London Math. Soc. Lecture Notes **41**, (Cambridge University Press, Cambridge).

Hebb, D.O [1949] *The Organization of Behavior*, (Wiley, New York).

Hegselmann, R. & Krause, U. [2002] "Opinion dynamics and bounded confidence models, analysis, and simulations," *J. Artificial Societies and Social Simulation* **5** 121–132.

Higgins, P.J. [1971] *Notes on Categories and Groupoids*, Van Nostrand Reinhold Mathematical Studies **32**, (Van Nostrand Reinhold, London).

Hotelling, H. [1993] "Analysis of a complex of statistical variables into principal components," *J. Educational Psychology* **24** 417–441, 498–520.

Hubel, D.H. & Wiesel, T.N. [1962] "Receptive fields, binocular interaction, and functional architecture of cat striate cortex," *J. Physiol. (Lond.)* **160** 106–154.

Iacaruso, M.F., Gasler. I.T., & Hofer, S.B. [2017] "Synaptic organisation of visual space in primary visual cortex," *Nature* **547** 449–452.

Ihrig, E. & Golubitsky, M. [1984] "Pattern selection with $\mathbf{O}(3)$ symmetry," *Physica* D **12** 1–33.

In, V., Kho, A., Longhini, P., Neff, J.D., Palacios, A., & Buono, P.L. [2022] "Meet ANIBOT: The first biologically-inspired animal robot," *Internat. J. Bif. Chaos* **32** 2230001; doi: 10.1142/S0218127422300014.

Iooss,G. & Joseph, D.D. [1990] *Elementary Stability and Bifurcation Theory* (2nd ed.), (Springer, New York).

Izhikevich, E.M. [2007] *Dynamical Systems in Neuroscience: The Geometry of Excitability and Bursting* (MIT Press, Cambridge MA).

Izquierdo, E. J. & Beer, R.D. [2018] "From head to tail: a neuromechanical model of forward locomotion in *Caenorhabditis elegans*," *Phil. Trans. R. Soc. Lond.* B; doi: 10.1098/rstb.2017.0374.

Jastrow, J. [1899] "The mind's eye," *Popular Science Monthly* **54** 299–312.

Jolliffe, I. T. [2002] *Principal Component Analysis*, Springer Series in Statistics, (Springer, New York); doi: 10.1007/b98835.

Kamei, H. & Cock, P.J.A. [2013] "Computational of balanced relations and their lattice for a coupled cell network," *SIAM J. Appl. Dyn. Syst.* **12** 352–382.

Kauffman, S. [2000] *Investigations*, (Oxford University Press, Oxford).

Kauffman, S. [2008] *Reinventing the Sacred*, (Basic Books, New York).

Klüver, H. [1966] *Mescal and Mechanisms of Hallucinations*, (University of Chicago Press, Chicago).

Kohonen, T. [1984] *Self-Organization and Associative Memory*, (Springer, Berlin).

Kopell, N. [1988] "Towards a theory of modelling central pattern generators," *Neural Control of Rhythmic Movements in Vertebrates*, eds. Cohen, A.H., Rossignol, S., & Grillner, S., (Wiley, New York).

Kopell, N. & Ermentrout, G.B. [1986] "Symmetry and phaselocking in chains of weakly coupled oscillators," *Comm. Pure Appl. Math.* **39** 623–660.

Kopell, N. & Ermentrout, G.B. [1988] "Coupled oscillators and the design of central pattern generators," *Math. Biosci.* **90** 87–109.

Kopell, N. & Ermentrout, G.B. [1990] "Phase transitions and other phenomena in chains of oscillators," *SIAM J. Appl. Math.* **50** 1014–1052.

Kopell, N. & LeMasson, G. [1994] "Rhythmogenesis, amplitude modulation, and multiplexing in a cortical architecture," *Proc. Nat. Acad. Sci. USA* **91** 10586–10590.

Kovács, I., Papathomas, T.V., Yang, M., & Fehér, A. [1996] "When the brain changes its mind: interocular grouping during binocular rivalry," *Proc. Nat. Acad. Sci. USA* **93** 15508–15511.

Kukalová-Peck, J. [1987] "New Carboniferous Diplura, Monura, and Thysanura, the hexapod ground plan, and the role of thoracic side lobes in the origin of wings (Insecta)," *Canad. J. Zool.* **65** 2327–2345.

Kupka, I. [1963] "Contribution à la théorie des champs génériques," *Contrib. Diff. Eqs.* **2** 457–484; **3** 411–420.

Kuramoto, Y. [1984] *Chemical Oscillations, Waves, and Turbulence*, (Springer, Berlin).

Leifer, I., Morone, F., Reis, S.D.S., Andrade J.S.Jr., Sigman, M., & Makse, H.A. [2020] "Circuits with broken fibration symmetries perform core logic computations in biological networks," *PLOS Compu-*

tational Biology; doi: 10.1371/journal.pcbi.1007776 0.
Leighton, F.T. [1982] "Finite common coverings of graphs," *J. Combinatorial Theory B* **33** 231–238.
Leite, M.C.A. & Golubitsky, M. [2006] "Homogeneous three-cell networks," *Nonlinearity* **19** 2313–2363.
Leopold, D.A. & Logothetis, N.K. [1999] "Multistable phenomena: changing views in perception," *Trends in Cognitive Science* **3** 254–264.
Liu, C., Chen, Q., & Zhang, J. [2009] "Coupled van der Pol oscillators utilised as central pattern generators for quadruped locomotion," *IEEE Chinese Control and Decision Conference* 3677–3682; doi: 10.1109/CCDC.2009.5192385.
MacFadden, B.J. [2005] "Fossil horses – evidence for evolution," *Science* **307** 1728–1730.
Makse, H. *et al.* [2021] *Symmetries of Living Systems: Graph Fibrations and Cluster Synchronization in Biological Networks*, Understanding Complex Systems series, (Springer, New York), in preparation.
McCollum, G., & Boyle, R. [2004] "Rotations in a vertebrate setting: evaluation of the symmetry group of the disynaptic canal-neck projection," *Biol. Cybern.* **90** 203–217. doi: 10.1007/s00422-003-0461-3.
McGhee, R.B. [1968] "Some finite state aspects of legged locomotion," *Math. Biosci.* **2** 67–84.
Miftakhov, R.N., Abdusheva, G.R, & Christensen, J. [1999] "Numerical simulation of motility patterns of the small bowel. 1. formulation of a mathematical model," *J. Theor. Biol.* **197** 89–112.
Miftakhov, R.N. & Wingate, D.L. [1993] "Mathematical modelling of the enteric nervous network. II: Facilitation and inhibition of the cholinergic transmission," *J. Biomed. Eng.* **15** 311–318.
Miftakhov, R.N. & Wingate, D.L. [1995] "Mathematical modelling of the enteric nervous network. 5. Excitation propagation in a planar neural network," *Med. Eng. Phys.* **17** 11–19.
Morone, F., Leifer, I., & Makse, H.A. [2020] "Fibration symmetries uncover the building blocks of biological networks," *Proc. Nat. Acad. Sci.* **117** 8306–8314.
Morone, F., & Makse, H.A. [2019] "Symmetry group factorization reveals the structure-function relation in the neural connectome of *Caenorhabditis elegans*," *Nature Communications* **10** 4961; doi: 10.1038/s41467-019-12675-8.
Moser, E., Roudi, Y., Witter, M., Kentros, C., Bonhoeffer, T., & Moser, M.-B. [2014] "Grid cells and cortical representation," *Nature Rev. Neurosci.* **15** 466–481; doi: 10.1038/nrn3766.
Murray, J. [1989] *Mathematical Biology*, (Springer, Berlin).
Muybridge, E. [1899] *Animals in Motion*, (Chapman and Hall, London); reprinted (Dover, New York).
Nagumo, J.S., Arimoto, S, & Yoshizawa, S. [1962] "An active pulse transmission line simulating nerve axon," *Proc. IRE* **50** 2061–2070.
Necker, L.A.[1832] "Observations on some remarkable optical phænomena seen in Switzerland; and on an optical phænomenon which occurs on viewing a figure of a crystal or geometrical solid," *London and Edinburgh Philosophical Magazine and Journal of Science* **1** 329–337.
Neumann, P.M., Stoy, G.A., & Thompson, E.C. [1994] *Groups and Geometry*, (Oxford University Press, Oxford).
Neumann, W.D. [2011] "On Leighton's graph covering theorem," *Groups, Geometry, and Dynamics* **4** 863–872.
Nicosia, V., Valencia, M, Chavez, M., Díaz-Guilera, A. & Vito Latora,V. "Remote synchronization reveals network symmetries and functional modules," *Phys. Rev. Lett.***110** 174102.
Norris, N. [1995] "Universal covers of graphs: isomorphism to depth $n-1$ implies isomorphism to all depths," *Discrete Appl. Math.* **56** 61–74.
Olivares, E., Izquierdo, E.J., & Beer, R.D. [2021] "A neuromechanical model of multiple network rhythmic pattern generators for forward locomotion in *C. elegans*," *Front. Comput. Neurosci.*; doi: 10.3380/fncom.2021.572339.
Olsen, O.H. & Calabrese, R.L. [1996] "Activation of intrinsic and synaptic currents in leech heart interneurons by realistic waveforms," *J. Neuroscience* **16** 4958–4970.
Olver, P. [1993] *Applications of Lie Groups to Differential Equations*, (Springer, New York).
Osterberg, G.A. [1935] "Topography of the layer of rods and cones in the human retina," *Acta Ophthalmologica* **6** 1–102.
Patterson, A. [1992] *Rock Art Symbols of the Greater Southwest*, (Johnson Books, Boulder CO).
Pearson, K. [1901] "On lines and planes of closest fit to systems of points in space," *Philosophical Magazine*

2: 559–572; doi: 10.1080/14786440109462720.

Pecora, L.M., Sorrentino, F., Hagerstrom, A.M., Murphy, T.E, & Roy, R. [2013] "Symmetries, cluster synchronization, and isolated desynchronization in complex networks," *Nature Communications* **5**; doi: 10.1038/ncomms5079.

Peixoto, M.M. [1966] "On an approximation theorem of Kupka and Smale," *J. Diff. Eq.* **3** 214–227.

Pillai, A.S. & and Jirsa, V.K. [2017] "Symmetry breaking in space-time hierarchies shapes brain dynamics and behavior," *Neuron* **94**; doi: 10.1016/j.neuron.2017.05.013.

Pinto, C.A. & Golubitsky, M. [2006] "Central pattern generators for bipedal locomotion," *J. Math. Biol.* **53** 474–489.

Pizlo, Z. & Acacio de Barros, J. [2021] "The concept of symmetry and the theory of perception," *Front. Comput. Neurosci.*; doi: 10.3389/fncom.2021.681162.

Pogromsky, A.Y. [2008] "A partial synchronization theorem," *Chaos* **18** 037107.

Poston. T. & Stewart, I. [1978] *Catastrophe Theory and Its Applications*, Surveys and Reference Works in Math. **2**, (Pitman, London).

Purcell, O., Savery, N.J., Grierson, C.S., & di Bernardo, M. [2010] "A comparative analysis of synthetic genetic oscillators," *J. R. Soc. Interface* **7** 1503–1524; doi:10.1098/rsif.2010.0183.

Roberts, S.K [1981] "Retinal log-polar mapping — solving the rotation-scaling problem in image recognition," Columbus, Ohio 1981; https://microship.com/log-polar-grid-rotation-scaling-vision/.

Rossi, L.F., Harris, K.D, & Carandini, M. [2020] "Spatial connectivity matches direction selectivity in visual cortex," *Nature* **588** 648–652.

Ryabakken, E., Baas, N., & Dunn, B. [2019] "Decoding of neural data using cohomological feature extraction," *Neural Comput.* **31** 68–93.

Sakamoto K., Soh, Z., Suzuki, M., Iino, Y., & Tsuji, T. [2021] "Forward and backward locomotion patterns in *C. elegans* generated by a connectome-based model simulation," *Nature Scientific Reports* **11** 13737; doi: 10.1038/s41598-021-92690-2.

Siegel, R.K. & Jarvik, M.E. [1975]. "Drug–induced hallucinations in animals and man," *Hallucinations: Behavior, Experience and Theory*, eds. Siegel, R.K. & West, L.J. (Wiley, New York) 81–161.

Simpson, G.G. [1951] *Horses*, (Oxford University Press, Oxford).

Singer, W. [1999] "Neuronal synchrony: a versatile code for the definition of relations," *Neuron* **24** 49–65.

Singh, R., Menon, S. & Sinha, S. [2016] "Complex patterns arise through spontaneous symmetry breaking in dense homogeneous networks of neural oscillators," *Sci. Rep.* **6** 22074; doi: 10.1038/srep22074.

Smale, S. [1963] "Stable manifolds for differential equations and diffeomorphisms," *Ann. Scuola Normale Superiore Pisa* **17** 97–116.

Smolen, P., Baxter, D., & Byrne, J.H. [1998] "Frequency selectivity, multistability, and oscillations emerge from models of genetic regulatory systems," *Amer. J. Physiol.* **274** C531–C542; doi: 10.1152/ajpcell.1998.274.2.C531.

Stephens, G.J., Johnson-Kerner, B., Bialek, W., & Ryu, W.S. [2008] "Dimensionality and dynamics in the behavior of *C. elegans*," *PLoS Comput Biol* **4** e1000028; doi:10.1371/journal.pcbi.1000028.

Stewart, G.W. [1993] "On the early history of the singular value decomposition," *SIAM Review* **35** 551–566; doi: 10.1137/1035134.

Stewart, I. [2007] "The lattice of balanced equivalence relations of a coupled cell network," *Math. Proc. Camb. Phil. Soc.* **143** 165–183.

Stewart, I. [2014] "Symmetry-breaking in a rate model for a biped locomotion central pattern generator," *Symmetry* **6** 23–66; doi:10.3390/sym6010023.

Stewart, I. [2017] "Spontaneous symmetry-breaking in a network model for quadruped locomotion," *Internat. J. Bif. Chaos* **27** 1730049.

Stewart, I. [2020a] "Finite characterization of the coarsest balanced colouring of a network," *Internat. J. Bif. Chaos* **30** 2050212; doi:10.1142/S0218127420502120.

Stewart, I. [2020b] "Overdetermined constraints and rigid synchrony patterns for network equilibria," *Portugaliae Mathematica* **77** 163–196.

Stewart, I. [2021] "Balanced colorings and bifurcations in rivalry and opinion networks," *Internat. J. Bif. Chaos* **31** 2130019; doi:10.1142/S0218127421300196.

Stewart, I. [2022] "Overdetermined ODEs and rigid periodic states in network dynamics," *Portugaliae Mathematica*, to appear; arxiv.org/abs/2112.15415.

Stewart, I., Elmhirst, T., & Cohen, J. [2003] Symmetry-breaking as an origin of species, in *Bifurcations, Symmetry, and Patterns*, eds. Buescu,J., Castro, S., Dias, A.P.S., & Labouriau, I., (Birkhäuser, Basel) 3–54.

Stewart, I. & Gökaydin, D.G. [2019] "Symmetries of quotient networks for doubly periodic patterns on the square lattice," *Internat. J. Bif. Chaos* **29** 1930026; doi: 10.1142/S021812741930026X.

Stewart, I. & Gökaydin, D.G. [2020] "Symmetries of quotient networks for doubly periodic patterns on the hexagonal lattice," *Internat. J. Bif. Chaos* **30** (2020) 2030004; doi: 10.1142/S0218127420300049.

Stewart, I. & Golubitsky, M. [2020] "Symmetric networks with geometric constraints as models of visual illusions," *Symmetry* **11** 799; doi: 10.3390/sym11060799.

Stewart, I., Golubitsky, M., & Pivato, M. [2003] "Symmetry groupoids and patterns of synchrony in coupled cell networks," *SIAM J. Appl. Dynam. Sys.* **2** 609–646.

Stewart, I. & Parker, M. [2007] "Periodic dynamics of coupled cell networks I: rigid patterns of synchrony and phase relations," *Dynamical Systems* **22** 389–450.

Stewart, I. & Parker, M. [2008] "Periodic dynamics of coupled cell networks II: cyclic symmetry," *Dynamical Systems* **23** 17–41.

Stewart, I. & Wood, D.A. [2022] "Stable synchronous propagation of signals by feedforward networks," in preparation.

Sullivan, L.H. [1896] "The tall office building artistically considered," *Lippincott's Magazine* 403–406.

Swindale, N.V. [1996] "Looking into a Klein bottle," *Current Biology* **6** 776–779.

Tanaka, S. [1985] "Topological analysis of point singularities in stimulus preference maps of the primary visual cortex," *Proc. R. Soc. Lond.* B **261** 81–88.

Tong, F., Meng, M., & Blake, R. [2006] "Neural bases of binocular rivalry," *Trends in Cognitive Sciences* **10** 502–511.

Uhlhaas, P.J., Pipa, G., Lima, B., Melloni, L. Neuenschwander, S., Nikolić, S.D., & Singer, W. [2009] "Neural synchrony in cortical networks: history, concept and current status," *Front. Integr. Neurosci.*; doi: 10.3389/neuro.07.017.2009.

A. Vanderbauwhede. [1980] *Local Bifurcation and Symmetry*, Habilitation Thesis, Rijksuniversiteit Gent.

Van Valkenburgh, B., Hayward, M.W., Ripple, W.J., Meloro, C., & Roth, V.L. [2016] "The impact of large terrestrial carnivores on Pleistocene ecosystems," *Proc. Nat. Acad. Sci.* **113** 862–867.

Varshney, L.R., Chen, B.L., Paniagua, E., Hall, D.H, & Chklovskii, D.B. [2011] "Structural properties of the *Caenorhabditis elegans* neuronal network," *PLoS Comput. Biol.* **7** (2011) e1001066.

Wei, X.-X., Prentice, J., & Balasubramanian, V. [2015] "A principle of economy predicts the functional architecture of grid cells," *eLife* **4** e08362. doiI:10.7554/eLife.08362.

White, J.G., Southgate, E. Thomson, J.N., & Brenner, S. [1986] "The structure of the nervous system of the nematode *Caenorhabditis elegans*," *Phil. Trans. R. Soc. Lond. B* **314** 1–340.

Wikipedia. [2023] "Latin rectangle," https://en.wikipedia.org/wiki/Latin_rectangle.

Wilshin, S., Haynes, G.C., Porteous, J., Koditschek, D., Revzen, S., & Spence, A.J. [2017] "Morphology and the gradient of a symmetric potential predicts gait transitions of dogs," *Biol. Cybernet.* **111** 269–277; doi 10.1007/s00422-017-0721-2.

Wilson, H.R. [2003] "Computational evidence for a rivalry hierarchy in vision," *Proc. Nat. Acad. Sci.* **100** 14499–14503.

Wilson, H.R. [2007] "Minimal physiological conditions for binocular rivalry and rivalry memory," *Vision Research* **47** 2741–2750.

Wilson, H.R. [2009] "Requirements for conscious visual processing," *Cortical mechanisms of vision*, eds. Jenkin, M. & Harris, L., (Cambridge University Press, Cambridge) 399–417.

Wilson, H.R. & Cowan, J.D. [1972] "Excitatory and inhibitory interactions in localized populations of model neurons," *Biophys. J.* **12** 1–24.

Wilson, R. & Clippingdale, S. [1996] "Self-similar neural networks based on a Kohonen learning rule," *Neural Networks* **9** 747–763; doi: 10.1016/0893-6080(95)00077-1.

Zeeman, E.C. [1977] *Catastrophe Theory: Selected Papers 1972–1977*, (Addison-Wesley, London).